FINAL REPORT

EVALUATIONS OF INDUCED SEISMICITY / SEISMIC HAZARDS AND RISK

FOR THE NEWBERRY VOLCANO EGS DEMONSTRATION

Prepared for
AltaRock Energy Inc.
2320 Marinship Way, Suite 300
Sausalito, California 94965

24 November 2010

Prepared by

Ivan Wong, Silvio Pezzopane, Mark Dober, and Fabia Terra
URS Corporation, Seismic Hazards Group
1333 Broadway, Suite 800
Oakland, California 94612

TABLE OF CONTENTS

TABLE OF CONTENTS

Tables

Figures

TABLE OF CONTENTS

AltaRock Energy Inc., as part of the Newberry Volcano Engineered Geothermal System (EGS) Demonstration Project, will develop an EGS reservoir in the high temperature, low permeability rock on the northwest flank of Newberry Volcano. AltaRock intends to quantitatively demonstrate that hydroshearing techniques can successfully induce and sustain fluid flow and heat extraction from one injection well and two production wells for the conceptual design of a commercial-scale wellfield and power plant.

In the first phase of the project, we have evaluated the potential EGS induced seismicity and seismic hazards in the Project Area and analyzed the seismic risk as part of the submittal of an environmental document to the governing regulatory agencies and stakeholders. The specific objectives of the study are to: (1) evaluate the baseline seismic hazards in the Project Area including at La Pine, the closest community to the site; (2) estimate the potential increase in seismicity rate and the maximum magnitude of an earthquake induced by the hydroshearing in the injection well NGC 55-29; and (3) evaluate the increased seismic risk imposed by the hydroshearing activities.

A priori estimates of the maximum induced earthquake and the rate of seismicity that might occur due to EGS activities at Newberry Volcano are difficult to predict prior to the undertaking of site-specific investigations including seismic monitoring and subsurface imaging of the pre-existing fault and fracture pattern in the affected rock volume. As a first-order characterization, estimates can be made based on global case histories of other EGS projects preferably in similar geologic and tectonic settings. Based on this approach, an upper-bound range of maximum magnitudes ranging from moment magnitude (**M**) 3.5 to 4.0 has been incorporated into the hazard analysis. A probably conservative range of rates of activity has been considered in the hazard analysis adopted from the observed induced seismicity at The Geysers, California.

The Project Area in central Oregon is characterized by a moderate level of tectonic and volcanic activity with a number of active faults and a low to moderate level of historical seismicity. In the probabilistic seismic hazard analysis performed in this study, active faults, volcanic sources of seismicity, and regional seismic source zones for background earthquakes were included. This included two local seismic sources associated with Newberry Volcano. The results of the probabilistic seismic hazard analysis indicate that there is no difference in hazard at La Pine, Sunriver, and the Project site (NGC 55-29) between the baseline conditions (which incorporates the hazard from both natural tectonic and volcanic seismicity) and the EGS induced seismicity. As a result, potential EGS induced seismicity poses no seismic risk to the residents in the neighboring communities.

Although there is no additional seismic risk due to EGS induced earthquakes, if events of **M** 3.0 and higher were to occur, and we judge the likelihood of their occurrence to be small, they will probably be felt in La Pine and Sunriver, but not at damaging levels of ground motions (> 0.10 g). Individual residents within 10 km of the Project site will feel the larger events. The strength of shaking will depend on the size of the event, and distance to and site conditions at each location. The effects of induced seismicity will be more of a nuisance than a hazard to the vast majority of local residents because of the small size of the events and distances to centers of population.

AltaRock Energy Inc., as part of the Newberry Volcano Engineered Geothermal System (EGS) Demonstration Project, will develop an EGS reservoir in the high temperature, low permeability rock on the northwest flank of Newberry Volcano (Figure 1). AltaRock intends to quantitatively demonstrate that hydroshearing techniques can successfully induce and sustain fluid flow and heat extraction from one injection well and two production wells for the conceptual design of a commercial-scale wellfield and power plant.

In the first phase of the project, evaluations of the induced seismicity and seismic hazards and a risk analysis need to be submitted as part of an environmental document for the governing regulatory agencies and stakeholders. As requested by AltaRock Energy, URS Corporation has performed such a study. The specific objectives of the study are to: (1) evaluate the baseline seismic hazards in the Project Area including La Pine, the closest community to the site; (2) estimate the potential increase in seismicity rate and maximum magnitude of an earthquake induced by the hydroshearing in the well NGC 55-29; and (3) evaluate the increased seismic risk imposed by the hydroshearing activities.

These objectives are consistent with Step Two, "Assess Natural Seismic Hazard Potential" and Step Three "Assess Induced Seismicity Potential" in the "Protocol for Induced Seismicity Associated With EGS" (Majer *et al.*, 2008) and the DOE protocol for the U.S. currently being developed.

1.1 SCOPE OF WORK

There are five specific tasks specified by AltaRock that were performed in this study. The following is a description of those tasks as described in the Request for Qualifications (RFQ):

Task 1. Review of Available Information and Data From Previous EGS Projects

The consultant will review available geologic, geophysical, and seismologic data for EGS projects, particularly those in volcanic environments similar to Newberry Volcano (e.g., EGS projects at Ogachi and Hijori geothermal projects in Japan). These data will be evaluated and if feasible, look-alike conceptual models generated. Relevant theoretical models should also be evaluated. AltaRock will make available to the consultant any relevant data requested that it possesses.

Task 2. Evaluation of Local Faults

Quaternary faults exist in and around the Project Area, including but not limited to ring structures associated with the Newberry nested caldera. The consultant must provide a defensible argument for the definition of the area to be investigated in this task. At a minimum, the area investigated should include the community of La Pine. This evaluation will include but not be limited to interpretation of LiDAR, aerial photographs, Landsat, and topographic maps to identify any geomorphic evidence for faulting at the surface (e.g., fault scarps). Note that AltaRock is part of the Oregon LiDAR Consortium Project flying LiDAR over the Newberry Volcano area. The consultant should include a brief field reconnaissance to field‐check potential fault scarps and surficial evidence of faulting in the proposed budget.

Note the LiDAR data was not made available to URS at the time of this study and so it was not evaluated.

Task 3. Site-Specific Probabilistic Seismic Hazard Analysis

The consultant will calculate the site-specific probabilistic ground motions resulting from natural seismicity and the potential increase resulting from hydroshearing activities for the Project Area defined in Task 2 above. The potential for induced seismicity could be derived by relating regional and site-specific conditions, including such parameters as the state of stress, presence or absence of favorably oriented faults and fractures, and hydroshearing plans (injection rates and pressures). The analysis will include but not be limited to contributions to strong ground shaking at the Project Area from seismic activity along known active structures, as well as other potential (e.g., suspected) contributing structures. The potential for induced seismicity should be characterized in terms of recurrence characteristics, rates, and maximum magnitudes for inclusion in the probabilistic hazard model. The analysis results should be presented at a minimum in a set of hazard curves that express ground motions as a function of annual exceedance probability. The basis and the potential for triggering of local faults should be included in the analysis. The consultant will define the uncertainties in any models used and in the model parameters.

Task 4. Seismic Risk Evaluation

A qualitative seismic risk evaluation will be performed based on the results of Task 3. The potential ground shaking as expressed in terms of peak ground acceleration, peak ground velocity, and/or intensity from induced events will be estimated. Estimates of their effects will be made on the local population, and the built and natural environment. The seismic vulnerability of typical buildings in the area will be considered. These potential impacts should be expressed in tangible measures of structural impacts and felt effects in the area investigated using for example, the Modified Mercalli (MM) intensity scale and standard blast vibration regulatory thresholds.

Task 5. Final Report

A final report that (1) describes the analysis approach and the results of each task performed, and (2) summarizes the results of the study will be produced and transmitted to AltaRock for their review. A Final Report will be produced.

1.2 ACKNOWLEDGMENTS

This study was supported by AltaRock Energy Inc. Our thanks to Joe Iovenitti and Will Osborn for their assistance. The seismic hazard and risk evaluations of the AltaRock Newberry Volcano EGS site were performed by the following personnel of URS Corporation:

Seismic Source Characterization	Silvio Pezzopane, Ivan Wong, and Mark Dober
Probabilistic Seismic Hazard Analysis	Mark Dober and Ivan Wong

Risk Analysis	Ivan Wong and Fabia Terra
Report Preparation	Ivan Wong, Silvio Pezzopane, Mark Dober, and Fabia Terra

Ivan Wong was the URS Project Manager. Our appreciation to Melinda Lee for her assistance in the preparation of this report and to Joe Iovenitti, Susan Petty, Trenton Cladouhos, and Will Osburn for their reviews of this study.

The Newberry Volcano EGS Project will be executed in three phases over a period of approximately three years (Davenport Newberry Holdings LLC, 2010). Phase I, *Pre-Stimulation*, will integrate all existing geoscience and well data along with any additional flow test and wellbore survey data into a comprehensive geologic model of the project. A detailed stimulation plan will be developed, an initial microseismic array (MSA) will be installed, public meetings and information forums will be conducted, and Phase I and II permits will be obtained. In Phase II, *Reservoir Creation and Characterization*, an existing deep well will be stimulated using hydroshearing techniques to create a fracture network. The initial MSA may be modified or augmented prior to stimulation. The stimulated injection well and surrounding fracture network will be characterized by a short flow test, and MSA and chemical tracer data will be interpreted to map the fracture locations.

Two production wells will be directionally drilled from the same well pad into the mapped fracture network. The first production well will be drilled into one flank of the newly created fracture network, and a connectivity test will be conducted. Groundwater, produced from on-site water wells, will be pumped into the injection well while the production well is flowed to an atmospheric separator, with the steam vented to the atmosphere and the residual liquid re-circulated to the injection well. A second similar production well will be drilled into the opposite flank of the fracture network. If necessary, stimulation of the production wells will be conducted to enhance connectivity. The final Phase II operation will be an extended circulation test to characterize system performance under steady-state conditions. In Phase III, *Long-Term Monitoring and Conceptual Modeling*, the static EGS system will be monitored to assess fracture evolution and reservoir response to production, and a conceptual model of a commercial-scale EGS wellfield and power generation facility will be developed.

In terms of progress to date, Davenport completed the drilling of two deep wells, NGC 55-29 and NGC 46-16, in August and November 2008, respectively. The injection well NGC 55-29 was completed to a depth of 3,066 m (10,060 ft), with an 8.5-inch-diameter open hole from 1,790 m (6,462 ft) to total depth. NGC 46-16 was completed to a depth of 3,553 m (11,599 ft), with a 12¼-inch-diameter open hole to 2,100 m (6,888 ft) and a 10-5/8-inch-diameter open hole to total depth. Both wells bottomed out in crystalline rock consisting of a mix of subvolcanic basalt and granodiorite.

The injection well and, if necessary, the production wells, will be stimulated using a process termed “hydroshearing.” The goal of hydroshearing stimulation is to create multiple hydraulic fracture network zones in crystalline rock to create the heat exchange area of an EGS system. Hydroshearing is the process of hydraulically inducing shear failure in subsurface rock formations along pre-existing natural fractures. Hydroshearing requires that stimulation pressure be maintained at levels less than formation breakdown pressure, unlike traditional oil and gas fracturing techniques. Exceeding the formation breakdown pressure can result in tensile failure, which can lead to short-circuiting in hot, dry rock formations. Inducing shear failure offers the greatest potential for creating an EGS reservoir that will provide sufficient surface area and residence time for injected fluids to reach optimum production temperature and maximize reservoir life by minimizing short-circuiting and premature injection fluid breakthrough. To create a network of optimum fracture width, density and overall dimension, hydroshearing stimulation is conducted at multiple levels in the target well. The advantages of multiple stimulations include:

- Creation of a larger reservoir volume, thereby doubling or tripling available heat exchange area.
- Enhancing system permeability and connectivity to allow for higher production rates and lower injection pressures, thereby increasing the economic viability of the project.
- Establishing a single-well production total mass flow rate 75 Kg/s.
- Forming a fracture network 'half-length', or radius, of 500 m.

The project planning purposes, the hydroshearing in NGC 55-29 is expected to occur over a period of 21 days at a pump rate of 420 to 1,260 gals/min. The objective of stimulation is to create up to three separate and stacked fracture networks. Well stimulation will use (1) rig-off with chemical diverters and/or (2) rig-on with mechanical and chemical diverters. In either case, stimulation will be accomplished by pumping groundwater into the injection well at relatively high pressure (but at a pressure low enough to prevent tensile failure and formation breakdown) to hydroshear the shallowest pre-existing wellbore fractures below the casing shoe. Chemical and mechanical diverters are used to direct the stimulation fluid to specific areas of pre-existing fractures, previously identified by borehole televiewer surveys. Chemical diverters, commonly and safely used in oil and gas operations, are used to temporarily block open fractures, but are later removed by thermal degradation or the addition of other chemical additives. Mechanical diverters are plugs and other tools used to isolate specific sections of the well bore. The Phase I Stimulation Plan will define the approach AltaRock will use, and will be reviewed and approved by BLM and DOE prior to field operations.

Microseismicity will be continuously monitored along with surface injection rates and pressures. A fiber optic monitoring system will be deployed in the wellbore to provide real-time distributed temperature information and bottomhole pressure. The orientation and shape of the fractured reservoir created by stimulation, controlled by the *in situ* stress regime at any given depth, will be determined by interpretation of MSA data. After the well has thermally recovered from stimulation, a three-day, single-well flow test will be conducted to characterize the newly created reservoir through tracer sampling and analysis. All resulting data (e.g., microseismic, hydraulic, fiber optic and flow back test data) will be thoroughly analyzed. The thermo-, hydro-, mechanical-, chemical-model of the reservoir will then be updated.

Once a fracture geometry with a long axis radius of about 500 m is achieved, a high-temperature, chemical diverter will be pumped in an attempt to redirect the hydraulic treatment to the next set of natural fractures. The resulting temperature, microseismic and pressure data will be analyzed to determine if the diversion has been successful. If the chemical diverter does not provide sufficient zonal isolation to allow creation of multiple fracture networks, a rig will be mobilized and a mechanical isolation device, such as a scab liner, will be installed in the well to ensure that at least two separate fracture networks are created.

Earthquakes that have been generated through human activity, i.e., induced seismicity, have been recognized for decades. One of the first examples was the recognition in 1945 that earthquakes were being caused by the impoundment of Lake Mead behind Hoover Dam. Earthquakes have also been induced by both surface and underground mining activities (e.g., McGarr, 1971; Cook, 1976) and fluid injection (e.g., Healy *et al.*, 1968; Nicholson and Wesson, 1990). In the past decade, the long-standing term "reservoir-induced seismicity" has been officially replaced by "reservoir-triggered seismicity" by the U.S. Committee on Large Dams. This term accurately characterizes the process of induced seismicity in that the effect of reservoir impoundment, mining, and fluid-injection is to "trigger" shear failure (earthquakes), along pre-existing pre-stressed zones of weakness, i.e., faults and fractures, that are favorably oriented in the current tectonic stress field. The act of triggering is to add an increment of stress or reduce the normal stress across pre-stressed faults or fractures resulting in seismic slip. Although this mechanism does not explain all induced seismicity such as tensile failure earthquakes due to hydraulic fracturing, it certainly explains the largest induced earthquakes such as those at the Rocky Mountain Arsenal and other cases of fluid-induced seismicity (Nicholson and Wesson, 1990), most mining cases (e.g., Wong and McGarr, 1990; Wong, 1993), and large reservoirs (e.g., Simpson, 1976; Wong *et al.*, 1991).

Seismicity induced by EGS activities has been described in a number of scientific papers. The subject has been reviewed and described in an overview paper by Majer *et al.* (2007). We briefly summarize that paper in the following.

Induced seismicity has been documented in a number of operating geothermal fields and EGS projects. The seismicity consists predominantly of microearthquakes (moment magnitude [**M**] or Richter local magnitude [M_L] < 3.0), which generally are not felt (unless at close distances of a few kilometers) although events in the **M** 4.0 to 5.0 range have occurred (Section 3.4). Microearthquakes have led to little or no damage worldwide (Majer *et al.*, 2007).

A number of mechanisms can lead to geothermal-induced seismicity (Majer *et al.*, 2007):

(1) pore pressure increase, which can decrease the static friction and induce seismic slip in a deviatoric stress field. In this process of effective stress reduction, pre-existing faults are already pre-stressed and the increase in pore pressure acts as a trigger;

(2) temperature decrease where cool fluids interact with hot rock causing contraction of fracture surfaces in a process called thermoelastic strain. As with the effective stress reduction, the slight opening of a pre-stressed fracture reduces the static friction and triggers slip already near failure in the local stress field;

(3) as fluid is produced from or injected into the reservoir rock, it may be compacted or stressed. These volume changes cause a perturbation in the local stress field and also can cause slip on pre-existing fractures or faults; and

(4) injecting non-native fluid into rock may cause a geochemical alteration of fracture surfaces thus changing the coefficient of friction on those surfaces. In this case of reduced friction, microearthquakes are more likely to occur.

All four mechanisms are relevant to EGS applications. The extent to which any of these processes is active in a specific situation is affected by a number of local and regional geologic conditions including (Majer *et al.*, 2007):

(1) the orientation and magnitude of the deviatoric stress field in relation to pre-existing faults;

(2) extent and orientation of faults and fractures;

(3) rock mechanical properties such as shear modulus, ductility, etc.;

(4) hydrologic factors such as permeability and porosity; and

(5) historical natural seismicity.

Majer *et al*. (2007) summarize several cases of geothermal-induced seismicity including The Geysers, California; Cooper Basin, Australia; Berlin, El Salvador, Soultz-sous-Forets, France, and Basel, Switzerland.

In the following we describe the induced seismicity at two EGS sites in Japan and the Fenton Hill site in New Mexico. All three sites are in similar volcanic caldera settings as Newberry Volcano. The Geysers has been the site of ongoing fluid-induced seismicity associated with geothermal production and has thus provided a field laboratory for studying their causes and effects. However, no EGS activities have been performed at The Geysers to date although the first experiment is scheduled to occur in early 2011. A brief description of The Geysers seismicity also follows.

3.1 OGACHI AND HIJORI, JAPAN

A Hot Dry Rock (HDR) geothermal project was initiated at the Ogachi site in northeast Japan in 1989. The site is located within a Neogene caldera with an uplifted granodiorite basement and a north-northwest-trending mylonite zone (Ito and Kitano, 2000). In the Ogachi experiment, a 1,000-m deep injection well and a 1,100-m deep production well were drilled into pre-Tertiary granite. Two reservoirs were developed by hydraulic fracturing in the injection well (Ito *et al.*, 2001). The deepest reservoir at the bottom of the injection well was created by injecting a total of 10,163 m^3 of water. The shallower reservoir at about 700 m depth was created by injecting 5,400 m^3 of water.

Both acoustic emissions (AE) and microearthquakes were monitored at the Ogachi site. Events appeared to be confined to a volume within 1,000 m of the injection well in an orientation consistent with the joint pattern (Kaieda *et al.*, 2010). With the exception of a single event of M (unknown scale) 2.0, the remainder were smaller than M -1.0 (Kaieda *et al.*, 2010).

A HDR project similar to the Ogachi experiment was performed at the Hijori site on the southern edge of the Hijori caldera in northern Japan (Kaieda *et al.*, 2010). An injection well HDR-1 was drilled to a depth of 2,205 m in granodiorite basement rock. Injection was carried out in three stages of flow rate: 1, 2, and 4 tons/min of water over a 12-hour period. Seismicity was very low the first 4 hours of stimulation similar to what was observed at Ogachi (Kaieda *et al.*, 2010). The events aligned along an east-west direction consistent with the natural joint pattern. The events propagated about 500 m from HDR-1. The maximum magnitude was M 0.3 with the remaining events smaller than M -1.0 (Kaieda *et al.*, 2010). In a comparison with the Cooper Basin Hot Fractured Rock Project, Kaieda *et al.* (2010) suggest that the microearthquakes at Ogachi and Hijori were relatively small compared to Cooper Basin (maximum **M** 3.7) because at the two

Japanese sites, the rock volume is highly fractured and the *in situ* stress conditions are relatively low.

3.2 FENTON HILL, NEW MEXICO

The first HDR experiments were initiated at a site at Fenton Hill, New Mexico in 1973 by the Los Alamos National Laboratory (Phillips *et al.*, 2001). The site is located on the southwest flank of the Jemez caldera, which was last active in the late-Pleistocene. During the 25-year lifetime of the Los Alamos HDR Project, two separate confined HDR reservoirs were created in hot crystalline rock, interrogated, and flow-tested for almost a year each. The first reservoir was developed at a depth of about 2,800 m in jointed granitic rock at a mean temperature of 195° C. (Brown, 2009). The second reservoir was created at a depth of about 2,500 m also in jointed granitic rock at a mean temperature of 235° C.

In December 1983, a massive hydraulic fracturing experiment was performed with more than 21,000 m^3 of water injected in 61 hours. The injection was conducted at a depth of 3,460 m in the deeper reservoir. More than 11,000 microearthquakes were recorded over the course of the injection. The events imaged a tabular volume 1 km by 1 km by 300 m striking N10°W and dipping 65° to the east (Phillips *et al.*, 2001). The local *in situ* stress field was extensional with the minimum principal stress oriented nearly northwest-southeast (Brown, 2009). Magnitudes of the events in three massive injections have ranged from M -6 to -2 (Albright and Pearson, 1982). The microearthquakes result from shear failure probably on pre-existing planes of weakness that intersect or make up the main hydraulic system (Albright and Pearson, 1982).

3.3 THE GEYSERS

The Geysers geothermal area is the site of a vapor-dominated steam field from which electric power has been generated since the early 1960's. Earthquakes are concentrated at the steam production field and extend to a depth of 6 km (Eberhart-Phillips and Oppenheimer, 1984). Prior to the onset of power production, the region surrounding The Geysers was characterized by a very low level of seismicity, albeit seismographic coverage was poor.

Eberhart-Phillips and Oppenheimer (1984) suggested that there are two plausible mechanisms that may explain the induced seismicity at The Geysers: (1) volumetric contraction due to mass withdrawal, which could perturb the stress field and cause faulting in the reservoir rock already near failure due to the regional stress field, and (2) aseismic deformation due to regional tectonism may be converted to strike-slip deformation due to an increase in the coefficient of friction along fault surfaces (Eberhart-Phillips and Oppenheimer, 1984). For both mechanisms, Eberhart-Phillips and Oppenheimer (1984) expected seismicity to continue to increase in spite of declining reservoir production and for seismicity to occur in areas where new production is initiated.

Stark (1990) made several significant observations on The Geysers seismicity: (1) earthquake clusters associated with injection wells image the injected fluid and this correlation is more apparent for hypocentral depths deeper than about 2 km; (2) temporal correlation between the onset of injection and seismicity is generally observed; and (3) not all injection is accompanied by seismicity and some seismicity, especially shallower events, does not correlate with injection.

The largest earthquake observed in The Geysers has been a **M** 4.6 event that occurred on 20 October 2006 on the northern margin of The Geysers area. It had a shallow focal depth (3.5 km) and it is believed to have been induced. The USGS catalog lists a total of 23 probable Geysers induced earthquakes of M_L or **M** 4.0 and greater. This translates to a rate of one **M** ≥ 4.0 event per 1.5 years since 1972. The rate, however, appears to have significantly increased since 2003 to about one **M** ≥ 4.0 event on average every 6 to 7 months, after a dramatic increase in injection. Although the largest earthquake observed at The Geysers has been a **M** 4.6, the value of **M** 5.0 is still generally agreed upon as an upper bound (Majer *et al.*, 2007).

3.4 MAXIMUM EGS EARTHQUAKE

Maximum magnitudes (Mmax) and earthquake rates are the two most important inputs into seismic hazard analyses. The magnitude of an earthquake is proportional to the area of the fault that slips in an event and the amount of stress that is released, i.e., stress drop. Several conditions must be met for a large and potentially damaging earthquake to occur. There must be a large enough fault, stresses must be high enough to cause slip, and the fault needs to be pre-stressed and near failure.

Predicting the Mmax of earthquakes due to EGS activities has been a difficult challenge. As recognized by many, the characteristics of induced seismicity are controlled by the nature and distribution of pre-existing fractures and faults and the local stress field in the volume of rock surrounding the well where fluid is being introduced (e.g., Majer *et al.*, 2007). A number of theoretical approaches have been developed to predict Mmax.

McGarr (1976) relates the sums of the seismic moment released in earthquakes to a change in volume. In the case of fluid injection, it is the volume added to the system by injection. McGarr (1976) applied this relationship to the injection-induced earthquakes at the Rocky Mountain Arsenal and obtained general agreement for the three largest events. A key constraint is the total seismic moment is not typically released in a single event but rather a sequence of events and so any estimate of Mmax would be conservative.

A second approach is to relate the seismic moment or maximum magnitude to the maximum length or area of pre-existing faults in the volume of rock that will be affected by fluid injection. The seismic moment and hence moment magnitude can be computed assuming a reasonable range of stress drops using the standard Brune (1970) source model. Stress drops have been computed for microearthquakes at Fenton Hill and they range from 0.1 to 20 bars (Fehler and Phillips, 1991). Seismic moments can also be computed based on a range of displacements that might occur on the faults. Leonard (2010) has developed a set of self-consistent scaling relationships between seismic moment and rupture area, length, width, and average displacement. Leonard (2010) contends that the scaling relationships are applicable to small rupture lengths and rupture areas (> 0 km or 0 km^2).

A third approach has been proposed by Shapiro *et al.* (2010) using the parameter "seismogenic index." Shapiro *et al.* (2007) observed that under "general conditions," the number of fluid-induced earthquakes with a magnitude larger than a given value increases approximately proportionally to the injected fluid volume. Using the seismicity rate of induced events and the fluid injection rate, Shapiro *et al.* (2010) derived the parameter seismogenic index. This parameter can be used to compare different locations of possible fluid injections. The

seismogenic index depends on the local maximum critical pressure for shear fracturing, the volume concentration of pre-existing fractures, and the poroelastic uniaxial storage coefficient (Shapiro *et al.*, 2010). Along with the injection parameters, the seismogenic parameter can be used to estimate the probability of a given number of such events during an injection period. Shapiro *et al.* (2010) tested this technique at six case studies of injection induced seismicity including Cooper Basin, Basel, and Ogachi and the results were reasonable.

All the approaches above depend on an *a priori* knowledge of the rupture characteristics of future induced seismicity, which requires subsurface characterization of the affected volume of rock around the well. This information is not yet available but will be obtained as further investigations are performed (Section 2).

In the absence of a characterization of the faulting and fracture pattern in the rock volume being affected by fluid injection at NGC 55-29, the estimation of Mmax needs to be based on suitable analogs. Although the number of analogs similar to Newberry Volcano are limited, the observations at EGS sites such Fenton Hill, Ogachi, and Hijori in similar geologic and tectonic settings suggest that Mmax may be less than **M** 3.0 (Figure 2). However, to reiterate, the value of Mmax is very dependent on the site-specific conditions of the affected rock volume as pointed out by numerous investigators and thus we need to allow for the probability, albeit small, of higher values.

In a review of Mmax associated with EGS, the highest observed value has been an earthquake of **M** 3.7 in Cooper Basin, Australia (Figure 2). The next largest event was a **M** 3.4 event in Basel, Switzerland. Although not an EGS site, The Geysers has recorded a **M** 4.6 earthquake, but this is for a well-developed geothermal field that has operated over four decades. The first **M** 4.0 induced earthquake occurred in 1982, nearly 20 years after geothermal production had begun (Wong *et al.*, 2010). In light of the Mmax values shown in Figure 2, with greater consideration of the EGS sites in similar geologic settings, a probable upper-bound Mmax for the Newberry EGS Project is **M** 3.5 to 4.0.

The seismotectonic setting and historical seismicity of the Project Area are described below.

4.1 SEISMOTECTONIC SETTING

An understanding of the seismotectonic setting of a site provides the framework in which the earthquake potential of geologic structures in a region can be identified and characterized. The following is a description of the seismotectonic setting of Newberry Volcano in central Oregon.

Central Oregon is dominantly influenced by the nearby seismically active convergent margin, which is marked by the boundary between the Juan de Fuca and North American plates (Figure 3). The northeastward (N60°E) motion of the Juan de Fuca plate relative to the North American plate occurs at a rate of approximately 40 to 45 mm/yr according to Riddihough (1984). Convergence is accommodated by underthrusting and subduction of the Juan de Fuca plate beneath the North American continent along the Cascadia trench. Oblique subduction of the Juan de Fuca plate has created a north-south trending volcanic arc that extends from northern California to southern British Columbia. This chain of Late-Cenozoic volcanoes makes up the Cascade Range (Figure 3). In central Oregon, the range is dominated by late Pleistocene stratovolcanoes including Mt. Jefferson, the Three Sisters, and Newberry Volcano (Figure 3).

Other major tectonic elements of the plate boundary include an active accretionary wedge complex in the offshore region east of the trench and a deformed Tertiary forearc basin that lies seaward of the volcanic arc. The present-day Coast Ranges consist of accreted marine sediments and fragments of oceanic crust that were subsequently deformed during early Tertiary plate convergence and subduction (Unruh *et al.*, 1994). Late Cenozoic deformation in the Coast Ranges is characterized by uplift, folding, distributed faulting, and rotation of crustal blocks about vertical axes (Unruh *et al.*, 1994). Geomorphic evidence (indices such as stream gradients, longitudinal profiles, sinuousity, and valley incision) suggests that uplift of the Coast Range may still be occurring today.

Oblique subduction along the Oregon coastline produces arc-parallel motion of the Cascadia forearc and adds an additional component of crustal deformation from the relative motions of distinct forearc blocks (Wells *et al.*, 1998; McCaffrey, 1994). Wells *et al.* (1998) differentiate between three forearc segments based on contrasting patterns of Neogene deformation, seismicity and volcanism, and crustal structure: the southern Sierra Nevada block, the central Oregon block, and the northern Washington block. The boundary of the Oregon block extends south from the Oregon-Washington border to the relatively aseismic Klamath Mountains which mark the northern boundary of the Sierra Nevada block (Wells *et al.*, 1998) (Figure 3). During the Cenozoic, the Oregon Coastal block (OC) has been rotating clockwise with respect to stable North America at about 1.5°/m.y. (Magill *et al.*, 1982), creating a diffuse transfer zone along its boundary with the Basin and Range to the east (Figure 3). The volcanic arc in this region is characterized by lower rates of seismicity, high extrusion rates, axial grabens, and overall extension (Wells *et al*., 1998). Due to the rapid translation of the Sierra Nevada block N50°W at a rate of 11 mm/yr, the volcanic arc along its eastern edge has generally higher rates of seismicity, high extrusion rates, and elements of transtension (Wells *et al*., 1998).

East of the Cascadia forearc is the Basin and Range Province which is undergoing east-west to southeast-northwest crustal extension at a rate of approximately 10 mm/yr (Wells *et al*., 1998; Zoback and Zoback, 1989) (Figure 3). This extension was initiated in the late Tertiary and has

resulted in an overall pattern of north-south trending normal faults that separate uplifted blocks from intervening grabens. This region is tectonically active with numerous fault scarps that indicate relatively youthful displacements, abundant geothermal activity, and low to moderate levels of historical seismicity.

Central Oregon is a complex transitional region, as the region is influenced in part by the northernmost extent of the Basin and Range extensional tectonics and also by volcanic processes that characterize the High Cascade region (Ake *et al.*, 2001). The dynamic interplay between extensional faulting and volcanic processes raises questions about whether the potential seismic sources are tectonic or volcanic in origin. (Ake *et al.*, 2001).

Regional active faulting in Oregon is largely concentrated along four north-trending fault zones within and east of the Cascade volcanic arc (Pezzopane, 1993). These broadly distributed zones in central and eastern Oregon appear to be the northern continuation of active faults of the Central Nevada Seismic Belt, north of the Walker Lane and the Eastern California Shear zones (Pezzopane and Weldon, 1993). Despite the paucity of large magnitude earthquakes in the historical record in Oregon, it is likely that active fault zones in Oregon serve to kinematically connect seismic activity in northeastern California and northwestern Nevada to seismically active fault zones in southern and central Washington (Pezzopane and Weldon, 1993).

The regional tectonics near Newberry Volcano is unique because of its location in the back-arc east of the Cascade Range, which is common to only three other nearby volcanic centers; Simcoe Mountain, Washington, and Medicine Lake and Hackamore in northern California (Hildreth, 2007). Newberry is similar to Medicine Lake and Hackamore insofar as they are influenced significantly by transtensional tectonics from impingement of Basin and Range faulting with Cascades faulting and volcanism (Gutmanis, 1989; Poland *et al.*, 2006; Hildreth, 2007; Donnelly-Nolan *et al.*, 2008). Extensional movements in the Newberry region are accommodated by slip along three principal fault zones that show Quaternary and Holocene displacements and probably intersect or merge beneath the caldera and shield, including the Northwest Rift zone, the Southeast Newberry fault zone, and the Southwest Newberry fault zone (Higgins, 1973; Fitterman, 1988; Gutmanis, 1989; Chitwood, 1990). On the northeast side of Newberry Volcano, the Brothers fault (Figure 9) offsets Miocene and Pliocene volcanics, yet does not appear to offset Quaternary lava flows (MacLeod and Sherrod, 1988; Walker and MacLeod, 1991). The Brothers zone is, nevertheless, included in this hazard analysis.

4.2 HISTORICAL SEISMICITY

The historical earthquake record can be divided into pre-instrumental and instrumental periods. Prior to about 1961, earthquake locations and size estimates are mostly based on felt reports. Earthquake data were gathered from newspaper accounts, which began with the establishment of settlements in the region. The pre-instrumental record for this region is estimated to be complete above **M** 5.0 since about 1850 (Wong and Bott, 1995). The historical catalog used in this analysis is from Wong *et al.* (2000) updated with data principally from the Advanced National Seismic Network and the U.S. Geological Survey (Figures 4 and 5).

4.2.1 Pre-Instrumental Seismicity

No earthquakes greater than **M** 5.0 have occurred within 100 km of Newberry Volcano between 1891 and 1961 (Figure 4). The closest large event is 165 km southwest of Newberry Volcano and was the **M** 6.0 Klamath Falls, Oregon earthquake that occurred on 21 October 1993. However several moderate-sized events have occurred since 1891. They include three M_L 4.3 or Modified Mercalli intensity (MM) V earthquakes in 1906, 1920 and 1921 none of which were felt at the site (Figure 4). There was a significant regional earthquake on 18 April 1936 about 340 km from the volcano which is discussed below.

The largest and most significant earthquake in eastern Oregon, known as the Milton-Freewater or Stateline earthquake, occurred at 11:08 p.m. on the night of 15 July 1936 (Neumann, 1938). The maximum intensity was MM VII+, and it was felt over an area of 275,000 km^2 (Figure 6). In a reevaluation of the event, Woodward-Clyde Consultants (1980) (also Foxall and Turcotte, 1979) calculated a magnitude of M_L 6.1, as recorded at 17 seismographic stations. Based on the isoseismal map and an empirical relationship between magnitude and total felt area developed by Toppozada (1975), the event was estimated to be a M_L 6.4 (Bott and Wong, 1993). The mainshock was preceded by two felt foreshocks at 10:30 p.m. and 11:20 p.m. local time and was followed by numerous aftershocks (Neumann, 1938).

The mainshock was felt most strongly and caused damage in and around Milton-Freewater, Umapine, and Stateline, Oregon. It was also strongly felt in Walla Walla, Washington just north of the border. Total damage amounted to $100,000 in 1936 dollars. Many chimneys were damaged, houses were moved off their foundations, canned goods were scattered in a cannery, plaster cracked, windows broke, and school buildings were damaged (Neumann, 1938).

Intense ground cracking occurred in a zone 25 m wide and 500 m long extending west-northwest along the base of a hill west of Milton-Freewater. Some cracks were 1 to 2 m wide, and in one place the ground dropped by 2.4 m. Water emerged from some of these cracks, indicating that liquefaction as well as ground slumping and landsliding had occurred. Groundwater flow generally increased in wells, and several springs were revived.

Though the epicentral location of this earthquake has been difficult to determine, an epicenter based on the isoseismal data gave a location about 10 km northeast of Milton-Freewater (Neumann, 1938). The isoseismal map depicted by in Stover and Coffman (1993) shows the Newberry Volcano just outside of the MM II to III isoseismal. However, it is possible that the event was felt (MM II) at or near the volcano (Figure 6).

4.2.2 Instrumental Seismicity

Although the earliest seismograph station was established in 1906 in Seattle, coverage using modern instrumentation did not begin until 1980 when the University of Washington extended its seismographic coverage into Oregon. Before this time, stations such as Corvallis (COR) installed in 1944 and Klamath Falls (KFO) in 1962 were few in number. Due to the lack of extensive seismographic coverage, the historical record is probably only complete in the study region for events of $M_L \geq 3.0$ since 1980.

There have only been six M_L 3.0 or greater earthquakes within 100 km of the Newberry Volcano since 1980 (Figure 4). Of these events, four were in 1999 consisting of a minor swarm of

earthquakes during April and May of that year. The largest event in the swarm was a M_L 4.3 earthquake on 28 April 1999, which was felt at Christmas Valley and Paisley, Oregon. It was located about 98 km southeast of the Newberry Volcano (Figure 4). Two other events were felt in Christmas Valley, a M_L 3.1 on 27 April and a M_L 3.3 earthquake the following day. The closest M_L 3.0 and larger earthquake to the site was an event estimated at M_L 3.0 in 1943 about 35 km north of the site (Figure 5). Based on the instrumental record, no earthquakes have been located within 10 km of well NGC 55-29 or Newberry Volcano (Figure 5).

Other significant earthquakes in the vicinity of the Newberry Volcano include a M_L 4.8 earthquake on 13 April 1976 located 150 km to the north (Figure 4). The Deschutes Valley earthquake cracked plaster and drywall in Dufur and Wamic, Oregon (Stover and Coffman, 1993). The M_L 4.8 event was felt throughout central Oregon and was possibly felt with MM II at the Newberry Volcano (Figure 7). The 15-km deep event was preceded by nine foreshocks ranging in magnitude from M_L 1.1 to 3.8. There were a total of 13 aftershocks, the largest measuring M_L 4.2 (Wong and Bott, 1995). Couch *et al.* (1976) computed a composite focal mechanism of the mainshock and other events in the sequence, which suggested a west-northwest-striking reverse fault as the source. Several anticlines in the epicentral area have similar orientations (Wong and Bott, 1995).

The probabilistic seismic hazard analysis (PSHA) approach used in this study is based on the model developed principally by Cornell (1968). The occurrence of earthquakes is assumed to be a Poisson process. The Poisson model is widely used and is a reasonable assumption in regions where data are sufficient to provide only an estimate of average recurrence rate (Cornell, 1968). The occurrence of ground motions at the site in excess of a specified level is also a Poisson process, if (1) the occurrence of earthquakes is a Poisson process, and (2) the probability that any one event will result in ground motions at the site in excess of a specified level is independent of the occurrence of other events.

The probability that a ground motion parameter "*Z*" exceeds a specified value "*z*" in a time period "t" is given by:

$$p(Z > z) = 1\text{-}e^{-\nu(z)\bullet t} \quad (1)$$

where $\nu(z)$ is the annual mean number (or rate) of events in which *Z* exceeds *z*. It should be noted that the assumption of a Poisson process for the number of events is not critical. This is because the mean number of events in time t, $\nu(z)\bullet t$, can be shown to be a close upper bound on the probability $p(Z > z)$ for small probabilities (less than 0.10) that generally are of interest for engineering applications. The annual mean number of events is obtained by summing the contributions from all sources, that is:

$$\nu(z) = \sum_{n} \nu_n(z) \quad (2)$$

where $\nu_n(z)$ is the annual mean number (or rate) of events on source n for which *Z* exceeds *z* at the site. The parameter $\nu_n(z)$ is given by the expression:

$$\nu_n(z) = \sum_{i}\sum_{j} ß_n(m_i) \bullet p(R=r_j|m_i) \bullet p(Z>z|m_i,r_j) \quad (3)$$

where:

$ß_n(m_i)$ = annual mean rate of recurrence of earthquakes of magnitude increment m_i on source n;

$p(R=r_j|m_i)$ = probability that given the occurrence of an earthquake of magnitude m_i on source n, r_j is the closest distance increment from the rupture surface to the site;

$p(Z > z|m_i,r_j)$ = probability that given an earthquake of magnitude m_i at a distance of r_j, the ground motion exceeds the specified level *z*.

The calculations were made using the computer program HAZ38 developed by Norm Abrahamson (PG&E). This program has been validated in the Pacific Earthquake Engineering Research (PEER) Center-sponsored "Validation of PSHA Computer Programs" Project (Thomas *et al.*, 2010).

5.1 SEISMIC SOURCE CHARACTERIZATION

Two types of earthquake sources are characterized in this seismic hazard analysis: (1) fault sources; and (2) areal source zones. Fault sources are modeled as three-dimensional fault

surfaces and details of their behavior are incorporated into the source characterization. Areal source zones are regions where earthquakes are assumed to occur randomly. Seismic sources are modeled in the hazard analysis in terms of geometry and earthquake recurrence.

The geometric source parameters for faults include fault location, segmentation model, dip, and thickness of the seismogenic zone. The recurrence parameters include recurrence model, recurrence rate (slip rate or average recurrence interval for the maximum event), slope of the recurrence curve (*b*-value), and maximum magnitude. Clearly, the geometry and recurrence are not totally independent. For example, if a fault is modeled with several small segments instead of large segments, the maximum magnitude is lower, and a given slip rate requires many more small earthquakes to accommodate a cumulative seismic moment. For areal source zones, only the areas, maximum magnitude, and recurrence parameters (based on the historical earthquake record) need to be defined.

Uncertainties in the seismic source parameters as described below, which are sometimes large, were incorporated into the probabilistic seismic hazard analysis using a logic tree approach (Figure 8). In this procedure, values of the source parameters are represented by the branches of logic trees with weights that define the distribution of values. A sample logic tree for a fault is shown in Figure 8. In general, three values for each parameter were weighted and used in the analysis. Statistical analyses by Keefer and Bodily (1983) indicate that a three-point distribution of 5th, 50th, and 95th percentiles weighted 0.185, 0.63, and 0.185 (rounded to 0.2, 0.6, and 0.2), respectively, is the best discrete approximation of a continuous distribution. Alternatively, they found that the 10th, 50th, and 90th percentiles weighted 0.3, 0.4, and 0.3, respectively, can be used when limited available data make it difficult to determine the extreme tails (i.e., the 5th and 95th percentiles) of a distribution. Note that the weights associated with the percentiles are not equivalent to probabilities for these values, but rather are weights assigned to define the distribution. We generally applied these guidelines in developing distributions for seismic source parameters with continuous distributions (e.g., M_{max}, fault dip, slip rate or recurrence) unless the available data suggested otherwise. Estimating the 5th, 95th, or even 50th percentiles is typically challenging and involves subjective judgment given limited available data.

5.1.1 Source Geometry

In a PSHA, it is assumed that earthquakes of a certain magnitude may occur randomly along the length of a given fault or segment. The distance from an earthquake to the site is dependent on the source geometry, the size and shape of the rupture on the fault plane, and the likelihood of the earthquake occurring at different points along the fault length. The distance to the fault is defined to be consistent with the specific attenuation relationship used to calculate the ground motions. The distance, therefore, is dependent on both the dip and depth of the fault plane, and a separate distance function is calculated for each geometry and attenuation relationship. The size and shape of the rupture on the fault plane are dependent on the magnitude of the earthquake; larger events rupture longer and wider portions of the fault plane. We modeled the rupture dimensions following the magnitude-rupture area and rupture width relationships of Wells and Coppersmith (1994).

Volcanic earthquakes are assumed to occur randomly with no preference for strike and dip, and only within a cylindrical source volume centered on the volcanic edifice. Volcano-tectonic

events are assumed to occur randomly along only the three fault zones that transect Newberry Volcano.

5.1.2 Earthquake Recurrence

Recurrence relationships for the earthquake sources are modeled using the truncated exponential Gutenberg-Richter, characteristic earthquake, and the maximum magnitude recurrence models. These models are weighted (Figure 8) to represent our judgment on their applicability to the sources. The truncated exponential recurrence relationship is assumed to be appropriate for the volcanic earthquake sources (eruption and volcano-tectonic) and the regional source zones.

The general approach of Molnar (1979) and Anderson (1979) is used to derive the recurrence for the truncated exponential model. The number of events exceeding a given magnitude, *N(m)*, for the truncated exponential relationship is

$$N(m) = \alpha(m^o)\frac{10^{-b(m-m^o)} - 10^{-b(m^u-m^o)}}{1 - 10^{-b(m^u-m^o)}} \quad (4)$$

where $\alpha(m^o)$ is the annual frequency of occurrence of earthquakes greater than the minimum magnitude, m^o; b is the Gutenberg-Richter parameter defining the slope of the recurrence curve; and m^u is the upper-bound magnitude event that can occur on the source. Typically, a m^o of **M** 5.0 is used for the hazard calculations because smaller events are not considered likely to produce ground motions with sufficient energy to damage well-designed structures. In this study, we have calculated the hazard at m^o of **M** 5.0 for the baseline hazard and **M** 4.0 when accounting for the EGS induced seismicity.

The numerical formula of Youngs and Coppersmith (1985) is used here for fault sources to model characteristic recurrence as described by Aki (1983) and Schwartz and Coppersmith (1984). In the characteristic model, the number of events exceeding a given magnitude is the sum of the characteristic events and the non-characteristic events. Characteristic events are distributed uniformly over ± 0.25 magnitude unit centered on the characteristic magnitude, and the remainder of the moment rate is distributed exponentially using the above equation with a maximum magnitude 0.25 lower than the characteristic magnitude (Youngs and Coppersmith, 1985).

The maximum magnitude model can be regarded as an extreme version of the characteristic model. We adopted the model proposed by Wesnousky (1986). In the maximum magnitude model, there is no exponential portion of the recurrence curve, i.e., events are modeled with a normal distribution about the characteristic magnitude, with a sigma of 0.25. The distribution is truncated at 0.5 units above the characteristic magnitude.

The recurrence rates for the fault sources are defined by either the slip rate or the average return time for the maximum or characteristic event and the recurrence *b*-value. The slip rate is used to calculate the moment rate on the fault using the following equation defining the seismic moment:

$$M_o = \mu A D \quad (5)$$

where M_o is the seismic moment, μ is the shear modulus, A is the area of the rupture plane, and D is the slip on the plane. Dividing both sides of the equation by time results in the moment rate as a function of slip rate:

$$M_o = \mu A S \quad (6)$$

where M_o is the moment rate and S is the slip rate. M_o has been related to moment magnitude, **M**, by Hanks and Kanamori (1979):

$$\mathbf{M} = 2/3 \log M_o - 10.7 \quad (7)$$

Using this relationship and the relative frequency of different magnitude events from the recurrence model, the slip rate can be used to estimate the absolute frequency of different magnitude events.

The average return time for the characteristic or maximum magnitude event defines the high magnitude (low likelihood) end of the recurrence curve. When combined with the relative frequency of different magnitude events from the recurrence model, the recurrence curve is established.

5.2 GROUND MOTION CHARACTERIZATION

To characterize the ground motions at a specified site as a result of the seismic sources considered in the PSHA, we used empirical ground motion prediction models for spectral accelerations. The relationships used in this study were selected on the basis of the appropriateness of the faulting type and site conditions for which they were developed (Figure 8).

The uncertainty in ground motion attenuation was included in the PSHA by using the log-normal distribution about the median values as defined by the standard error associated with each attenuation relationship. Three standard deviations about the median value were included in the analysis.

As required by Task 3, the probabilistic seismic hazard at selected locations (e.g., La Pine) is calculated for (1) the baseline conditions due to natural seismicity, in this case both tectonic and volcanic earthquakes, and (2) with the added effects of potential fluid injection-induced seismicity due to the EGS activities. The following section describes the characterization of the seismic sources considered in the PSHA and the empirical ground motion prediction models selected and used.

6.1 SEISMIC SOURCES

Seismic source characterization is concerned with three fundamental elements: (1) the identification of significant sources of earthquakes; (2) the maximum magnitude of these earthquakes; and (3) the rate at which they occur. All significant sources of earthquake ground shaking should be included in state-of-the-art PSHAs. Given the close proximity of the geothermal well site to Newberry Volcano, the seismic hazards from naturally-occurring volcano-tectonic earthquakes are also considered important in this analysis.

Thus three types of seismic sources were included: active seismotectonic faults including the Cascadia subduction zone (CSZ), active volcanoes and volcano-tectonic sources, and regional background source zones. An "active" fault or volcano must typically show recurrent movements or eruptions, respectively, within Holocene or latest Pleistocene time to be considered potentially seismogenic and thus included here. Regional seismic source zones account for potential random background earthquakes on structures that are buried or may be too small or too deep to rupture to the surface. Although the downdip edge of the CSZ megathrust rupture is more than 250 km away, its ability to generate relatively frequent great earthquakes (**M** 9) will result in some contribution to the hazard for sites in central Oregon. The specific parameters used in this analysis for these three types of seismic sources are discussed in the following sections.

6.1.1 Tectonic Earthquakes on Faults

A search for all known or suspected Quaternary faults within a 100-km radius from the Newberry Volcano was performed using mainly the maps from the USGS Quaternary Faults and Fold Database of the United States (http://earthquake.usgs.gov/regional/qfaults/) and available published reports and geologic maps. The compilation located 14 known or suspected late Quaternary fault zones located within a 100-km radius of the Project Area that could contribute to the ground motion hazard (Table 1; Figure 4). Each fault was characterized with a probability distribution for activity, fault geometry and rupture length, maximum magnitude, and slip rate on the basis of the results of several previous seismic hazard studies and regional investigations (e.g., Ake *et al.*, 2001, Geomatrix Consultants, 1995; Pezzopane, 1993, Hawkins *et al.*, 1988, Schapiro *et al.*, 2004). The following section describes the methodology used to characterize the crustal faults, and discusses the attributes of significant Quaternary fault zones in the region near Newberry Volcano.

Table 1 lists the earthquake source parameters and Figure 9 shows the location of the fault zone sources used as input to the hazard calculations. Table 1 is an inventory of all known and suspected active tectonic fault sources that potentially contribute to the probabilistic ground-shaking hazard because of their potential activity, rupture length, and proximity to the geothermal wells and sites nearby. Shorter, individual faults (< 10 km) were not included as

separate independent sources because they are accounted for by use of the areal background source.

The probability of activity, P(a) for each fault source is considered to be the likelihood that the structure is seismogenic and capable of generating an earthquake independently in the current neotectonic stress regime. Many factors were used in these determinations including: fault orientation with respect to the contemporary stress regime, fault geometry, relation to other seismogenic structures, relation to volcanoes and volcanic vents, age of youngest movement, rates of activity, geomorphic expression, amount of cumulative offset, and evidence for a non-tectonic origin. Generally, faults with definitive evidence of late Quaternary (post-middle Pleistocene) activity were assigned a P(a) of 1.0. Other faults were judged on an individual basis. Zones having any fault or splay that shows definitive evidence for repeated Quaternary activity were assigned a P(a) of 1.0 (Table 1). Exceptions include faults that may be secondary and dependent on other faults, faults or fault features that may have a non-seismogenic origin, and faults that may be too short (≤ 10 km) to independently generate significant earthquakes. The P(a) for faults and fissure zones that merge with Newberry Volcano was reduced to account for the probability that the high heat flow does not allow a brittle crust to be thick enough to produce moderate- to large-magnitude tectonic earthquakes, and that local extension and regional fault slip is partially aseismic and accommodated partially by dike intrusion. The P(a) values for all the faults range from 0.3 to 1.0 (Table 1).

The maximum magnitude earthquake for each fault was estimated from the maximum mapped fault length and the empirical relationship of Wells and Coppersmith (1994) between **M** and surface rupture length (SRL), for all fault types, where **M** = 1.16*log (SRL) + 5.08. The standard deviation in this determination is ± 0.3 magnitude units, which is taken to form the 2-sigma tails of the distribution. For some fault zones, two values of Mmax are used and weighted to account for the likelihood of shorter ruptures and smaller magnitude events on these broad zones of graben-type faults, which in places have a volcano-tectonic signature. To account for the probability of smaller magnitude earthquakes on certain "volcanic" faults, this study places a lower weight on the maximum rupture length and a higher weight on a preferred rupture length that is based on the length of the longest continuous fault (or vent alignment) and not the total length of the zone.

In the site region, almost all faults are dominantly normal-slip faults, but occur in zones, commonly associated with grabens, some with volcanic vents and vent alignments. The Holocene (Quaternary) rupture behavior of many of the faults in this region is poorly understood. Many of the regional fault zones can be projected along strike to connect with adjacent fault zones, however, available geologic maps indicate most faults are short and rarely rupture multiple fault segments. Actual fault behavior may be more complex than what is assumed in this analysis. For example, one reason fault displacement may not be expressed at the surface in this region is because the slip during a typical large magnitude (~**M** 7) earthquake is distributed onto more than one fault splay and may die out rapidly upwards on the numerous faults in these nested graben zones. Thus, for the hazard calculations, all faults are modeled as planar sources that extend the full depth of the seismogenic crust, which varies spatially in the study area. Probability distributions for the maximum seismogenic depth for fault and background earthquake sources (Tables 1 and 3) were assigned on the basis of the maximum depth of historical seismicity in that region, if available. In all rupture models, fault dip values are averaged over the total depth of the seismogenic crust.

Depending on the available data, the slip rate distributions relied on long-term (≤ 1.6 Ma) and short-term (≤ 130 ka) geological data. However, most faults have no specific data at all. Commonly, in this study, only one or two sites along a young, well-expressed fault scarp might provide slip rate or displacement-per-event or recurrence information. Only two or three faults in Table 1 have reliable data to calculate a Holocene or late Pleistocene slip rate. For a fault having little or no slip rate data, the distribution was commonly established by a comparison to other better-studied faults in the area, taking into account factors such as location of the zone, style of deformation, geomorphic expression, and age of youngest movement.

Most uncertainties in slip rates are based on geological constraints, dating, or measurement uncertainties, which commonly vary by factors of 2 to 3 from the average or preferred slip rate. Factors of 2 or 3 are not uncommon for geological uncertainties. The discrete probability distribution weights the preferred slip rate higher than the tails. In most cases, the two tails of the distributions commonly span an order of magnitude in slip rate, which we consider to form the 2-sigma or 95% confidence limits. For most of these faults, the slower slip rate estimate may be the most accurate, given they generally lack abundant evidence of repeated paleoearthquakes or multiple event scarps. If slip rates on the principal fault zones in this region were 2 or 3 times greater than the preferred estimates, we would likely see it expressed as more scarps or more relief in the topography. On the other hand, perhaps the +2-sigma slip rates can be considered to account, at least conceptually, for an incomplete record of the active faulting in the region (burial or erosion), or for a hypothetical rise in seismic moment rate, perhaps associated with regional stress triggering of events related to locking and unlocking of the CSZ, or with temporal clustering of earthquakes, as seen most commonly on longer, multi-segment fault zones. Thus, slip rate uncertainties that commonly span an order of magnitude (± 2-sigma) about the preferred value are taken here to be an appropriate approach for estimating uncertainty in slip rates for ground motion hazard analysis.

Earthquake recurrence for most fault sources is modeled with two recurrence models: the maximum magnitude and characteristic earthquake recurrence (Section 5.1.2). The characteristic model is preferred and weighted 0.6 and the maximum magnitude model is assigned a weight of 0.4. Volcanic and volcano-tectonic earthquake sources are modeled with the truncated exponential recurrence. Observations of historical seismicity and paleoseismic investigations suggest that characteristic behavior is more likely for individual faults, whereas a truncated exponential model seems to fit better the seismicity that occurs in zones (Schwartz and Coppersmith, 1984), including volcanic and volcano-tectonic events.

The most significant Quaternary faults in terms of seismic hazard to the areas of interest are summarized below. Table 1 includes a more detailed description of some of the regional Quaternary faults and tectonic earthquake source parameters.

Significant Faults

Late Pleistocene and Holocene fault activity in Oregon is concentrated along four regional through-going fault zones that trend approximately north-south across Oregon and appear to connect active faults in northern California and the Central Nevada seismic belt with those in southern Washington and the High Cascades (Pezzopane, 1993; Pezzopane and Weldon, 1993). Several of the crustal faults within the western two zones of Pezzopane (1993), the Cascade zone and the Central Oregon zone (not shown here), are potential seismic sources that could generate

a ground-shaking hazard to the EGS site on Newberry Volcano, and the towns of La Pine and Sunriver, Oregon (Figure 10). The Cascade zone, the westernmost zone in Oregon, begins near Mount Lassen in California and consists primarily of normal faults in the High Cascade graben. In the 100-km-radius study area, principal fault zones of the Cascade zone include the Chemult graben, the La Pine graben, the Southwest Newberry zone, the Northwest Rift, the Tumalo, the Sisters fault zone, and Warm Springs fault zone (Figure 9).

The Central Oregon zone, east of the Cascade zone, consists of several long, range-bounding normal and normal-oblique faults that form a regional zone that merges into the High Cascades along the Southeast Newberry fault zone at Newberry Volcano. This fault trend continues northwestward along the Northwest Rift zone, the Tumalo, and Sisters fault zones, and along graben faults towards Mount Hood and other faults towards Mount St Helens. The Southeast Newberry fault zone marks the volcano-tectonic transition from more-purely tectonic transtensional faulting to the south and southwest, in the northwestern Basin and Range Province, to more-purely volcanic at Newberry Volcano and into the Sisters Volcanoes and High Cascades. Young, voluminous fissure eruptions along the Northwest Rift zone indicate it is much more volcano-tectonically active than the Southwest Newberry or Southeast Newberry fault zones. All three of these fault zones are characterized as volcano-tectonic earthquakes sources in this hazard study.

The Southeast Newberry fault zone intersects the southeast flank of the volcano and likely is structurally connected or kinematically related to the Northwest Rift zone (Higgins, 1973; Pezzopane and Weldon, 1993), perhaps in a left-stepping *en echelon* style, with Newberry caldera in a pull-apart graben (e.g., Gutmanis, 1989). The Southwest Newberry fault zone is the third Quaternary fault zone to converge at Newberry Volcano and offset early Newberry lava flows. Several workers have suggested that the Chemult Graben (Walker Rim), Southwest Newberry faults, and the Northwest Rift-Tumalo-Sisters fault zones may be extensions of the same regional fault zone, partially buried under the Newberry shield (Higgins, 1973; Fitterman, 1988; MacLeod and Sherrod, 1988; Chitwood, 1990).

The Northwest Rift is a series of discontinuous, northwest-striking, *en echelon*, normal faults that offset late Pleistocene and early Holocene lava flows on the northern shield of Newberry Volcano. Peterson and Groh (1964) map the Rift Zone for 30 km length, from The Fissure at East Lake, within Newberry Caldera, to beyond Lava Butte, and they describe eight separate Holocene basaltic lava flows that have erupted from vents along the Rift Zone. Higgins and Waters (1967) describe several N-S and NW-striking faults exposed on the north and south walls of the caldera, one that may have as much as 122 to 183 m of stratigraphic throw. On the basis of vent alignments and topographic linears on both the north and southern shield of Newberry we speculate that the Rift Zone may continue southeastwards beneath the caldera as a stepover from The Fissure to the NW-trending vent alignment including the Interlake Obsidian Flow, the Pumice Cone Crater Obsidian Flow, and the Game Hut Obsidian Flow. Perhaps the Rift Zone steps west again to near the Big Obsidian Flow and faults that cross West Lake (Higgins and Waters, 1967). All these west steps are curving the zone to connect with the Southwest Newberry fault zone and Walker Rim faults to the south.

The alignment and spatial association of volcanic fissures and cinder cones along some zones suggests that certain faults may have a volcanic association (e.g., Geomatrix Consultants, 1995; Ake *et al*., 2001). The distinction between volcanic faulting and tectonic faulting is significant

because faults that slip as a result of dike intrusion may only be capable of generating a maximum magnitude earthquake of **M** 5.5 (e.g., Jackson, 1994). Therefore, it is important to try to distinguish the point where a tectonic fault that projects beneath a volcanic center becomes a "volcanic" fault associated with magma migration and dike intrusion (Ake *et al.*, 2001). Faults in the latter category include the Northwest Rift zone, and portions of the Southeast and Southwest Newberry fault zones in the vicinity of Newberry Volcano. However, Newberry is a hybrid between High Cascades and Basin and Range volcano-tectonics and seismo-tectonics, and not completely similar to the "volcanic rifting" within the Eastern Snake River Plains and associated magmatism and neotectonics related to hotspot migration at Yellowstone caldera. Newberry Volcano has bimodal volcanic chemistry and is located at the intersection of several regional fault zones in the backarc of Cascadia. This is a quite different seismotectonic setting than purely volcanic rifting and basaltic dike intrusions following a major hotspot as it melts into the edge of a craton.

The close proximity of the Northwest Rift with Newberry Crater and the spatial association of faults in this zone with aligned cinder cones and fissure vents have been interpreted to indicate that the Northwest Rift Zone is more closely associated with volcanic extension and dike emplacement rather than tectonic extension as slip along a dipping fault (Ake *et al*., 2001; Geomatrix Consultants, 1995). Yet, the relatively long (~30 km), straight, surface expression, the NW-strike, and potential connection to the Tumalo fault, are similar features that it shares with other active faults in the Central Oregon zone. The northern portion of the Rift zone connects with the Tumalo fault far north of Newberry Caldera, maybe beyond the influence of its volcanism. The Rift may have a volcanic association, but is also favorably oriented to accommodate slip within the current tectonic stress field, and it probably reaches to the base of the seismogenic crust even below the volcano. The Rift and Tumalo faults and La Pine graben faults serve to accommodate a significant portion of the regional strain associated with the Southeast and Southwest Newberry fault zones, which merge with the Brothers fault zone beneath Newberry Volcano (Pezzopane and Weldon, 1993).

This study uses a P(a) of 0.5 to account for the possibility the Northwest Rift structure is seismogenic and thus infer it is to some extent related to volcanic processes and thus may be partially aseismic. Perhaps also the La Pine graben faults, the Tumalo, and Sisters fault zones may in part be associated with magmatic extension and dike intrusion (Ake *et al.*, 2001). This study uses a P(a) of 1 for all the other faults near Newberry, simply because they serve to accommodate extension in the High Cascades graben and nearby Basin and Range province. However, to account for the likelihood these three nearby faults are to some extent related to volcanic processes and thus may be smaller in magnitude, this study places a lower weight on a maximum rupture length based on the length of the longest continuous fault in the zone, and not the total length of the zone (Table 1). A higher weight is placed on a preferred maximum magnitude of **M** 6.0 for volcano-tectonic earthquakes on the 3 faults near Newberry Volcano, as described in the next section.

6.1.2 Volcanic Earthquake Sources

Commonly, volcanic earthquakes occur in sequences that accompany the movement of magma at different depths. Thus, the tectonic setting of seismicity at volcanoes can be classified into sequences of eruption earthquakes and sequences of volcano-tectonic earthquakes, some of

which are not clearly associated with eruptions (Zobin, 2003). Eruption earthquakes hypothetically occur at the center of the volcano and during every major volcanic eruption. Volcano-tectonic (VT) earthquakes are associated with magma injection or withdrawal along fault zones in the proximity (~<10 to 20 km) of active volcanoes, including near the central eruption during caldera collapse and during flank vent and fissure eruptions. Many VT events are relatively deep for volcanic regions and thus are not expressed as movement along faults at the surface. Movement of magma and associated gas and fluids can serve to overpressure and load to failure the caldera faults, ring fracture systems, and, local tectonic faults, especially if they have accumulated strain and are situated favorably in the local and regional stress field (Zobin, 2003).

Given the close proximity of the EGS Demonstration to Newberry Caldera, the earthquake hazards posed by Newberry Volcano, like any other active volcano, are in part independent of regional tectonic slip accommodated on faults. Volcanic earthquakes are associated directly with dike intrusion and magma movement. Seismicity occurs during either injection or withdrawal, and commonly as earthquake swarms within a few kilometers of the edifice, vent, or caldera (Tilling *et al*., 1987; Lahr *et al*., 1994; Simkin and Siebert, 2002; Roman and Cashman, 2006). Many volcanoes and volcanic centers, do in fact display various unique geological, geophysical, or seismotectonic features that reflect the stress and strain fields and style of faulting in the region. Long Valley Caldera, Medicine Lake, and Mount St. Helens are just a few examples where regional dextral shear and extension (transtension) has been expressed in earthquake focal mechanisms beneath and in the vicinity of the volcanic centers (e.g., Prejean *et. al.*, 2006; Poland *et. al.*, 2006; Weaver *et. al.*, 1987). Newberry is probably similar given its setting where transtension in the Basin and Range Province merges with extension and magmatism in the High Cascade graben (Figure 4).

Four volcanic earthquake sources are used in this study to model the seismicity associated with the largest Holocene volcanoes in the 100-km area, these include Bachelor Butte, South Sister, and North (and Middle) Sister volcanoes in the Cascades, and Newberry Volcano (Table 2; Figure 10). These volcanoes were selected among the other numerous volcanic vents and vent alignments because of their recurrent Holocene eruption history and their assumed potential to generate much larger magnitude volcanic earthquakes than other vents and cinder cones in the area. In particular for Newberry, this volcanic earthquake source is inferred to account for events that might accompany slip on ring-fracture and intra-caldera faults mapped or inferred to be under the caldera (Figure 9).

In this study, eruption earthquakes and volcano-tectonic earthquakes are characterized for Newberry Volcano and the nearby fault zones, whereas only eruption earthquakes are characterized for the three other Cascade volcanoes within 100 km of the EGS well sites. Volcanic earthquake source parameters related to eruption sequences are characterized for the four volcanoes (Table 2). Three VT "fault" sources (Northwest Rift, Southwest Newberry, and Southeast Newberry fault zones) are inferred to have smaller preferred Mmax (**M** 6.0) and at most, maximum rupture lengths are assume equivalent to the lengths of the longest individual faults in the zone, rather than total length of the zone (Table 1). The VT model is preferred (0.7 weight) over the fault rupture model (0.3 weight).

On the basis of a literature review of volcanic seismicity (e.g., Jackson, 1994; Zobin, 2001, 2003), particularly at shield volcanoes and bimodal volcanic centers, earthquakes associated with

basalt dike-intrusion usually have small maximum magnitudes (~ **M** 5) because dike intrusion ruptures along the fault incrementally and at shallow depths (less than 4 to 7 km) where crustal rocks have lower strengths. However, some volcanic centers considered similar to Newberry, have experienced events as large as **M** 6 to 6.5, especially if they have a more complicated history or explosive chemistry, and if they have regional fault zones in the vicinity or that transect the volcanic center (e.g., Zobin, 2001; 2003). For the hazard calculations, the maximum volcanic earthquake for Newberry and Bachelor Butte is assumed to be **M** 6.0, and for the more complex and explosive Sisters stratovolcanoes the Mmax is **M** 6.5. These assumed Mmax may be considered conservative for eruption sequences, based on available empirical data (e.g., Zobin, 2003), yet are probably appropriate and accurate to use to model volcano-tectonic events in the conduit deeper (~ 10 to 20+ km) beneath the volcanic edifice.

By analogy and reference to historical volcanic seismicity patterns, most volcanic eruption events occur within approximately 5 to 10 km of the edifice, caldera or volcanic vent, whereas volcano-tectonic events occur as deep as 20 km and within a horizontal distance of ~10 km of the volcanic center (e.g., Walker, 1993; Zobin, 2003). Thus, in this study, a cylindrical source volume with a diameter of 10 km is assumed centered on the volcano. The source area is only to account for earthquakes within and beneath the volcano. By analog, most volcanic swarms occur in the upper few kilometers of the crust, although in several cases, seismicity begins at deeper levels. In this study, the volcanic earthquake sources are assumed to extend to 10 km in depth beneath the volcano. Thus, the source volume is shaped like a cylinder with diameter of 10 km and long axis of 10 km oriented vertically.

The recurrence rate of volcanic earthquakes is estimated from the history of volcanic eruptions, including major eruptive events as well as minor flows or pumice falls. Newberry Volcano, the closest volcano to the site, is a broad shield volcano built by thousands of eruptions. These began about 600,000 years ago and continued for several eruptive episodes over the past 10,000 years at as many as 25 vents on the flanks and summit (Sherrod *et al*., 1997). The most recent eruption 1,300 years ago produced the Big Obsidian Flow. The caldera has been the focus of Newberry's volcanic activity for at least the past 10,000 years, with as many as 4 to 6 major eruptions in 10 to 12 kyr (e.g., Higgins and Waters, 1967; Chitwood, 1990; Sherrod *et al*., 1997; Simkin and Siebert, 2002). Other eruptions during this time have occurred along Northwest Rift zone on the volcano's northwest shield and, to a lesser extent, the southwest and southeast flanks. Certainly, large eruptions are accompanied by moderate magnitude earthquakes near the caldera. Earthquakes that might accompany the flank eruptions, such as along the Northwest Rift, are accounted for by the background source and by assuming a volcano-tectonic source model where a portion of the slip is seismic.

The observation that many volcanoes have earthquake swarms that do not have eruptions, is the basis to estimate that volcanic earthquakes occur at minimum every eruption and in places occur much more frequent than every eruption. This analysis makes the assumption that volcanic earthquakes occur ~ 2 to 3 times more often than the eruption record (e.g., Zobin, 2001, 2003). Thus, basic averages of the number of eruptions per time were used to establish an estimate of the maximum (longer) recurrence rate, which was divided by 2.5 to estimate the preferred and minimum (shorter) recurrence rates (Table 2). For example, for Newberry Volcano, on the basis of having 4 major eruptions in 12 kyr (Sherrod *et al*., 1997; Simkin and Siebert, 2002), the average maximum eruption recurrence rate is once every 3 kyr (Table 1). Divide the maximum by ~2.5 provides the preferred average recurrence rate of ~1 kyr, and divide again provides a

minimum recurrence rate of ~0.5 kyrs. Similarly, taking 6 major eruptions in 10 kyr (e.g., Chitwood, 1990), is an average of 1 major eruption (earthquake) sequence every ~1.7 kyr; and thus, assuming 2 or 3 earthquake sequences for every major eruption, a Mmax event is assumed to occur on average every 0.5 to 0.6 kyrs. This is an example of how the recurrence rates were determined for the volcanic eruption earthquake sources. The maximum and minimum recurrence values commonly vary by a factor of approximately 5 to 6 (2-sigma range), which is taken to be an appropriate characterization of the uncertainties for the hazard calculations.

6.1.3 Newberry Background Earthquake Zone

The Newberry background earthquake zone (NBEZ) accounts for the hazard from background earthquakes that are associated with volcanic processes and with smaller buried faults beneath the young volcanic deposits in the area. The Holocene lava flows and pyroclastic deposits form a young volcanic carapace near Newberry that has buried fault and fissure zones beneath the shield. Also the NBEZ is assumed to account for the random occurrence of earthquake swarms related to fault fissure movements, dike intrusions, and magma emplacement, but without a recorded eruption.

In the Basin and Range Province and most of the western U.S., the maximum magnitude of earthquakes that do not produce surface rupture usually ranges from **M** 6 to 6.5, like in this study for those adjacent regions (Table 2). However, in the vicinity of Newberry Volcano, the high heat flow serves to elevate the brittle-ductile transition depth to 10 to 12 km, and locally as shallow as 7 km (Catchings and Mooney, 1988; Stanley *et al*., 1990), which is substantially shallower than that for the surrounding regions. The shallower seismogenic zone depth serves to limit the potential rupture source dimensions of earthquakes, which places limits on maximum magnitude. In this study, the NBEZ is assumed to have maximum seismogenic zone depth of 10 km and maximum background earthquake of **M** 5.5 ± 0.3. The relatively smaller maximum background earthquake used for the NBEZ source zone corresponds to the relatively high heat flow and shallower seismogenic depth near Newberry Volcano, and thus to a VT source model that uses relatively smaller Mmax on the three fault zones that intersect Newberry Volcano (Table 1, discussion above).

The NBEZ is assumed to have a P(a) 0.5 to account for the inferred potential aseismic character of volcanic and fault deformation in this area and for the probability that "typical" (tectonic and volcano-tectonic) background earthquakes in the region near Newberry may not be as common as in adjacent areas. Recurrence rates for NBEZ are based on the historical catalogue for the Southern Cascades region (Section 6.1.4) and the Long Valley Caldera. The latter is scaled down on the basis of comparisons of regional seismicity and strain rates. The model assumes that Long Valley caldera accommodates ~10 times more regional strain (extension, shear, or both) than Newberry Volcano, and that otherwise, the shape and slope (but the scaled a-value) of the recurrence curve from Long Valley earthquakes are analogous to what might be expected at Newberry during an eruption (earthquake) sequence like the 1980 Mammoth Lake sequence (i.e., Hill, 2006). Long Valley and Medicine Lake are considered the best seismotectonic analogs to Newberry insofar as they are located in similar tectonic settings in the western U.S., but they are in different stages of evolution, getting older to the south. Long Valley was chosen as an analog to Newberry simply because the 1980 sequence was recorded well and yet the earthquake sequence was not associated with an eruption. Thus, the pre-1980 record and seismicity before

and since then is a conservative analog for calculating recurrence statistics for a volcano-tectonic earthquake sequence and background seismicity at Newberry Volcano. Medicine Lake has not had a significant historical earthquake sequence like at Long Valley.

In the PSHA, we assign a weight of 0.95 that the NBEZ will have a rate similar to the Southern Cascades and a weight of 0.05 that the NBEZ could enter a seismic phase similar to the 1980 Mammoth Lakes earthquake sequences and reactivation.

6.1.4 Regional Seismic Source Zones

To account for the hazard from background crustal earthquakes that are not associated with known or mapped faults, regional seismic source zones were incorporated into the analyses. In most of the western U.S., the maximum magnitude of earthquakes not associated with known faults usually ranges from **M** 6 to 6.5. Repeated events larger than these magnitudes probably produce recognizable fault-or-fold related features at the earth's surface (e.g., Doser, 1985; dePolo, 1994).

Earthquake recurrence estimates in the site region are required in order to assess the hazard from background earthquakes. The region was divided into four seismic source zones, in part based on the tectonic model of Wells *et al.* (1998) (Figure 10): Southern Cascades, Oregon Block, Fold and Thrust Belt, and Northern Great Basin. The recurrence for the Long Valley Caldera discussed in Section 6.1.5 was also computed. Recurrence for the Oregon Block was adopted from Wong *et al.* (2000). The recurrence relationship for each seismic source zone was estimated using the maximum likelihood procedure developed by Weichert (1980) and the estimated completeness intervals for the region (Figures 11 to 14). Completeness intervals were estimated based on the history of settlement and the seismographic installation and operation in the region. Dependent events, such as aftershocks, foreshocks, and smaller events within an earthquake swarm, were also identified and removed from the catalogs using the technique developed by Youngs *et al.* (2000). The resulting mean recurrence relationship assumed the truncated exponential form of the Gutenberg-Richter relationship of $\log N = a - b\mathbf{M}$. The recurrence parameters with their standard deviations curves are summarized on Table 4. The standard errors only reflect the goodness-of-fit of the recurrence curves. Other sources of epistemic uncertainty, such as the definition of the boundaries of the regional source zones and magnitudes, are not included in these errors.

6.1.5 Cascadia Subduction Zone Megathrust

Considerable new and significant data and information has become available in the past decade on the megathrust. In particular, there is now convincing evidence that the most recent megathrust earthquake occurred in January 1700, and that it was about a **M** 9 in size, thus probably rupturing the full length of the CSZ (Satake *et al.*, 1996). Although the CSZ appears to be segmented in its southern half (Goldfinger *et al.*, 2010), we only considered full rupture events in our model because the hazard from the southern segments would be negligible in central Oregon. Three scenarios were considered for the eastern extent of the megathrust rupture based on the model of the subduction zone by Flück *et al.* (1997): (1) at the boundary between the locked and transition zones; (2) halfway into the transition zone; and (3) at the boundary between the transition and ductile zones. We believe these scenarios capture the range of

uncertainty presently known on the extent of the megathrust rupture (Wong and Silva, 2000). The recurrence of the megathrust earthquakes are characterized by recurrence intervals of 250, 450, and 650 years based on Goldfinger *et al.* (2010), weighted 0.3, 0.4, and 0.3, respectively. The characteristic and maximum magnitude recurrence model were considered for the megathrust and weighted 0.20 and 0.80, respectively, given the absence of any historical seismicity (**M** ≥ 5.0) along the megathrust with the possible exception of the 1992 **M** 7.2 Cape Mendocino earthquake.

The Wadati-Benioff zone within the CSZ was not incorporated into the PSHA because previous studies (e.g., Shapiro *et al.*, 2004) indicate it does not contribute to the hazard in central Oregon given the distance and low activity rate.

6.2 EGS INDUCED SEISMICITY

An EGS zone was defined as the area of 1 km radius centered on Well NGC 55-29 based on observations from other EGS sites (Section 2). Computing a future rate of seismicity for EGS at Newberry Volcano is not possible until future investigations have been performed including seismic monitoring. However, we can consider a range of rates from other geothermal areas and therefore we have used recurrence parameters for The Geysers since 1972 as an upper-bound rate in the PSHA. The b-value computed was 1.25 and we also included a + 0.2 uncertainty in the b-value to incorporate a large uncertainty in the recurrence rates (Figure 15).

The distribution of Mmax adopted for the EGS induced seismicity based on global analogs (Section 3) was estimated to be **M** 3.0, 3.5, and 4.0 weighted 0.4, 0.4, and 0.2 (Figure 8). The 0.2 weight assigned to the value of **M** 4.0 translates to the 95th percentile value. As will be demonstrated in Section 7, the EGS seismicity has an insignificant impact on the probabilistic hazard at the three locations where the hazard was computed.

6.3 GROUND MOTION PREDICTION MODELS

To characterize the attenuation of ground motions in the PSHA, we have used recently developed empirical attenuation relationships appropriate for tectonically active regions such as the western U.S. These new attenuation relationships were developed as part of the Next Generation of Attenuation (NGA) Project sponsored by the PEER Center Lifelines Program and have been published in the *Earthquake Spectra*. The NGA models have a substantially better scientific basis than previous relationships (e.g., Abrahamson and Silva, 1997) because they are developed through the efforts of five selected attenuation relationship developer teams working in a highly interactive process with other researchers who have: (a) developed an expanded and improved database of strong ground motion recordings and supporting information on the causative earthquakes, the source-to-site travel path characteristics, and the site and structure conditions at ground motion recording stations; (b) conducted research to provide improved understanding of the effects of various parameters and effects on ground motions that are used to constrain attenuation models; and (c) developed improved statistical methods to develop attenuation relationships including uncertainty quantification.

The relationships have benefited greatly from a large amount of new strong motion data from large earthquakes (**M** > 7) at close-in distances (< 25 km). Data include records from the 1999 **M** 7.6 Chi Chi, Taiwan; 1999 **M** 7.4 Kocaeli, Turkey; and 2002 **M** 7.9 Denali, Alaska

earthquakes. Review of the NGA relationships indicate that, in general, ground motions particularly at short-periods (e.g., peak acceleration) are significantly reduced particularly for very large magnitudes (**M** 7.5) compared to earlier relationships. The relationships by Chiou and Youngs (2008), Campbell and Bozorgnia (2008), Abrahamson and Silva (2008), and Boore and Atkinson (2008) were used in the PSHA for all crustal seismic sources (Figure 8). The relationships were weighted equally in the PSHA.

A critical input into the NGA models is V_S30, the average shear-wave velocity (V_S) in the top 30 m. No *in situ* near-surface V_S investigations have been performed in the Project Area. The PSHA was calculated at the injection well (NGC 55-29) and the two closest communities, La Pine and Sunriver. The site geology and V_S30 values at these three locations are described in Section 6.4.

Other input parameters include $Z_{2.5}$, the depth to the Vs of 2.5 km/sec (a proxy for basin effects), which is only used in one model, Campbell and Bozorgnia (2008). We have used the default value of 2.0 km as recommended by the authors in lieu of site-specific data. Other parameters such as depth to the top of rupture (zero for all surficial faults unless specified otherwise), dip angle, rupture width, and aspect ratio of each fault are specified or calculated within the PSHA code.

For the CSZ megathrust, the Youngs *et al.* (1997), Zhao *et al.* (2006), and Atkinson and Macias (2009) attenuation relationships were used with equal weights (Figure 8). The Zhao *et al.* (2006) model is based on Japanese strong motion data.

The above ground motion prediction models are for tectonic earthquakes of **M** ≥ 5.0. However, to estimate the hazard from smaller induced earthquakes in the Project Area, a ground motion prediction model is needed. Obviously, no such model exists for the Project Area and models appropriate for geothermally-induced seismicity have not been developed and published.

A model by Chiou *et al.* (2010) has been recently developed for tectonic earthquakes **M** 3.0 to 5.5 in California. They observed that the strong motion data from induced seismicity at The Geysers, California indicated lower than average amplitudes for the parameters they investigated and so they did not include The Geysers data in their model. We investigate this issue and have plotted the PGA values derived from ShakeMaps (Wald *et al.*, 1999) of Geysers events onto the Chiou *et al.* (2010) curves for **M** 3.5, 4.0, and 4.5 and a soil site condition (Figures 16 to 18). The events range from M_L 3.25 to 4.5 and were binned by 0.5 magnitude unit centered on the magnitude above. As can be seen, the stations within 10 km show PGA values significantly above the attenuation curves. Some of this exceedance may be due to local site effects since the close-in PGA values are from the Calpine strong motion sites in the communities of Anderson Springs and Cobb, California (Wong *et al.*, 2010). The values beyond 10 km are either within the 2 sigma curves or well below. Thus the Chiou *et al.* (2010) curves underestimate ground motions at short distances (< 10 km) and are conservative at longer distances (> 10 km). This result is not surprising given the shallow nature of fluid-injection induced seismicity compared to natural tectonic earthquakes and the highly attenuating crust in which they occur.

This comparison is for The Geysers and northern California and so the question arises how would ground motions from induced earthquakes near Newberry Volcano compare with The Geysers seismicity ground motions? It is possible, there may be differences due to different source parameters and crustal attenuation between the Project Area and The Geysers.

Obviously, we have no area-specific data so we are relying on analogs as is necessary in assessing potential EGS seismicity in the Project Area. We believe that in terms of seismic source parameters, the assumption that EGS seismicity in the Project Area will be similar to seismicity at The Geysers is reasonable. Induced earthquakes in different geothermal areas whether EGS-related or otherwise probably have similar seismic source parameters as tectonic earthquakes as has been observed in several studies (e.g., Fenton Hill, Section 2). In terms of crustal attenuation, we are only interested in distances out to 30 km because the ground motions, e.g., PGA are too small (< 0.001 g) to have any hazardous impact (Figures 16 to 18). Hence, we use the Chiou *et al.* (2010) model in our PSHA since it is the only model that is appropriate for **M** < 5.0 earthquakes. The differences noted above will be considered in evaluating the hazard results.

6.4 SITE GEOLOGY

The site geology is described for the three sites where the probabilistic hazard was computed. No site-specific V_S data are available for these sites to classify them.

6.4.1 La Pine

La Pine is in a basin between the Cascade Volcanic chain and Newberry Volcano in the Upper Deschutes River valley near the Little Deschutes River. The basin is filled with 250 m to ~1 km of Quaternary and Tertiary volcanic and sedimentary deposits (Walker and McLeod, 1991; Lite and Gannett, 2002). Hundreds of meters of fine-grained pyroclastic and glacial sediments are interbedded with lava and tuff deposits from Newberry Volcano and the Cascade Range. Thick sedimentary sequences occur with Mazama ash near the top and lacustrine sediments and glacial outwash gravels with tephra and lava flows. Walker and McLeod (1991) and Lite and Gannett (2002) map the units as Pleistocene to Holocene lacustrine and fluvial sedimentary deposits (Qs), but they contain thick Mazama ash, so they could map as Holocene Mazama pumice deposits (Qmp) in Cascade Range (Wang *et al.*, 1998). The depth to bedrock varies considerably in the area, from ~1 to 3 m on the pumice-mantled lava slopes, to a few tens of meters in the center of the basin and depressions on stream terraces. These units are probably the equivalent of National Earthquake Hazard Reduction Program (NEHRP) site class D (Table 5) for sites higher in elevation on the river terraces although many swampy saturated areas in the river flood plain fall into NEHRP E. Perhaps most sites in the Upper Deschutes River Valley could be characterized by NEHRP E, given the low-density volcanic ash, the thick young, alluvial and lacustrine sediments, and shallow water table. Based on this geologic site description, we adopted a V_S30 of 320 m/sec, an average value appropriate for NEHRP D (Table 5). NEHRP E sites will produce lower seismic hazard at higher ground motions because of nonlinear soil effects.

6.4.2 Sunriver

Sunriver is located downstream of La Pine, where the Upper Deschutes River Valley is constrained between the Cascade Range volcanic vents and flows and lava flows on the northwest shield of Newberry Volcano. Lava flows have periodically damned the river and helped fill the basin with lacustrine and fluvial sediments, through which the river has cut to leave numerous stream terraces. Sunriver is on the eastern edge of the alluvial valley and the

western shield of Newberry. Sunriver is mapped as Pleistocene to Holocene lacustrine and fluvial sedimentary deposits (Qs) and Pleistocene to Holocene basalt and basaltic andesite (Qb) by Walker and McLeod (1991) and Lite and Gannett (2002), but near the Deschutes River, some sites contain thick alluvial and fluvial gravel and basin lacustrine sediments. The bedrock units map to Holocene Youngest basalt (Qyb) of Wang *et al*. (1998). The sites closer to Newberry where lava flows are shallow in the section are probably NEHRP B to C and sites closer to or on the river flood plain are closer to NEHRP C to D. A V_S30 of 480 m/sec was adopted appropriate for NEHRP site class C (Table 5).

6.4.3 Well NGC 55-29

The geothermal wells are on the upper northwest flank of Newberry Volcano, near the caldera margin. The sites are mapped as Pleistocene pyroclastic flows (Qp) and Pleistocene to Holocene basalt and basaltic andesite (Qb), and likely correlate with Holocene Youngest basalt (Qyb) of Wang *et al*. (1998). Pyroclastic flow, pumice fall, and cinder deposits are interbedded with ignimbrites and lava flows, and Mazama ash mantles the surface except in swales and valleys where it has been washed away. At increasing depths, tuffaceous and pumiceous units are interbedded with thicker lava flows. The geothermal wells are in the flank of the volcano and are not associated with soft soils or saturated sediments. However, the pyroclastic deposits, which might vary considerably spatially, in thickness and composition, can reduce the average shear wave velocities. The sites can be classified as NEHRP B overall, given the shallow bedrock and lack of sediments or a deep soil profile. A V_S30 of 550 m/sec appropriate for basalt was adopted for input into the PSHA.

Several factors control the level and character of earthquake ground shaking. These factors are in general: (1) rupture dimensions, geometry, orientation, rupture type of the causative fault; (2) distance from the causative fault; (3) magnitude of the earthquake; (4) the rate of attenuation of the seismic waves along the propagation path from the source to site; and (5) site factors including the effects of near-surface geology particularly from soils and unconsolidated sediments. Other factors, which vary in their significance depending on specific conditions, include slip distribution along the fault, rupture directivity, footwall/hanging-wall effects, and the effects of crustal structure such as basin effects.

Several parameters may be used to characterize earthquake ground motions. The common parameters include: peak ground acceleration, velocity, and displacement; response spectral accelerations or velocities; duration; and time histories in acceleration, velocity, or displacement. In this analysis, we have estimated peak horizontal ground acceleration (PGA) and 0.3 and 1.0 sec horizontal spectral accelerations (SA).

PGAs can be roughly correlated to perceived shaking or MM intensity using the classification of Wald *et al.* (1999). They have classified the following levels of ground shaking.

PGA (g)	Perceived Shaking	MM Intensity
< 0.002	Not felt	I
0.002 – 0.014	Weak	II – III
0.014 – 0.039	Light	IV
0.039 – 0.092	Moderate	V
0.092 – 0.18	Strong	VI

Correlations between any single ground motion parameter and intensity are highly uncertain. The above relationship has been found to be not well correlated for The Geysers since it was developed based upon eight larger California earthquakes of **M** ≥ 5.8 (Wald *et al.*, 1999) that were tectonic events, which occur much deeper than the shallow Geysers earthquakes (Wong *et al.*, 2010). However, the model has found widespread use in the fluid-induced seismicity community.

The results of the PSHA are described below and they are compared with the USGS National Seismic Hazard Maps.

7.1 HAZARD RESULTS

The results of the PSHA for the three locations La Pine, Sunriver, and Well NGC 55-29 are presented in terms of ground motion as a function of annual exceedance probability (i.e., hazard curves). The annual exceedance probability is the reciprocal of the average return period. At the standard return periods of 475, 975, and 2,475 years (10%, 5%, and 2% exceedance in 50 years, respectively), the baseline hazard PGAs and 0.3 and 1.0 sec SAs without EGS induced seismicity based on the hazard curves are listed in Table 6. The complete hazard results are presented in the Appendix.

Figures 19 to 21, show in terms of hazard curves, which seismic sources contribute to the mean (total) hazard at the three locations. At La Pine and Sunriver, the PGA hazard is controlled by

background earthquakes in the Basin and Range Province (Figures 19 and 20). At Well NGC 55-29, the hazard is dominated by the Newberry Volcano source (Figure 21).

Next we included the potential EGS seismicity in the PSHA but we used a minimum magnitude of **M** 4.0 for the induced earthquakes even though **M** 5.0 is the generally accepted threshold for structural damage (Bommer *et al.*, 2001). **M** 5.0 was still used for the sources of natural earthquakes. As summarized in Table 6, there is basically no contribution to the probabilistic hazard at La Pine, Sunriver at Well NGC 55-29 from EGS seismicity. The relatively low rate of $\mathbf{M} \geq 4.0$ induced earthquakes and associated low ground motions result in no differences in the hazard when EGS events are included.

7.2 COMPARISON WITH NATIONAL HAZARD MAPS

In the 2008 version of the U.S. Geological Survey's National Hazard Maps, which are the basis for the U.S. building code, the International Building Code, Petersen *et al.* (2008) have estimated probabilistic ground motions for the U.S. for the annual exceedance probabilities of 2%, 5%, and 10% in 50 years (2,475, 975, and 475-year return periods, respectively). The USGS PGA values at La Pine, Sunriver, and NGC 55-29 for a firm rock (NEHRP B/C) site condition average only about 0.09 g for a return period of 2,475 years significantly lower than the values computed in this study (Table 6) because they do not include many of the local seismic sources that are typically addressed in a site-specific PSHA.

Figures 22 and 23 show the distribution of population and buildings in the Project Area based on the HAZUS (FEMA, 1997) default demographic database (2000 census) and default building stock inventory. As shown, the area in the vicinity of Well NGC 55-29 is largely unpopulated and the seismic risk exposure due to EGS seismicity is low. The results of the hazard analysis described in Section 7 indicate that there is no increase over the baseline probabilistic seismic hazard in the towns of La Pine and Sunriver as well as at NGC 55-29 due to EGS induced seismicity even though conservative ranges of rates were used in the PSHA. The two towns are too distant (> 10 km) for EGS seismicity to contribute to the hazard. Thus the seismic risk, even in terms of minor structural damage, to the residents of La Pine and Sunriver and local residents near Well NGC 55-29 is judged to be very low based on the results of this study.

This is not to be construed that potentially larger EGS earthquakes of **M** 3.0 and higher, should they occur, will not be felt in La Pine and Sunriver. It is highly possible they will be felt but not at damaging levels of ground motions (> 0.10 g) (Figures 16 to 18). Individual residents within 10 km of the project site will feel the larger events should they occur. The strength of shaking will depend on the size of the event, and distance to and site conditions at the location. However, the effects of induced seismicity will be more of a nuisance rather than a hazard to the vast majority of local residents because of the small size of the events and distance to centers of population.

Abrahamson, N.A. and Silva, W.J., 1997, Empirical response spectral attenuation relations for shallow crustal earthquakes: Seismological Research Letters, v. 68, p. 94-127.

Abrahamson, N.A. and Silva, W.J., 2008, Summary of the Abrahamson and Silva NGA ground motion relations. Earthquake Spectra, v. 24, p. 67-97.

Ake, J., LaForge, R., and Hawkins, F., 2001, Probabilistic seismic hazard analysis, Wickiup Dam, Deschutes project, central Oregon: U.S. Bureau of Reclamation Seismotectonic Report 2000-04.

Aki, K., 1983, Seismological evidence in support of the existence of "Characteristic Earthquakes": Earthquake Notes, v. 54, p. 60-61.

Albright, J.N. and Pearson, C.F., 1982, Acoustic emissions as a tool for hydraulic fracture locations: experience at the Fenton Hill hot dry rock site: SPE Journal, v. 22, p. 523-530.

Anderson, J.G., 1979, Estimating the seismicity from geological structure for seismic risk studies: Bulletin of the Seismological Society of America, v. 69, p. 135-158.

Atkinson, G.M. and Macias, M., 2009, Predicted ground motions for great interface earthquakes in the Cascadia subduction zone: Bulletin of the Seismological Society of America, (in press).

Bommer, J.J., Georgallides, G. Tromans, I.J., 2001, Is there a near field for small-to-moderate-magnitude earthquakes? Journal of Earthquake Engineering, v. 5, p. 395-423.

Boore, D.M., and Atkinson, G.M., 2008, Ground motion predictive equations for the average horizontal component of PGA, PGV, and 5% damped PSA at spectral periods between 0.01s to 10.0s: Earthquake Spectra, v. 24, p. 99-138.

Bott, J.D.J. and Wong, I.G., 1993, Historical earthquakes in and around Portland, Oregon, Oregon Geology, v. 55, p. 116-122.

Brown, D.W., 2009, Hot dry rock geothermal energy: important lessons from Fenton Hill: Proceedings, Thirty-Fourth Workshop on Geothermal Reservoir Engineering, Stanford University, Stanford, California.

Brune, J.N., 1970, Tectonic stress and the spectra of seismic shear waves from earthquakes, Journal of Geophysical Research, v. 75, p. 4997-5009.

Campbell, K.W. and Bozorgnia, Y., 2008, NGA ground motion model for the geometric mean horizontal component of PGA, PGV, PGD, and 5% damped linear elastic response spectra for periods ranging from 0.01 to 10s: Earthquake Spectra, v. 24, p. 139-171.

Catchings, R.D. and Mooney, W.D., 1988, Crustal structure of the Columbia Plateau: evaluation for continental rifting: Journal of Geophysical Research, v. 93, p. 459-474.

Chiou, B.S.J. and Youngs, R.R., 2008, An NGA model for the average horizontal component of peak ground motion and response spectra: Earthquake Spectra, v. 24, p. 173-215.

Chiou, B., Youngs, R., Abrahamson, N., and Addo, K., 2010, Ground-motion attenuation model for small-to-moderate shallow crustal earthquakes in California and its implications on regionalization of ground-motion prediction models: Earthquake Spectra (in press).

Chitwood, L.A., 1990, Newberry, Oregon, in Wood, C.A. and Kienle, J. (eds.) Volcanoes of North America. Cambridge University Press, p. 200-202.

Cook, N.G.W., 1976, Seismicity associated with mining: Engineering Geology, v. 10, p. 99-122.

Cornell, C.A., 1968, Engineering seismic risk analysis: Bulletin of the Seismological Society of America, v. 58, p. 1583-1606.

Couch, R., Thrasher, G., and Keeling, K., 1976, The Deschutes Valley earthquake of April 12, 1976, Oregon Department of Geology and Mineral Industries, Ore Bin, v. 38, p. 151-161.

Davenport Newberry Holdings LLC, 2010, Plan of exploration, operations plan and drilling program, Newberry Volcano EGS Demonstration Project.

Denlinger, R.P. and Bufe, C.G., 1982, Reservoir conditions related to induced seismicity at The Geysers steam reservoir, northern California: Bulletin of the Seismological Society of America, v. 72, p. 1317-1327.

dePolo, C.M., 1994, The maximum background earthquake for the Basin and Range Province, western North America: Bulletin of the Seismological Society of America, v. 84, p. 466-472.

Donnelly-Nolan, J.M., Grove, T.L., Lanphere, M.A., Champion, D.E., Ramsey, D.W., 2008, Eruptive history and tectonic setting of Medicine Lake volcano, a large rear-arc volcano in the southern Cascades: Journal of Volcanic Geothermal Research, v. 177, p. 313-328.

Doser, D.I., 1985, The 1983 Borah Peak, Idaho and 1959 Hebgen Lake, Montana earthquakes—Models for normal fault earthquakes in the Intermountain Seismic Belt, *in* R.S. Stein and R.C. Bucknam (eds.), Proceedings of Workshop XXVIII on the Borah Peak, Idaho, Earthquake: U.S. Geological Survey Open-File Report 85-290, p. 368-384.

Eberhart-Phillips, D. and Oppenheimer, D.H., 1984, Induced seismicity in The Geysers geothermal area, California: Journal of Geophysical Research, v. 89, p. 1191-1207.

Federal Emergency Management Agency (FEMA), 1997, Earthquake loss estimation methodology HAZUS 99 Technical Manual, prepared by National Institute of Building Sciences.

Fehler, M.C. and Phillips, W.S., 1991, Simultaneous inversion for Q and source parameters of microearthquakes accompanying hydraulic fracturing in granitic rock: Bulletin of the Seismological Society of America, v. 81, p. 553-575.

Fitterman, D.V., 1988, Overview of the structure and geothermal potential of Newberry Volcano, Oregon: Journal of Geophysical Research, v. 93, p. 10,059–10,066.

Flück, P., Hyndman, R.D., and Wang, K., 1997, Three-dimensional dislocation model for great earthquakes of the Cascadia subduction zone, Journal of Geophysical Research, v. 102, p. 20,539-20,550.

Foxall, B. and Turcotte, T., 1979, Seismological investigation of the Walla Walla/Milton-Freewater area [abs.]: Earthquake Notes, v. 50, p. 7.

Geomatrix Consultants, 1995, Seismic design mapping, state of Oregon: Report prepared for Oregon Department of Transportation, Proj. No. 2442.

Goldfinger, C., Nelson, C.H., Johnson, J.E., Morey, A.E., Gutiérrez-Pastor, J., Karabanov, E., Eriksson, A.T., Gràcia, E., Dunhill, G., Patton, J., Enkin, R., Dallimore, A., Vallier, T., and the Shipboard Scientific Parties, 2010. Turbidite event history: methods and implications for Holocene paleoseismicity of the Cascadia Subduction Zone, U.S. Geological Survey Professional Paper 1661-F (in press).

Greensfelder, R.W. for Parsons Engineering, 2003, Induced seismicity analysis, Santa Rosa Incremental Recycled Water Program: prepared for City of Santa Rosa.

Gutmanis, J.C., 1989, Wrench faults, pull-apart basins, and volcanism in central Oregon: A new tectonic model based on image interpretation: Geological Journal, v. 24, p.183–192.

Hanks, T.C. and Kanamori, H. 1979, A moment magnitude scale: Journal of Geophysical Research, v. 84, p. 2348-2350.

Hawkins, F.F., LaForge, R.C., and Gilbert, J.D., 1989, Seismotectonic study for Wickiup and Crane Prairie Dams, Deschutes Project, Oregon: U.S. Bureau of Reclamation Seismotectonic Report 89-2.

Hawkins, F.F., LaForge, R.C., Templeton, M., and Gilbert, J.D., 1988, Seismotectonic study for Arthur R. Bowman and Ochoco Dams, Crooked River Project, Oregon: U.S. Bureau of Reclamation Seismotectonic Report 88-10, 57 p.

Healy, J.H., Rubey, W.W., Griggs, D.T., and Raleigh, C.B., 1968, The Denver earthquakes: Science, v. 161, p. 1301-1310.

Hemphill-Haley, M., 2001, Letter summarizing PSHA Field Trip to Wickiup Reservoir, November, 1998; in Ake, J., LaForge, R., and Hawkins, F., 2001, Probabilistic seismic hazard analysis, Wickiup Dam, Deschutes project, central Oregon: U.S. Bureau of Reclamation Seismotectonic Report 2000-04.

Herrero-Bervera, E., Helsley, C.E., Sarna-Wojcicki, A.M., Lajoie, K.R., Meyer, C.E., McWilliams, M.O., Negrini, R.M., Turrin, B.D., Nolan, J.M.D., and Liddicoat, J.C., 1994, Age and correlation of a paleomagnetic episode in the western United States by 40Ar/39Ar dating and tephrochronology: The Jamaica, Blake, or a new polarity episode?, Journal of Geophysical Research, v. 99, p. 24,091–24,103.

Higgins, M.W., 1973, Petrology of Newberry Volcano, central Oregon: Geological Society of America Bulletin, v. 84, p. 455-488.

Higgins, M.W. and Waters, A.C., 1967, Newberry caldera, Oregon; a preliminary report: The Ore Bin, v. 29, p. 37-60.

Hildreth, W., 2007, Quaternary magmatism in the Cascades; geologic perspectives: U.S. Geological Survey Professional Paper 1744, 125 p.

Hill, D.P., 2006, Unrest in Long Valley Caldera, California, 1978–2004, in Troise, C., De Natale, G., and Kilburn, C.R.J. (eds.), Mechanisms of Activity and Unrest at Large Calderas. Geological Society, London, Special Publications, v. 269, p. 1–24.

Ito, H., Kaieda, H., Suzuki, K., Suenaga, H., Kiho, K., Shin, K., Kusunoki, K., Kitano, K., and Hori, Y., 2001, An overview of the Ogachi HDR project – verification of the reservoir evaluation methods using data from Well OGC-3: Geothermal Resources Council Transactions, v. 25, p. 173-176.

Ito, H. and Kitano, K., 2000, Fracture investigation of the granitic basement in the HDR Ogachi project, Japan: Proceedings, World Geothermal Congress, p. 3,743-3.747.

Jackson, S., 1994, Magnitudes of earthquakes associated with basaltic dike injection for use in INEL seismic hazards evaluations: EG&G informal report, EGG-EES-11375.

Kaieda, H., Sasaki, S., and Wyborn, D., 2010, Comparison of characteristics of micro-earthquakes observed during hydraulic stimulation operations in Ogachi, Hijiori and Cooper Basin HDR projects: Proceedings World Geothermal Congress 2010, Bali, Indonesia.

Keefer, D.I. and Bodily, S.E., 1983, Three-point approximations for continuous random variables: Management Science, v. 26, p. 595-609.

Lahr, J.C., Chouet, B.A., Stephens, C.D., Power, J.A., and Page, R.A., 1994, Earthquake classification, location, and error analysis in a volcanic environment: implications for the magmatic system of the 1989-1990 eruptions at Redoubt Volcano, Alaska: Journal of Volcanology and Geothermal Research, v. 62, p. 137-151.

Lawrence, R.D., 1976, Strike-slip faulting terminates the Basin and Range Province in Oregon: Geological Society of America Bulletin, v. 87, p. 846–850.

Leonard, M., 2010, Earthquake fault scaling: self-consistent relating of rupture length, width, average displacement, and moment release: Bulleting of the Seismological Society of America, v. 100, p. 1971-1988.

Lite, K.E. Jr. and Gannett, M.W., 2002, Geologic framework of the regional ground-water flow system in the Upper Deschutes Basin, Oregon: U.S. Geological Survey Water-Resources Investigations Report 02-4015, 44 p.

Lyon, E.W., Jr., 2001, Late Quaternary geochronology and recent faulting along the eastern margin of the Shukash basin, central Cascadia range, Oregon: Boise State University, unpublished M.S. thesis, 99 p.

MacLeod, N.S. and Sherrod, D.R., 1988, Geologic evidence for a magma chamber beneath Newberry volcano, Oregon: Journal of Geophysical Research, v. 93, p. 10,067-10,079.

MacLeod, N.S., and Sherrod, D.R., 1992, Reconnaissance geologic map of the west half of the Crescent 1° by 2° quadrangle, central Oregon: U.S. Geological Survey Miscellaneous Investigations Map I–2215, scale 1:250,000.

Magill, J. R., Wells, R. E., Simpson, R. W., and Cox, A. V., 1982, Post-12 m.y. rotation of southwest Washington: Journal of Geophysical Research, v. 87, p. 3761-3776.

Majer, E.L., Baria, R., and Stark, M., 2008, Protocol for induced seismicity associated with enhanced geothermal systems, in International Energy Agency-Geothermal Implementing Agreement, C. Bromley, W. Cumming, A. Jelacic, and L. Byback, 8 pp.

Majer, E.L., Baria, R., Stark, M., Oates, S., Bommer, J., Smith, B., and Asamuma, H., 2007, Induced seismcity associated with Enhanced Geothermal Systems: Geothermics, v. 26, p. 185-222.

McCaffrey, R., 1994, Global variability in subduction thrust zone-fore arc systems: Pure and Applied Geophysics, v. 142, p. 173-224.

McGarr, A., 1971, Violent deformation of rock near deep-level, tabular excavations – seismic events: Bulletin of the Seismological Society of America, v. 61, p. 1453-1466.

McGarr, A., 1976, Seismic moments and volume changes: Journal of Geophysical Research, v. 81, p. 1487.

Molnar, P., 1979, Earthquake recurrence intervals and plate tectonics: Bulletin of the Seismological Society of America, v. 69, p. 115-133.

Neumann, F., 1938, United States earthquakes 1936-1940: U.S. Coast and Geodetic Survey Serial No. 6510, p. 45.

Nicholson, C. and Wesson, R.L., 1990, Earthquake hazard associated with deep well injection: U.S. Geological Survey Bulletin, v. 1951, 74 p.

Oppenheimer, D.H., 1986, Extensional tectonics at The Geysers geothermal area, California: Journal of Geophysical Research, v. 91, p. 11,463-11,476.

Petersen, M.D., Frankel, A.D., Harmsen, S.C., Mueller, C.S., Haller, K.M., Wheeler, R.L., Wesson, R.L., Zeng, Y., Boyd, O.S., Perkins, D.M., Luco, N., Field, E.H., Wills, C.J., and Rukstales, K.S., 2008, Documentation for the 2008 update of the United States National Seismic Hazard Maps: U.S. Geological Survey Open-File Report 2008-1128, 61 p.

Peterson, N.V. and Groh, E.A., 1964, Crack-in-the-ground, Lake County, Oregon: The ORE BIN, v. 26, p. 158-167.

Peterson, N.V., Groh, E.A., Taylor, E.M., and Stensland, D.E., 1976, Geology and mineral resources of Deschutes County, Oregon: State of Oregon, Department of Geology and Mineral Industries Bulletin 89, 66 p., 4 pls.

Pezzopane, S.K., 1993, Active faults and earthquake ground motions in Oregon, Ph.D. Thesis, University of Oregon, 208 p.

Pezzopane, S.K. and Weldon, R.J., 1993, Tectonic role of active faulting in central Oregon, Tectonics, v. 12, p. 528-521.

Phillips, W.S., Rutledge, J.T., House, L.S., and Fehler, M.C., 2001, Induced microearthquake patterns in hydrocarbon and geothermal reservoirs: Review submitted to PAGEOPH, Los Alamos National Laboratory.

Pitts, S. and Couch, R., 1978, Complete Bouguer gravity anomaly map of the Cascade Mountain Range, central Oregon: Oregon Department of Geology and Mineral Industries Geologic Map Series GMS-8, 1 sheet.

Poland, M., Burgmann, R., Dzurisin, D., Lisowski, M., Masterlark, T., Owen, S., Fink, J., 2006, Constraints on the mechanism of long-term, steady subsidence at Medicine Lake volcano, northern California, from GPS, leveling, and InSAR: Journal of Volcanology and Geothermal Research, v. 150, p. 55-78.

Prejean, S., Ellsworth, W., Zoback, M., and Walhouser, F., 2002, Fault structure and kinematics of the Long Valley Caldera region, California, revealed by high-accuracy earthquake

hypocenters and focal mechanism stress inversion: Journal of Geophysical Research, v. 107, p. 2355.

Riddihough, R., 1984, Recent movements of the Juan de Fuca plate system, Journal of Geophysical Research, v. 89, p. 6980-6994.

Roman, D.C. and K.V., Cashman, 2006, The origin of volcano-tectonic earthquake swarms, Geology, v. 34, p. 457-460.

Satake, K. Shimazaki, K., Tsuji, Y., and Ueda, K., 1996, Time and size of a giant earthquake in Cascadia inferred from Japanese tsunami records of January 1700: Nature, v. 379, p. 246-249.

Shapiro, S.A., Dinske, C., and Kummerow, J., 2007, Probability of a given-magnitude earthquake induced by a fluid injection: Geophysical Research Letters, v. 34, p. L22314.

Shapiro, S.A., Dinske, C., Langebruch, C., and Wenzel, F., 2010, Seismogenic index and magnitude probability of earthquakes induced during reservoir fluid stimulations: The Leading Edge, Special Section: Microseismic, p. 304-309.

Schapiro, R., Dober, M., Nemser, E., and Wong, I., 2004, Screening/scoping level probabilistic seismic hazard analyses, Arthur R. Bowman and Ochoco Dams: unpublished report prepared for the U.S. Bureau of Reclamation.

Schwartz, D.P. and Coppersmith, K.J., 1984, Fault behavior and characteristic earthquakes–examples from the Wasatch and San Andreas fault zones: Journal of Geophysical Research, v. 89, p. 5681-5698.

Scott, W.E., Iverson, R.M., Schilling, S.P., and Fischer, B.J., 2001, Volcano hazards in the Three Sisters Region, Oregon: U.S. Geological Survey Open-File Report 99-437, 14p.

Sherrod, D.R., Mastin, L.G., Scott, W.E., and Schilling, S.P., 1997, Volcano hazards at Newberry Volcano, Oregon: U.S. Geological Survey Open-File Report 97-513.

Sherrod, D.R. and Smith, J.G., 2000, Geologic map of upper Eocene to Holocene volcanic and related rocks of the Cascade Range, Oregon: U.S. Geological Survey Geologic Investigations Map I–2569, scale 1:500,000.

Sherrod, D.R., Taylor, E.M., Ferns, M.L., Scott, W.E., Conrey, R.M., and Smith, G.A., 2004, Geologic map of the bend 30- 60- Minute Quadrangle, Central Oregon: U.S. Geological Survey Geologic Investigations Series I-2683, 48 p.

Simkin T. and Siebert, L., 2002, Global Volcanism FAQs. Smithsonian Institution, Global Volcanism Program Digital Information Series, GVP-5.

Simpson, D.W., 1976, Seismicity changes associated with reservoir loading: Engineering Geology, v. 10, p. 12-150.

Stanley, W.D., Mooney, W.D., and Fuis, G.S., 1990, Deep crustal structure of the Cascade Range and surrounding regions from seismic refraction and magnetotelluric Data, Journal of Geophysical Research, v. 95, p. 19,419–19,438.

Stark, M.A., 1990, Imaging injected water in The Geysers reservoir using microearthquake data: Geothermal Resources Council Transactions, v. 14, p. 1697-1704.

Stover, C.W. and Coffman, J.L., 1993, Seismicity of the United States, 1568-1989 (Revised): U.S. Geological Survey Professional Paper 1527, 415 p.

Thomas, P.A., Wong, I.G., and Abrahamson, N., 2010, Verification of probabilistic seismic hazard analysis software programs: PEER Report 2010/106, Pacific Earthquake Engineering Research Center, Report 2010/10, 173 p.

Tilling et al., 1987, Eruptions of Hawaiian volcanoes: past, present, and future: USGS General Interest Publication.

Toppozada, T.R., 1975, Earthquake magnitude as a function of intensity data in California and western Nevada: Bulletin of the Seismological Society of America, v. 61, p.1223-1238.

Unruh, J.R., Wong, I.G., Bott, J.D.J., Silva, W.J., and Lettis, W.R., 1994, Seismotectonic Evaluation: Scoggins Dam, Tualatin Project, Northwestern Oregon; William Lettis & Associates and Woodward-Clyde Federal Services, unpublished final report prepared for the U.S. Bureau of Reclamation, Denver, CO.

U.S. Geological Survey, 2009, Cascades Volcano Observatory - Volcanic Hazards Assessment Reports and Maps Online Database [http://vulcan.wr.usgs.gov/Publications/ hazards_reports.html].

Wald, D.J., Quitoriano, V., Heaton, T.H., and Kanomori, H., 1999, Relationships between peak ground acceleration, peak ground velocity, and Modified Mercalli intensity in California: Earthquake Spectra, v. 15, p. 557-564.

Walker, G.P.L., 1993, Basaltic-volcano systems, in Magmatic Processes and Plate Tectonics, Geological Society Special Publication, v. 76, p. 3–38.

Walker, G.W. and MacLeod, N.S., 1991, Geologic map of Oregon: U.S. Geological Survey, scale 1:500,000.

Wang, Y., Weldon, R., and Fletcher, D., 1998, Creating a map of Oregon UBC soils: Oregon Geology, v. 60, p. 75-80.

Weaver, C.S., Grant, W.C., and Shemeta, J.E., 1987, Local crustal extension at Mount St. Helens, Washington, Journal of Geophysical Research, v. 92, p. 10,170–10,178.

Weichert, D.H., 1980, Estimation of the earthquake recurrence parameters for unequal observation periods for different magnitudes: Bulletin of the Seismological Society of America, v. 70, p. 1337-1346.

Weldon, R.J., II, Fletcher, D.K., Weldon, E.M., Scharer, K.M., and McCrory, P.A., 2003, An update of Quaternary faults of central and eastern Oregon: U.S. Geological Survey Open-File Report 02-301, 1 CD-ROM.

Wells, D.L. and Coppersmith, K.J., 1994, New empirical relationships among magnitude, rupture length, rupture width, rupture area, and surface displacement: Bulletin of the Seismological Society of America, v. 84, p. 974-1002.

Wells, R.E., Weaver, C.S., and Blakely, R.J., 1998, Forearc migration in Cascadia and its neotectonic significance: Geology, v. 26, p. 759-762.

Wesnousky, S.G., 1986, Earthquakes, Quaternary faults, and seismic hazard in California: Journal Geophysical Research, v. 91, p. 12,587-12,631.

Wong, I.G., 1993, The role of geologic discontinuities and tectonic stresses in mine seismicity (Chpt. 15), in Comprehensive Rock Engineering, Principles, Practice and Projects, v. 5, Surface and Underground Project Case Histories, J.A. Hudson and E. Hoek (eds.), Pergamon Press, p. 393-410.

Wong, I.G. and Bott, J.D.J., 1995, A look back at Oregon's earthquake history, 1841-1994: Oregon Geology, v. 57, p. 125-139.

Wong, I.G., Dober, M., Hemphill-Haley, M., and Schapiro, R., 2002, Probabilistic seismic hazard analyses Owyhee Dam, Owyhee Project, Eastern Oregon and Mann Creek Dam, Mann Creek Project, Western Idaho: unpublished report prepared for the U.S. Bureau of Reclamation.

Wong, I.G. and McGarr, A., 1990, Implosional failure in mining-induced seismicity: A critical review, in Rockbursts and Seismicity in Mines, Proceedings of the Second International Symposium, C. Fairhurst (ed.), A.A. Balkema Publishers, p. 45-51.

Wong, I.G., Voos, K., Kulkarni, R., and Lawton, G., 1991, An updated probabilistic approach for evaluating reservoir-induced seismicity (abs.): Seismological Research Letters, v. 62, p. 36.

Wong, I.G. and Silva, W.J., 2000, Predicting great earthquake ground shaking in the Pacific Northwest from the Cascadia subduction zone (abs.): Penrose Conference 2000, Great Cascadia Earthquake Tricentennial, Program Summary and Abstracts, Oregon Department of Geology and Mineral Industries Special Paper 33, p. 141-143.

Wong, I., Silva, W., Bott, J., Wright, D., Thomas, P., Gregor, N., Li, S., Mabey, M., Sojourner, A., and Wang, Y., 2000, Earthquake scenario and probabilistic ground shaking maps for the Portland, Oregon, metropolitan area, Oregon Department of Geology and Mineral Industries Interpretive Map Series IMS-16, scale 1:62,500, 11 sheets with 16 p. text.

Wong, I., Terra, F., Zachariasen, J., and Lowenthal-Savy, D., 2010, Evaluation of the environmental impacts of induced seismicity at the Calpine proposed Wildhorse Power Plant Project, The Geysers, California: unpublished report submitted to Calpine Corporation.

Wood and Kienle, 1990, Volcanoes of North America: United States and Canada: Cambridge University Press, 354, p.185-187

Woodward-Clyde Consultants, 1980, Evaluation of the potential for resolving the geologic and seismic issues at Humboldt Bay Power Plant Unit Number 3, Appendices A, B and C: Technical report to Pacific Gas and Electric Company.

Youngs, R.R., Chiou, S.-J, Silva, W.J., Humphrey, J.R., 1997, Strong ground motion attenuation relationships for subduction zone earthquakes: Seismological Research Letters, v. 68, p. 58-73.

Youngs, R.R. and Coppersmith, K.J., 1985, Implications of fault slip rates and earthquake recurrence models to probabilistic seismic hazard estimates: Bulletin of the Seismological Society of America, v. 75, p. 939-964.

Youngs, R.R., Swan, F.H., Power, M.S., Schwartz, D.P., and Green, R.K., 2000, Probabilistic analysis of earthquake ground shaking hazard along the Wasatch Front, Utah, *in* P.L. Gori and W.W. Hays (eds.), Assessment of Regional Earthquake Hazards and Risk Along the Wasatch Front, Utah: U.S. Geological Survey Professional Paper 1500-K-R, p. M1-M74.

Zhao, J.X., Zhang, J., Asano, A., Ohno, Y., Oouchi, T., Takahashi, T., Ogawa, H., Irikura, K., Thio, H.K., Somerville, P.G., Fukushima,Y., and Fukushima, Y., 2006, Attenuation relations of strong ground motion in Japan using site classification based on predominant period: Bulletin of the Seismological Society of America, v. 96, p. 898-913.

Zoback, M.D. and Zoback, M.L., 1989, Tectonic stress field of the continental United States, *in* Pakiser, L.C. and Mooney, W.D (eds.), Geophysical Framework of the Continental United States: Geological Society of America Memoir 172, p. 523-541.

Zobin, V.M., 2001, Seismic hazard of volcanic activity: Journal of Volcanology Geothermal Research, v. 112, p. 1-14.

Zobin, V.M., 2003, Introduction to volcanic seismology: Elsevier, Amsterdam, 304 pp.

Table 1. Fault Parameters

Fault[1]	P(a)[2]	Style[3]	Rupture Length[4] (km)	Mmax (M)[5]	Fault Dip	Slip Rate (mm/yr)	Seismogenic Depth (km)	Approximate Distance to Well (km)	Data Sources	Comments
La Pine Graben Faults	1.0	N	30 (0.5) 42 (0.5)	6.8 7.0	70° W (0.4) 90° (0.4) 70° E (0.2)	0.01 (0.2) 0.1 (0.6) 0.3 (0.2)	7 (0.2) 12 (0.6) 15 (0.2)	28.5	Pitts and Couch, 1978; Hawkins *et al*., 1989; Lyon, 2001; Ake *et al*., 2001; Geomatrix Consultants 1995; MacLeod and Sherrod, 1992; Pezzopane 1993	The La Pine graben faults include mostly buried, composite graben structures located between Newberry Volcano and the High Cascades (Hawkins *et al*., 1988; MacLeod and Sherrod, 1992; Pezzopane, 1993; Geomatrix Consultants, 1995; Ake *et al*., 2001). The Deschutes River and numerous glacial lakes have filled the basins west of La Pine with ~250 m to ~1 km of mostly Quaternary glacial outwash and pyroclastic sediments from the High Cascade and Newberry volcanoes (Pitts and Couch, 1978; Ake *et al*., 2001; Lyon, 2001). The basin is bisected by a NNW-trending horst coincident with a chain of aligned volcanic vents (Gilchrist, Wampus, and Pringle Buttes) that have built upon the basin fill. Ake *et al*., 2001 discuss how eruptions from Newberry along the Northwest Rift at times dammed the Deschutes River, and they pose whether the basin may be a result of volcanic extrusion and basin subsidence rather than tectonic faulting. Ake *et al.* (2001) and Lyon (2001) discuss the Wampus fault zone and Dilman Meadows fault, which are considered in this study to be the surface expression of active faults in the La Pine graben zone. Dilman Meadows fault offsets the Pringle Falls tephra layer (218 ± 10 ka, Herrero-Bervera *et al*., 1994), middle Pleistocene lacustrine units, last-glacial-maximum outwash deposits, several younger fluvial (outwash?) terraces, and deposits containing the 7.6 ka Mazama ash (Lyon, 2001). Dilman Meadows fault dips east, antithetic to Wampus fault zone that dips west to vertical, according to geological and geophysical interpretations (Pitts and Couch, 1978; Ake *et al*., 2001). Gravity data (Pitts and Couch, 1978) define a subsurface fault zone at least 30 km in length. Surface expression of the Wampus fault is mapped for 15 km, whereas volcanic vent and fault alignments, and the regional basin trend and topography imply the Wampus and Dilman Meadow faults are probably part of a longer (~42 km) structural zone of nested grabens and en echelon step-over faults.
Northwest Rift Zone (southern section of the Metolius fault zone)	0.5	N	VT[3] (0.7) 10 (0.3)	6.0 6.2	70° W (0.2) 90° (0.6) 70° E (0.2)	0.01 (0.2) 0.1 (0.6) 0.2 (0.2)	7 (0.4) 10 (0.4) 12 (0.2)	7.0	Ake *et al*. (2001); Geomatrix Consultants (1995); Hawkins *et al*. (1988)	The Northwest Rift is a series of discontinuous, NW-striking, right-stepping, en echelon, normal faults that offset late Pleistocene and early Holocene lava flows on the northern shield of Newberry Volcano. It is the southern section of the Metolius fault zone. Hawkins *et al*. (1988) interpreted fault scarps that are 2 to 25 m in height in Pleistocene lava flows (~300 – 400 ka) including the Shevlin Park Tuff (~170 ka). The most recent fault activity was likely pre-Holocene (>6.6 to 7.3 ka) based on the age of unfaulted lava flows. Peterson and Groh (1964) map the Rift Zone for 30 km length, from The Fissure at East Lake, within Newberry Caldera, to beyond Lava Butte, and they describe eight separate Holocene basaltic lava flows that have erupted from vents along the Rift Zone. Higgins and Waters (1967) describe several N-S and NW-striking faults exposed on the north and south walls of the caldera, one with as much as 400 to 600 feet of stratigraphic throw. On the basis of vent alignments and topographic linears on both the north and southern shield of Newberry we speculate that the Rift Zone may continue southeastwards beneath the caldera as a west stepover from The Fissure to the NW-trending vent alignment including the Interlake Obsidian Flow, the Pumice Cone Crater Obsidian Flow, and the Game Hut Obsidian Flow. Perhaps the Rift Zone steps west again to near the Big Obsidian Flow and faults that cross West Lake (Higgins and Waters, 1967). The close proximity of the Northwest Rift with Newberry Crater and the spatial association of faults in this zone with aligned cinder cones and fissure vents have been interpreted to indicate that the Rift Zone is more closely associated with volcanic extension and dike emplacement rather than tectonic extension as slip along a dipping fault (Ake *et al*., 2001; Geomatrix Consultants, 1995). Yet, the relatively long (~30 km), straight, surface expression and the NW-strike are similar to other active faults in Central Oregon, and the northern portion is far north of Newberry Caldera, probably beyond the influence of its volcanism. The Rift probably accommodates some portion of the regional strain associated with the Southeast and Southwest Newberry fault zones, which merge with the Brothers fault zone beneath Newberry Volcano (Pezzopane and Weldon, 1993). P(a) of 0.5 accounts for the possibility this fault structure is more often than not related to volcanic processes and thus may be partially aseismic. Maximum rupture length (10 km), given a VT earthquake source model, is estimated from the lengths of the longest individual faults in the zone (rather than total length of the zone). VT earthquakes are modeled to occur randomly along the zone because rupture of these smaller magnitude events (~M 6.0), theoretically does not encompass the rupture area inferred from maximum fault length and downdip seismogenic width.
Tumalo Fault (central section of the Metolius fault zone)	1.0	N	32 (0.7) 45 (0.3)	6.8 7.0	70° W (0.6) 90° (0.4)	0.01 (0.2) 0.1 (0.6) 0.3 (0.2)	7 (0.2) 12 (0.6) 15 (0.2)	26.4	Ake *et al*. (2001); Geomatrix Consultants (1995) Hawkins *et al.* (1988); Hemphill-Haley (2001)	Normal fault that forms the central section of the Metolius fault zone (94 km length; Hawkins *et al*.,1988) and the western margin of the Sisters fault zone. Differentiated from the Sisters zone on the basis of having a more-continuous scarp, evidence for repeated late- Pleistocene events and greater cumulative displacements. Prominent fault scarps are as much as 70 m high in Miocene-Pliocene volcanic rocks, 2- to 10-m-high scarps in middle Pleistocene ash-flow tuffs and lavas (Hawkins *et al*., 1988; Hemphill-Haley, 2001; Sherrod *et al.*, 2004), and in places have been mapped as faulting glacial outwash (Peterson *et al*., 1976). In a quarry, the Tumalo fault displaces the Bend Pumice (~300-400 ka) and overlying gravels (~100-140 ka) (Ake *et al*., 2001; Hawkins *et al*., 1988). Cumulative displacement on the overlying deposits (~ 5 m) exceeds the displacement that could result from a single earthquake, which led Ake *et al*. (2001) to conjecture that multiple surface rupture events were accountable.
Green Ridge - Tumalo Fault Zone (northern and central section of the Metolius fault zone)	0.2	N	29 (0.7) 81 (0.3)	6.8 7.3	70° W (0.6) 90° (0.4)	0.01 (0.2) 0.1 (0.6) 0.3 (0.2)	7 (0.2) 12 (0.6) 15 (0.2)	26.4	Geomatrix Consultants (1995) Hawkins *et al.* (1988)	Green Ridge is prominent ~700 m escarpment in Miocene volcanic rocks that forms the eastern margin of the High Cascades, and the northern section of the Metolius fault zone (Hawkins *et al*.,1988), north of the Tumalo fault and Sisters fault zone. Tonal and topographic linears across late Quaternary slope and fan deposits and the relatively large vertical displacements on early and middle Quaternary volcanic deposits suggests Quaternary fault activity on Green Ridge. However, evidence is weak, and surface expression, although prominent, may not be as youthful as other faults like Tumalo, Sisters, and Northwest Rift zones. Rupture length of 81 km is a Mmax model that assumes rupture of Green Ridge and Tumalo fault zones, the central and northern Metolius fault zone. P(a) of 0.2 accounts for the possibility that Green Ridge and Tumalo fault zones could rupture together in a Mw 7.3 earthquake. Complete rupture (~105 km) including along the southern Metolius zone, Northwest Rift, is not modeled in this study.

Table 1. Fault Parameters

Fault[1]	P(a)[2]	Style[3]	Rupture Length[4] (km)	Mmax (M)[5]	Fault Dip	Slip Rate (mm/yr)	Seismogenic Depth (km)	Approximate Distance to Well (km)	Data Sources	Comments
Sisters Fault Zone	1.0	N/NO	30 (0.7) 55 (0.3)	6.8 7.1	70° W (0.2) 90° (0.6) 70° E (0.2)	0.01 (0.2) 0.05 (0.6) 0.1 (0.2)	7 (0.2) 12 (0.6) 15 (0.2)	26.5	Ake *et al*. (2001); Geomatrix Consultants (1995); Hawkins *et al*. (1988)	Sisters is a broad zone (6 to 13 km in width) of short (< 15 km) NNW-striking normal faults that form the eastern margin of the High Cascades, from southeast of Bend to east of the town of Sisters. Sense of displacement is down-to-the-east and down-to-the-west with scarps from a few meters to several tens of meters in height in late Teriary basalts, and lower scarps in Quaternary gravels (Ake *et al*., 2001). Hemphill-Haley (2001) identified scarps in Pleistocene gravels, and trenched across fault strands near Rudi Road, north of Tumalo. Trench exposures evidence at least two paleoevents, each with as much as 1 m vertical displacement in outwash gravels estimated to be ~<100 ka (Hemphill-Haley (2001). Ake *et al*. (2001) assigned Max 6.75 on the basis of the discontinuous nature of the scarps in the zone and to match the displacement per event results of Hemphill-Haley (2001). The association of cinder cones along many of the scarps in the Sisters fault zone has been used to infer that the faults may not generate tectonic earthquakes, but rather be related to dike intrusion and volcanic earthquakes (Geomatrix Consultants, 1995; Ake *et al*., 2001). The Tumalo fault lies along the western margin of the Sisters zone and exhibits obviously more evidence of recent activity, and therefore is treated as a separate fault source.
Chemult Graben (western section)	1.0	N	30 (0.5) 41 (0.5)	6.8 6.9	70° W (0.2) 90° (0.6) 70° E (0.2)	0.01 (0.2) 0.1 (0.6) 0.3 (0.2)	7 (0.2) 12 (0.6) 15 (0.2)	40.8	Ake *et al*. (2001) Geomatrix Consultants (1995) MacLeod and Sherrod (1992)	Graben is defined by series of discontinuous, north- to northeast-trending fault scarps, approximately 30 km long, that displace volcanic rocks of late Tertiary and Quaternary age (MacLeod and Sherrod, 1992). Youngest displacement dated at ~0.88 Ma (MacLeod and Sherrod, 1992). Relatively subdued scarps, so slow slip rates seem likely compare to the Walker Rim faults that form the eastern escarpment, which is much more prominent but composed of older rock. The longest continuous scarp is 16 km in length. Northern traces may extend into La Pine Graben. Rupture length of 30 km is from Ake *et al*. (2001). Rupture of 41 km is assumed to reach the southern end of the La Pine graben and Deschutes basin. Faults continue farther south, where they are buried by Mazama tephra, so rupture length is poorly known and probably a minimum value.
Chemult Graben Faults (Walker Rim section)	1.0	N	41 (0.7) 66 (0.3)	6.9 7.2	70° W (0.4) 90° (0.4) 70° E (0.2)	0.01 (0.2) 0.1 (0.6) 0.3 (0.2)	7 (0.2) 12 (0.6) 15 (0.2)	32.2	Weldon *et al*. (2002) Ake *et al*. (2001) Geomatrix Consultants (1995) Pezzopane (1993) MacLeod and Sherrod (1992)	Walker Rim is a prominent 300-m-high, west-facing escarpment of upper Miocene to lower Pliocene volcanic rocks formed by a series of splaying and anastamosing west-side down faults along the eastern margin of the Chemult Graben. Southward in the graben, the numerous, mostly west-side-down fault scarps are in places mostly buried by the Mount Mazama tephra (~7 ka). Northward, the fault zone curves from a NNW strike to a NE strike and projects towards Newberry volcano, and possibly steps east to connect with the Southwest Newberry faults. To date, no Quaternary fault scarps have been described along this section, perhaps in part because of the blanket of Mazama ash. Weldon *et al* (2002) observe lineaments across Quaternary deposits using 1:100,000-scale DEMs of the area. Walker Rim faults appear to be less active than more N-striking faults in the western Chemult graben (MacLeod and Sherrod, 1992; Pezzopane, 1993; Geomatrix Consultants Inc., 1995; Ake and others, 2001.) The total curved length of the Walker Rim zone is 66 km, which is assumed for Mmax, although considered to have a weight of only 0.3. Rupture length of 41 km and slip rate are assumed from the western section of the Chemult graben.
Southwest Newberry Fault Zone	1.0	N	VT[3] (0.7) 14 (0.3)	6.0 6.4	70° W (0.4) 90° (0.4) 70° E (0.2)	0.01 (0.2) 0.05 (0.6) 0.1 (0.2)	7 (0.2) 10 (0.6) 12 (0.2)	21.1	Geomatrix Consultants (1995) MacLeod and Sherrod (1992) Sherrod and Smith (2000)	A zone of east-and west-facing normal faults that projects northeastward from the Walker Rim faults towards Newberry Volcano. Individual faults in this zone are short (<12 km), discontinuous, and offset Pleistocene lava flows, but not Holocene. Scarps appear to be buried by Newberry lava flows, yet, the 1-m DEM maps show several NE-trending lineations that project across the southwestern shield of Newberry towards the caldera. Cinder cones and fissure vents on the south shield are oriented parallel to these faults, which has been taken to indicate the faults are associated with volcanism and dike intrusion rather than tectonic slip (MacLeod and Sherrod, 1992; Geomatrix Consultants, 1995); Sherrod and Smith, 2000). These faults lie along the transitional boundary zone between Basin and Range faulting to the east and High Cascades volcanism and faulting to the west. The zone probably merges with the Southeast Newberry zone near or beneath Newberry Volcano. Maximum rupture length (14 km), assuming a VT model, is estimated from the lengths of the longest individual faults in the zone.
Southeast Newberry Fault Zone	1.0	N	VT[6] (0.7) 21 (0.3)	6.0 6.6	70° W (0.4) 90° (0.4) 70° E (0.2)	0.01 (0.2) 0.2 (0.6) 0.5 (0.2)	7 (0.2) 10 (0.6) 12 (0.2)	29.2	Peterson and Groh (1964); Geomatrix Consultants (1995); Pezzopane (1993)	The Southeast Newberry fault zone strikes northwest from the southern end of Viewpoint fault in the Fort Rock basin, through the Four Craters, to near two volcanic buttes (East Butte and China Hat) on the Newberry shield ~20 km SE of Newberry caldera. Mainly northwest-striking normal faults form small scarps on Plio-Pleistocene volcanic rocks and late Quaternary fluvial-lacustrine deposits with both down-to-the-east and down-to-the west displacements that are, in places, Holocene in age (Pezzopane, 1993). Radiocarbon dating on the Viewpoint fault indicates the most recent event is younger than 11 kyr, and geomorphic evidence suggests activity as recently as 4 kyr. Crack-In-The-Ground is part of a late Pleistocene graben that bounds the Four Craters volcanic center and offsets 740 ± 60 ka Green Mountain lava flows (Peterson and Groh, 1964; Pezzopane, 1993; Geomatrix Consultants, 1995). Maximum rupture length (21 km) is estimated from the lengths of the longest individual faults in this VT zone.
Unnamed Faults near Antelope Mountain	0.5	N	38 (1.0)	6.9	70° SW (0.5) 90° (0.5)	0.005 (0.2) 0.01 (0.6) 0.05 (0.2)	7 (0.2) 12 (0.6) 15 (0.2)	45.9	MacLeod and Sherrod, 1992; Weldon *et al*., 2002	Northwest-striking faults that offset the Miocene to Pliocene volcanic vent complex at Antelope Mountain and a large basalt complex in the surrounding region (MacLeod and Sherrod, 1992). The tall escarpment at Antelope Mountain and several small nested grabens are fault controlled and show significant throw, although no Quaternary scarps have been mapped. Weldon *et al*. (2002) observed linears across Quaternary deposits on 1:100,000-scale DEMs of the area. P(a) of 0.5 is based on the lack of definitive evidence for late Quaternary activity.
Paulina Marsh Faults	1.0	N/NO	35 (1.0)	6.9	70° W (0.2) 90° (0.6) 70° E (0.2)	0.01 (0.2) 0.05 (0.6) 0.1 (0.2)	7 (0.2) 12 (0.6) 15 (0.2)	53.0	Walker and MacLeod, 1991; MacLeod and Sherrod, 1992; Pezzopane, 1993; Weldon *et al*., 2002	Northwest-striking faults that offset Miocene and Pliocene volcanic rocks in the southwestern corner of the Fort Rock Valley (Walker and MacLeod, 1991; MacLeod and Sherrod, 1992). Paulina Marsh fault is marked on the floor of the marsh by a <2-m-high, down-to-the-southwest fault scarp on deposits that may contain Mazama ash (Pezzopane, 1993). Possible right-lateral displacement of small stream channels on the marsh floor. Other faults are normal and high-angle and dip NE and SW so as to form two prominent grabens. Weldon *et al*. (2002) observed lineaments across Quaternary deposits on 1:100,000-scale DEMs.

Table 1. Fault Parameters

Fault[1]	P(a)[2]	Style[3]	Rupture Length[4] (km)	Mmax (M)[5]	Fault Dip	Slip Rate (mm/yr)	Seismogenic Depth (km)	Approximate Distance to Well (km)	Data Sources	Comments
Faults North of Summer Lake	0.5	N	38 (1.0)	6.9	70° W (0.2) 90° (0.6) 70° E (0.2)	0.005 (0.2) 0.01 (0.6) 0.05 (0.2)	10 (0.2) 12 (0.6) 15 (0.2)	91.5	Walker and MacLeod, 1991; Pezzopane, 1993; Weldon *et al*., 2002	Anastomosing zones of mostly NW- and many NE-striking normal faults that form tall bedrock escarpments with Pliocene and Miocene volcanic rocks (Walker and MacLeod, 1991). No fault scarps on Quaternary deposits have been described along these faults, but Quaternary displacement is inferred on the basis of the significant throw in the prominent bedrock escarpments associated with these faults. P(a) of 0.5 is based on the lack of definitive evidence for late Quaternary activity.
Brothers Fault Zone	0.3	NO/SS	55 (0.8) 247 (0.2)	7.1 7.8	70° SW (0.5) 90° (0.5)	0.005 (0.2) 0.01 (0.6) 0.05 (0.2)	10 (0.2) 12 (0.6) 15 (0.2)	28.5	Lawrence, 1976	Brothers fault zone marks a significant geologic, geophysical, and seismotectonic boundary between transtensional faulting in the northern Basin and Range Province and transpression in the Yakima Fold belt and Columbia Plateau in southern Washinton. Brothers fault zone was considered to be the tectonically active “termination” of the NW Basin and Range faulting (Lawrence, 1976). Brothers fault zone is included although neither published nor informal information reveals substantial evidence for late Quaternary fault activity, which is not unusual for many faults in this area where young slip is not obvious. P(a) of 0.1 is based on the lack of evidence for faults or scarps in known or suspected Quaternary deposits. Slip rate is assumed to be similar to other faults that show significant throw in late Tertiary deposits yet lack demonstrable Quaternary activity. P(a) of 0.3 is based on the lack of any evidence for Quaternary fault activity.
Warm Springs Fault Zone Shitake Creek Faults	0.5	N	30 (1.0)	6.8	70° W (0.4) 90° (0.4) 70° E (0.2)	0.005 (0.2) 0.01 (0.6) 0.05 (0.2)	7 (0.2) 12 (0.6) 15 (0.2)	110.6	Geomatrix Consultants, 1995; Pezzopane, 1993	Warm Springs zone consists of discontinuous, north-south- trending, mostly down-to-the west normal faults along the eastern boundary of the High Cascades. Pezzopane (1993) describes young fault scarps in Pleistocene alluvium that resemble some scarps on the Sisters fault zone. P(a) of 0.5 is based on the lack of definitive evidence for late Quaternary activity.

Note: Values in parentheses are probability weights.

1 Faults included in this analysis are all known or suspected late Quaternary faults within a 100-km radius from Newberry Volcano. See text for further information.

2 P(a) is a normalized probability (from 0 to 1.0) coefficient for the subjective certainty that the fault structure has demonstrable or inferable capability of generating significant earthquakes.

3 N Normal; O Oblique; N/O Normal-Oblique; SS Strike-Slip.

4 Measured in a straight line, end-to-end, unless otherwise noted. Most mapped faults taken from Geomatrix Consultants (1995).

5 Mmax is calculated from rupture length and other considerations as described in the text.

6 Volcano-tectonic (VT) earthquakes are associated with magma injection or withdrawal along fault zones in the proximity (~<10 km) of active volcanoes or volcanic rift areas, including the central eruption, caldera collapse, central eruption and flank eruptions, and flank fissure eruptions. In this study, VT sources are assumed to have maximum rupture lengths equivalent to the lengths of the longest individual faults in the zone, rather than total length of the zone. VT earthquake locations are modeled to occur randomly along the idealized fault source zone, because rupture of these inferred smaller-magnitude VT events (~M 6.0 ± 0.5) theoretically does not encompass the maximum tectonic rupture area inferred from maximum fault length and seismogenic width. VT sources are modeled with a truncated exponential recurrence rather than a characteristic recurrence model.

Table 2. Volcanic Earthquake Parameters

Volcano	P(a)	Mmax (Mw)	Recurrence Rate (kyr)	Approximate Distance to Well (km)	Data Sources	Comments
Newberry Volcano	1.0	M 6.0	3 (0.3) 1 (0.4) 0.5 (0.3)	3.0	Sherrod *et al.*, 1997; Simkin and Siebert, 2002; U.S. Geological Survey, 2009	Newberry Volcano, situated east of the Cascade Range, is one of the largest volcanoes in the conterminous United States, covering an area of about 1600 sq km. The low-angle basaltic to basaltic-andesite shield volcano is dotted with more than 400 cinder cones; however Newberry has also produced major silicic eruptions associated with formation of a 6 x 8 km wide summit caldera containing two caldera lakes. The earliest eruptive products (<0.73 million years ago) (Ma) consist of a sequence of ash-flow and airfall tuffs. Caldera collapse is thought to be associated with major ash flows emplaced about 0.5 and 0.3-0.5 Ma. These eruptions were preceded by the emplacement of numerous mafic cones and vents and silicic lava domes and flows, many of which are aligned NNW and NNE parallel to regional fault zones. A rhyolitic magma chamber has been present throughout the Holocene. Six major eruptive episodes from the early Holocene to about 1300 years ago have included both the eruption of basaltic lava flows from flank vents and the explosive ejection of rhyolitic pumice and pyroclastic flows and the extrusion of obsidian flows within the caldera. USGS leveling surveys near Newberry Volcano in 1985, 1986, and 1994 suggests that the volcano's summit area had risen as much as 97±22 mm with respect to a third-order survey in 1931. The 1931 and 1994 surveys measured a 37-km-long, east–west traverse across the entire volcano. The 1985 and 1986 surveys, on the other hand, measured only a 9-km-long traverse across the summit caldera with only one benchmark in common with the 1931 survey. Comparison of the 1985, 1986, and 1994 surveys revealed no significant differential displacements inside the caldera. A possible mechanism for uplift during 1931–1994 is injection of approximately 0.06 km^3 of magma at a depth of approximately 10 km beneath the volcano's summit. Volcano Type: Shield volcano Volcano Status: Radiocarbon Last Known Eruption: 690 AD ± 100 years Summit Elevation: 2434 m 7,985 feet
Bachelor Butte	1.0	M 6.0	5 (0.3) 3 (0.4) 1 (0.3)	37.0	Wood and Kienle, 1990; Simkin and Siebert, 2002; U.S. Geological Survey, 2009	The 25-km-long Mount Bachelor volcanic chain consists of a symmetrical late-Pleistocene to Holocene stratovolcano SE of South Sister volcano and a roughly N-S-trending chain of scoria cones and small shield volcanoes. The youthful basaltic-andesite and basaltic Mount Bachelor volcanic chain was formed in four eruptive episodes dating back to about 18,000-15,000 years before present (BP). Construction of the NNW-SSE scoria cone chain south of Mount Bachelor was completed by about 12,000 years BP. The 2763-m-high Mount Bachelor (formerly known as Bachelor Butte) on the north topographically dominates the chain and is one of its youngest features. The latest activity from the chain produced early Holocene lava flows from Egan scoria cone on the north flank of Mount Bachelor that slightly preceded the eruption of the Mazama ash from Crater Lake about 6850 years ago. Volcano Type: Stratovolcano Volcano Status: Tephrochronology Last Known Eruption: 5800 BC ± 1000 years Summit Elevation: 2763 m 9,065 feet
South SisterVolcano	1.0	M 6.5	5 (0.3) 3 (0.4) 1 (0.3)	57.0	Scott *et al.*, 2001; Simkin and Siebert, 2002; U.S. Geological Survey, 2009	South Sister is the highest and youngest of the Three Sisters volcanoes that dominate the landscape of the central Oregon Cascades. The main edifice of 3157-m-high South Sister is constructed of andesitic and dacitic lava flows capped by a symmetrical summit cinder cone of probable latest-Pleistocene age. The late Pleistocene or early Holocene Cayuse Crater on the SW flank of Broken Top volcano and other flank vents such as Le Conte Crater on the SW flank of South Sister mark mafic vents that have erupted at considerable distances from South Sister itself. Late-Holocene eruptions formed a chain of dike-fed rhyodacitic lava domes and flows on the volcano's SE-to-SW flanks about 2000 years ago. Satellite radar interferometry (InSAR) data obtained by U S Geological Survey scientists detected continuing long-term slight uplift of the ground surface over a broad region centered 5 km west of South Sister volcano that began in 1997. Volcano Type: Complex volcano Volcano Status: Radiocarbon Last Known Eruption: 50 BC (?) Summit Elevation: 3157 m 10,357 feet
North SisterVolcano	1.0	M 6.5	50 (0.4) 30 (0.4) 10 (0.2)	57.0	Scott *et al.*, 2001; Simkin and Siebert, 2002; U.S. Geological Survey, 2009	North and Middle Sister volcanoes anchor the northern end of the Three Sisters volcano group that dominates the landscape of the central Oregon Cascades. Glaciers have deeply eroded the Pleistocene andesitic-dacitic North Sister stratovolcano, exposing the volcano's central plug. North Sister was constructed over the remnants of the basaltic Little Brother shield volcano to the NW. Construction of the main edifice ceased at about 55,000 yrs ago, but N-S-trending fissures north of the volcano were active until at least the latest Pleistocene. Middle Sister volcano is located 2 km to the south. The basaltic-to-rhyolitic Middle Sister and its flank vents is less-eroded, but Holocene activity in the North Sister area is restricted to a group of cinder cones north and NW of the North Sister that have produced a series of fresh-looking blocky lava flows on both sides of McKenzie Pass. The youngest lava flow, from Collier Cone, which was erupted about 1600 years ago and traveled 13.5 km to the west, is a prominent feature of the McKenzie Pass area. North Sister was constructed in four central volcano eruptive stages. Stages are bounded by unconformities and include (1) the Lower Shield Stage (ca. 400 ka), (2) the Glacial Stage (99–182 ka), (3) the Upper Shield Stage (ca. 80 ka), and (4) the Stratocone Stage (55–70 ka). We estimate that ~90% of the total 40 km^3 volume of North Sister was produced during the first two stages. The >11-km-long, north-trending Matthieu Lakes Fissure (75–11 ka) transects North Sister and erupted in three magmatic pulses, yielding a series of thick lavas, scoria cones, and subglacially erupted flow-dominated tuyas. Time-integrated eruption rates at North Sister appear to have slowed from 0.18 to 0.12 km^3 per k.y. between < ca. 400–300 ka and 100 ka to 0.08 km^3 per k.y. between ca. 100 ka and 50 ka. Toward the end of volcanism at North Sister, dikes changed from a radial pattern to a N-S pattern, parallel to faults and vent alignments associated with E-W extension of the High Cascades graben. The Matthieu Lakes Fissure represents the final overprinting of the edifice and distribution of magma supply away from the North Sister center. Volcano Type: Complex volcano Volcano Status: Radiocarbon Last Known Eruption: 440 AD ± 150 years Summit Elevation: 3074 m 10,085 feet

Note: Values in parentheses are weights.

Table 3
Earthquake Parameters for the Seismic Source Zones

Source Zone	Seismogenic Depths (km)	Mmax (M)
Newberry	10 ± 2	5.5
Southern Cascades	12 ± 3	6.0
Northern Great Basin	15 ± 3	6.5
Oregon Block	20 ± 5	6.75
Fold and Thrust Belt	20 ± 5	6.75

Table 4
Recurrence Parameters for Local and Regional Seismic Source Zones

	Area (km2)	a-value	a-value (area)	b-value	Magnitude (M)	Return Period	n (for whole area)
Fold and Thrust	74,172	-0.29	4.58	1.33	6	2511	0.0004
					5	117	0.0085
					4	5.5	0.1821
Southern Cascade	25,100	-2.11	2.29	0.94	6	2240	0.0004
					5	257	0.0039
					4	29.5	0.0339
Northern Great Basin	117,578	-2.44	2.63	0.82	6	195	0.0051
					5	29.5	0.0339
					4	4.5	0.2240
Oregon Block	100,000	-1.5	3.5	1.05	6	631	0.0016
					5	56.2	0.0178
					4	5	0.1995
Long Valley Caldera	4,827	-0.73	2.95	0.69	6	15.6	0.0651
					5.5	6.9	0.1441
					5	3.1	0.3189
					4	0.6	1.5620

Table 5
NEHRP Site Class Definitions

Site Class	Soil Profile Name	Average Properties in Top 100 Feet
		Shear-Wave Velocity, $\bar{v}_s$, (ft/s)
A	Hard Rock	$\bar{v}_s > 5{,}000$
B	Rock	$2{,}500 < \bar{v}_s \leq 5{,}000$
C	Very Dense Soil and Soft Rock	$1{,}200 \leq \bar{v}_s \leq 2{,}500$
D	Stiff Soil Profile	$600 \leq \bar{v}_s \leq 1{,}200$
E	Soft Soil Profile	$\bar{v}_s < 600$

Table 6
Probabilistic PGA and 0.3 and 1.0 sec SA Values

Site	Without EGS Seismicity* Return Period (years)			With EGS Seismicity** Return Period (years)		
	475	**975**	**2,475**	**475**	**975**	**2,475**
La Pine						
PGA	0.21	0.28	0.37	0.21	0.28	0.37
0.3 Sec	0.45	0.58	0.78	0.45	0.58	0.78
1.0 Sec	0.16	0.22	0.31	0.16	0.22	0.31
Sunriver						
PGA	0.18	0.24	0.34	0.18	0.24	0.34
0.3 Sec	0.37	0.49	0.69	0.37	0.49	0.69
1.0 Sec	0.10	0.14	0.20	0.10	0.14	0.20
Well NGC 55-29						
PGA	0.19	0.26	0.36	0.19	0.26	0.36
0.3 Sec	0.34	0.47	0.67	0.34	0.47	0.67
1.0 Sec	0.09	0.12	0.17	0.09	0.12	0.17

* Mmin 5.0

** Mmin 4.0 for EGS Zone

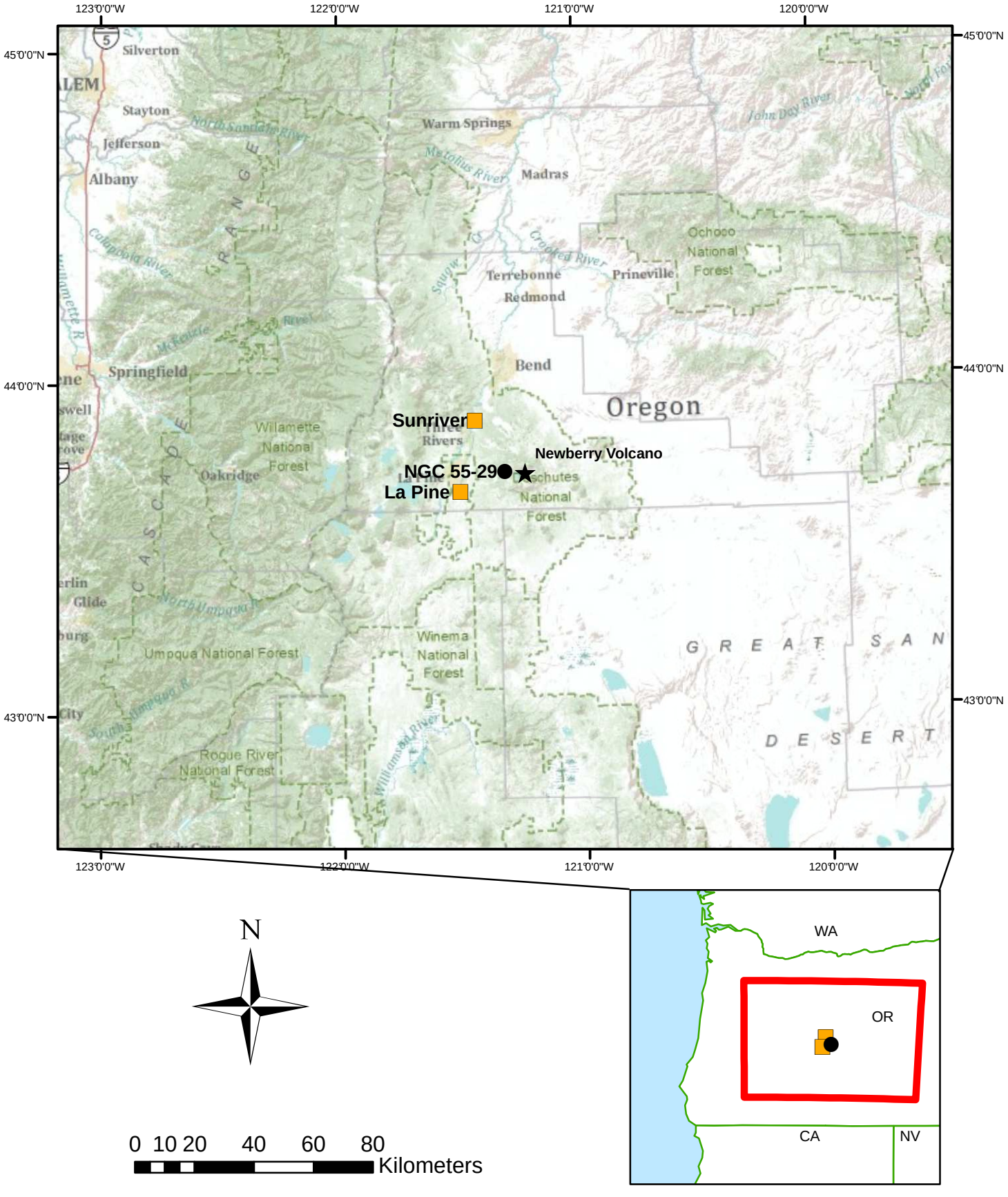

URS	Project No. 26817879 Newberry Volcano, Oregon	LOCATION MAP OF PROJECT AREA	Figure 1

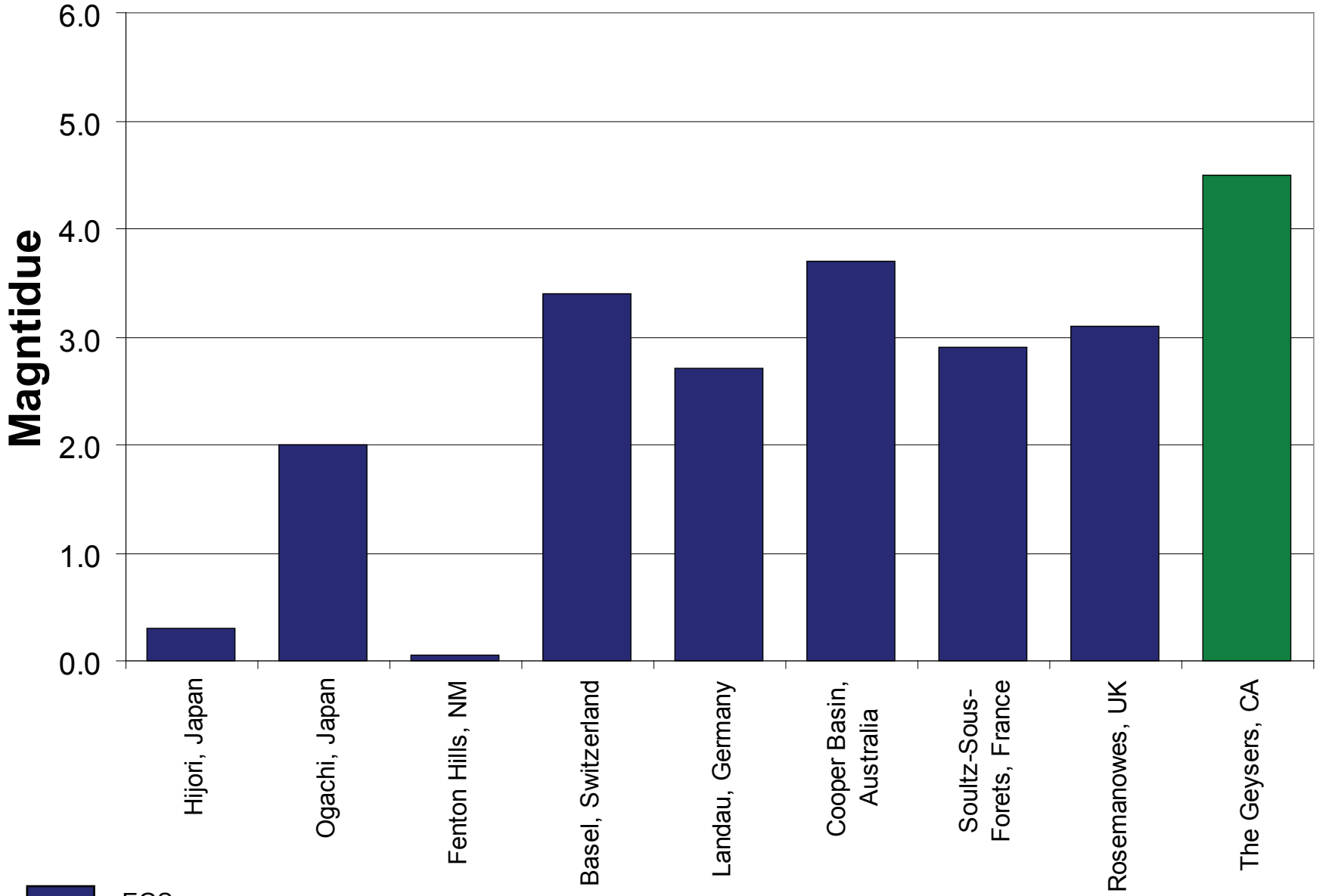

URS

Project No. 26817879

Newberry Volcano, Oregon

MAXIMUM INDUCED EARTHQUAKES FROM GLOBAL GEOTHERMAL ACTIVITIES

Figure 2

Modified from: Wells *et al.* (1998)

URS	Project No. 26817879 Newberry Volcano Oregon	SEISMOTECTONIC SETTING OF NEWBERRY VOLCANO	Figure 3

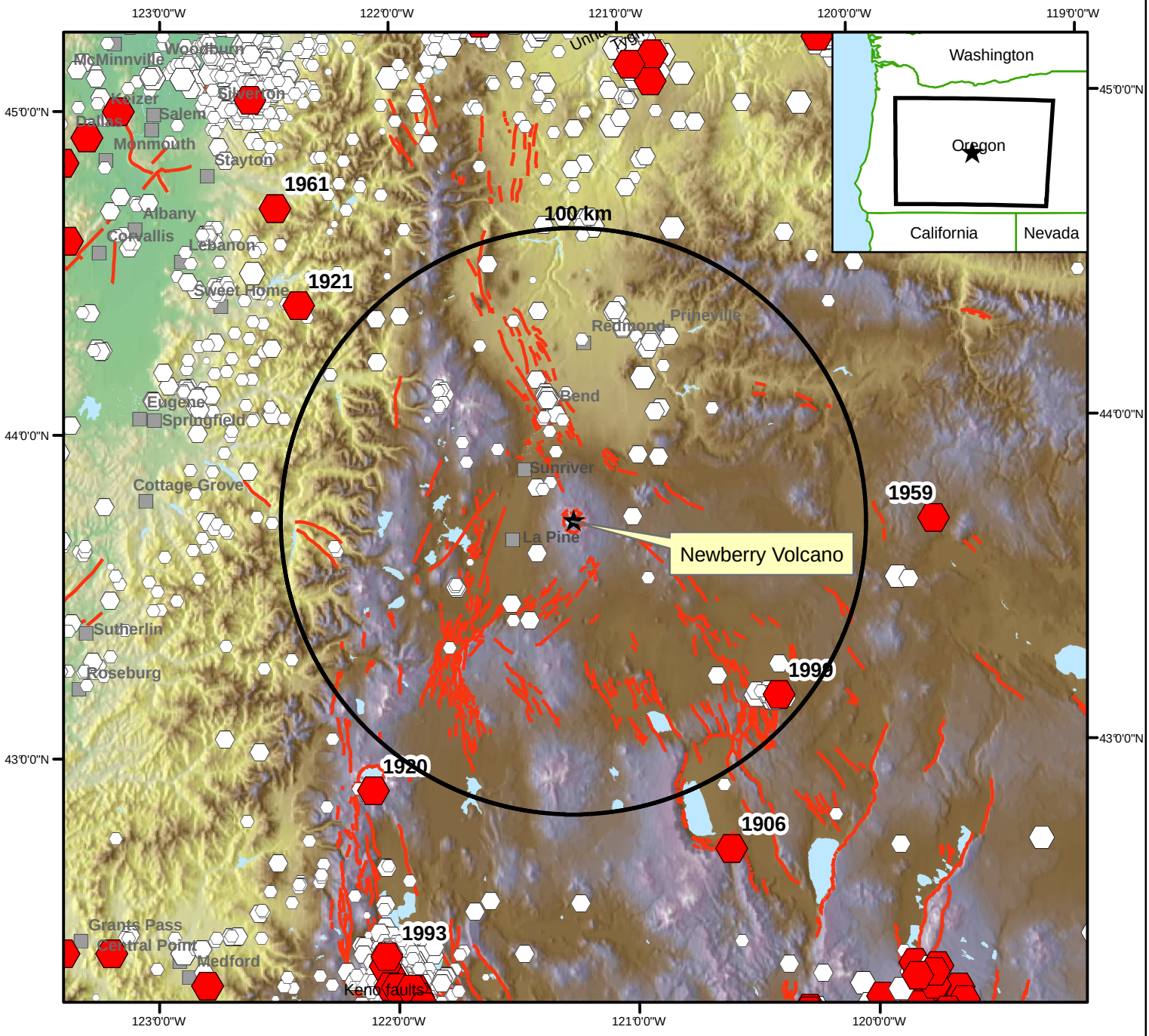

Magnitudes

- 0.1 to 1
- 1.1 to 2.0
- 2.1 to 3.0
- 3.1 to 4.0
- 4.1 to 5.0
- No Magnitude

MM Intensities

- 0
- I to III
- III to IV
- IV to V
- above V

N

- Towns
- Site Location
- Faults

0 10 20 40 60 80 100 Kilometers

URS	Project No. 26817879 Newberry Volcano Oregon	HISTORICAL SEISMICITY OF THE SITE REGION (1840 to 2009)	Figure 4

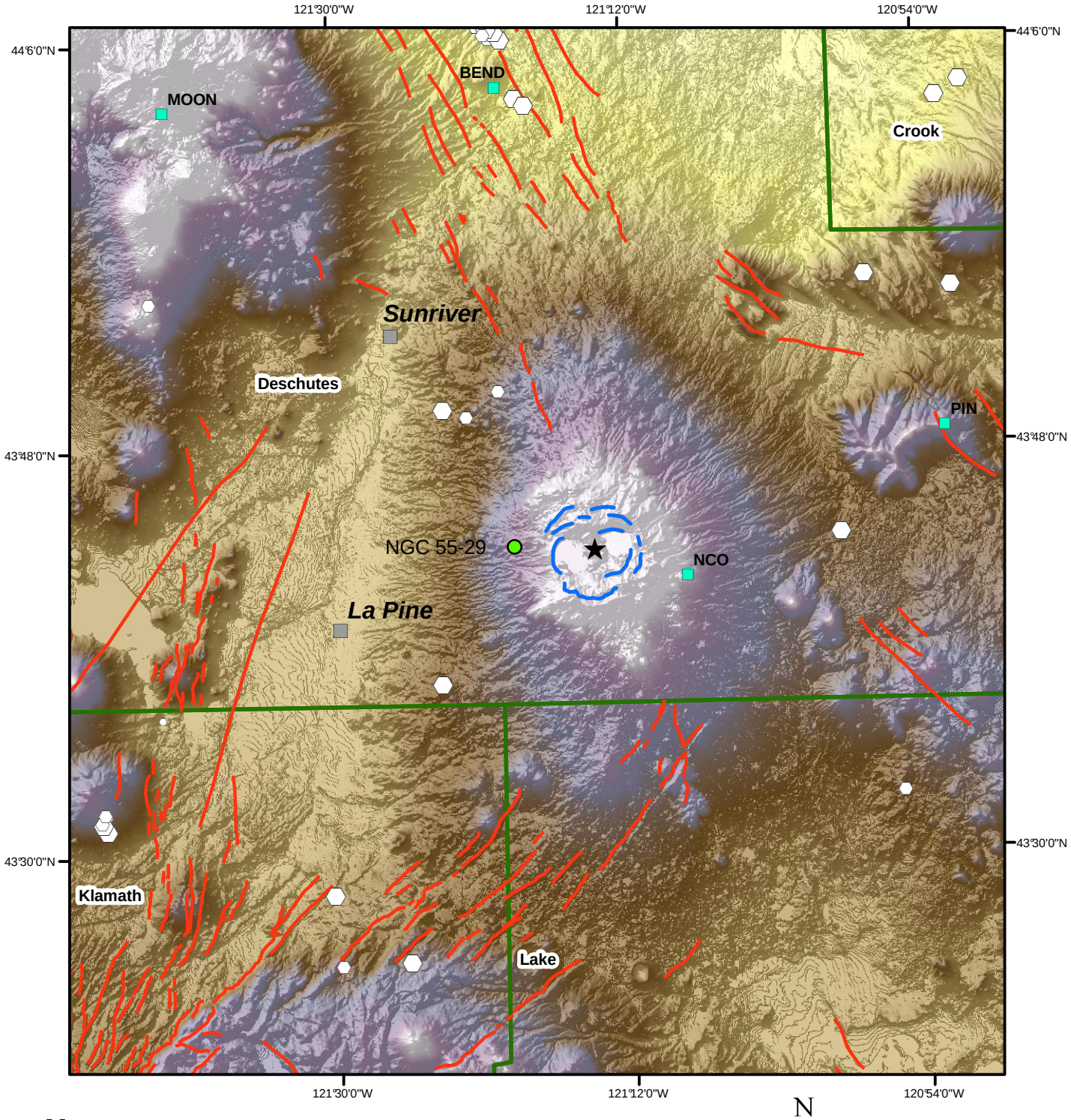

Mag

- 1.00 - 2.00
- 2.00 - 3.00
- 3.00 - 4.00

PNSN Stations

Counties

Class A faults, USGS Quaternary Fault Database

Class B faults, USGS Quaternary Fault Database

N

Kilometers

0 15 30

URS	Project No. 26817879 Newberry Volcano Oregon	HISTORICAL SEISMICITY IN THE VICINITY OF THE SITE (1840 to 2009)	Figure 5

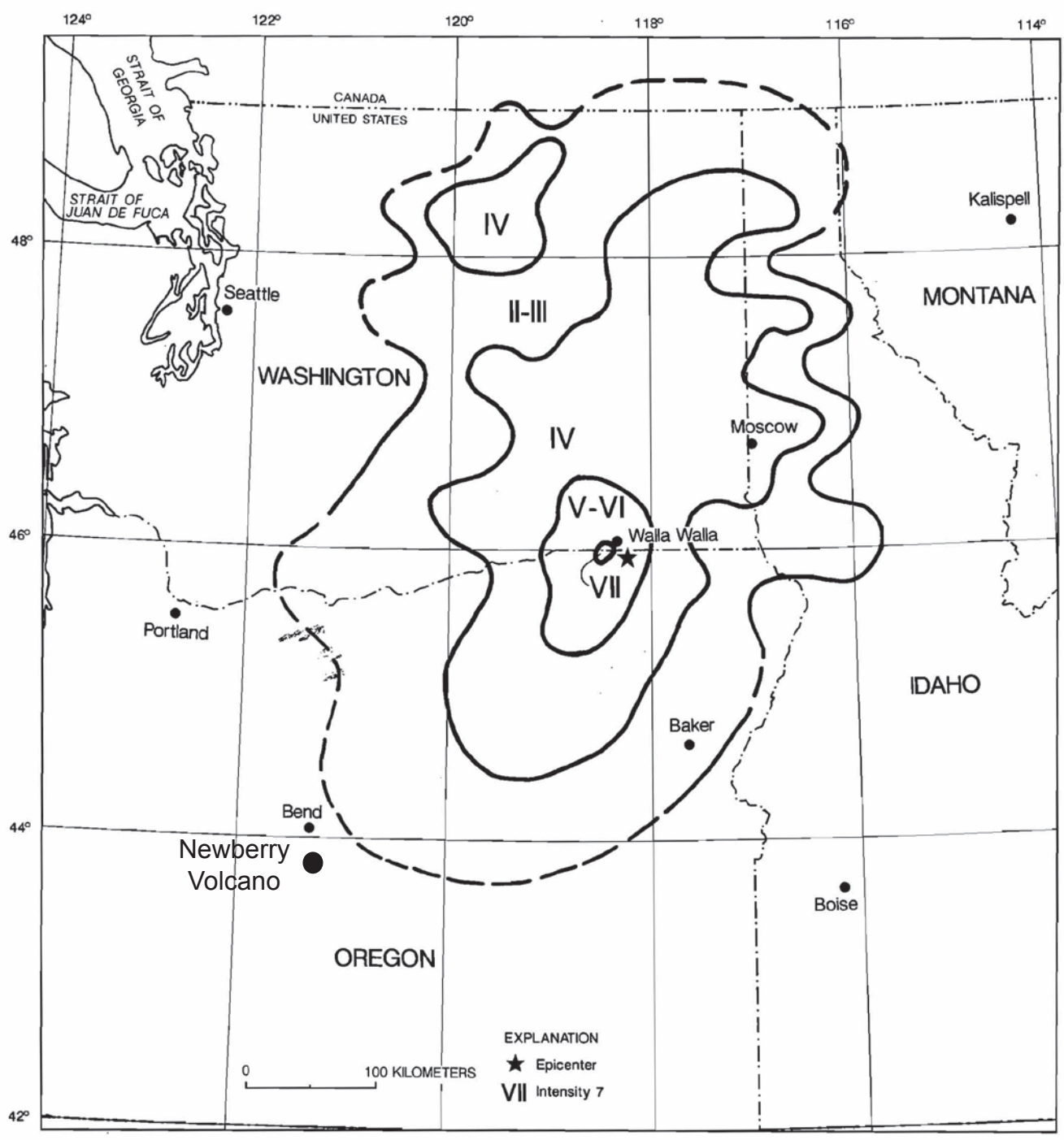

Source: Stover and Coffman (1993)

URS	Project No. 26817879 Newberry Volcano, Oregon	ISOSEISMAL MAP FOR THE 15 JULY 1936 MILTON FREEWATER EARTHQUAKE	Figure 6

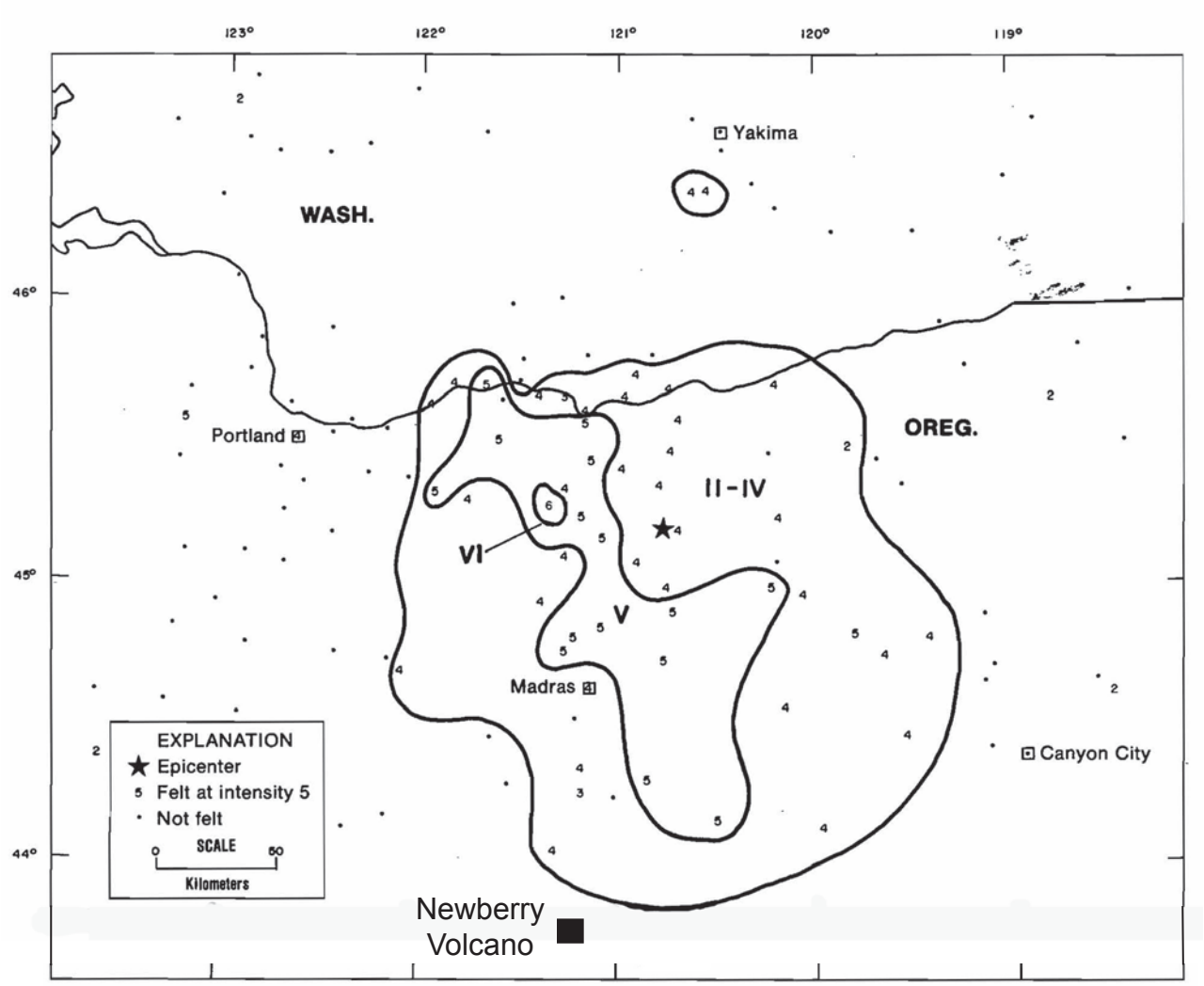

Modified from: Coffman (1979)

URS	Project No. 26817879 Newberry Volcano Oregon	ISOSEISMAL MAP FOR THE 13 APRIL 1976 DESCHUTES VALLEY, OREGON EARTHQUAKE	Figure 7

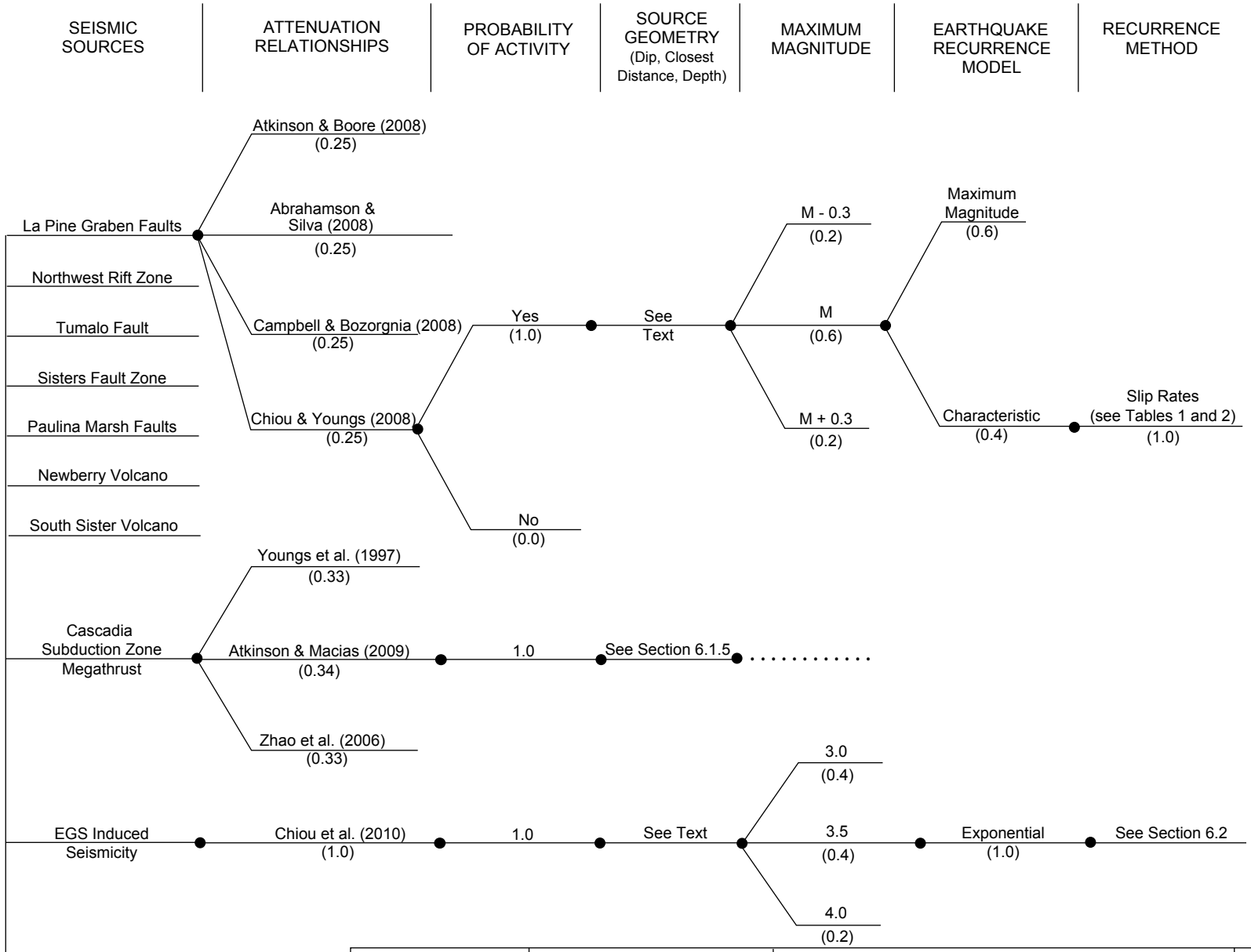

URS

Project No. 26817879

Newberry Volcano, Oregon

SEISMIC HAZARD MODEL LOGIC TREE

Figure 8

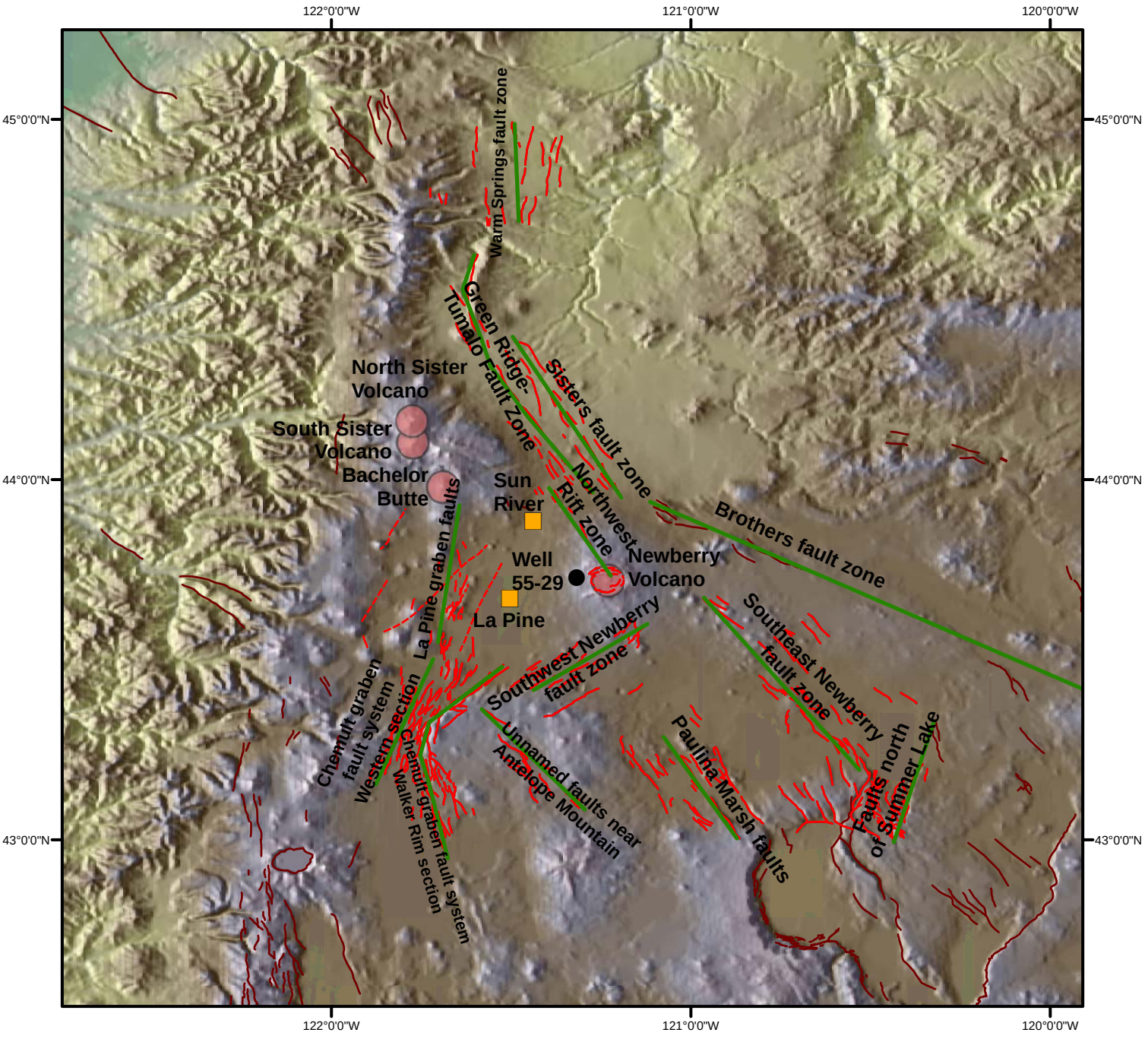

URS Seismic Source Model

USGS Quaternary Fault Database

USGS Quaternary Fault Database
Not Included in URS Analysis

N

0 10 20 40 60 80
Kilometers

URS	Project No. 26817879 Newberry Volcano Oregon	ACTIVE FAULTS INCLUDED IN THE ANALYSIS	Figure 9

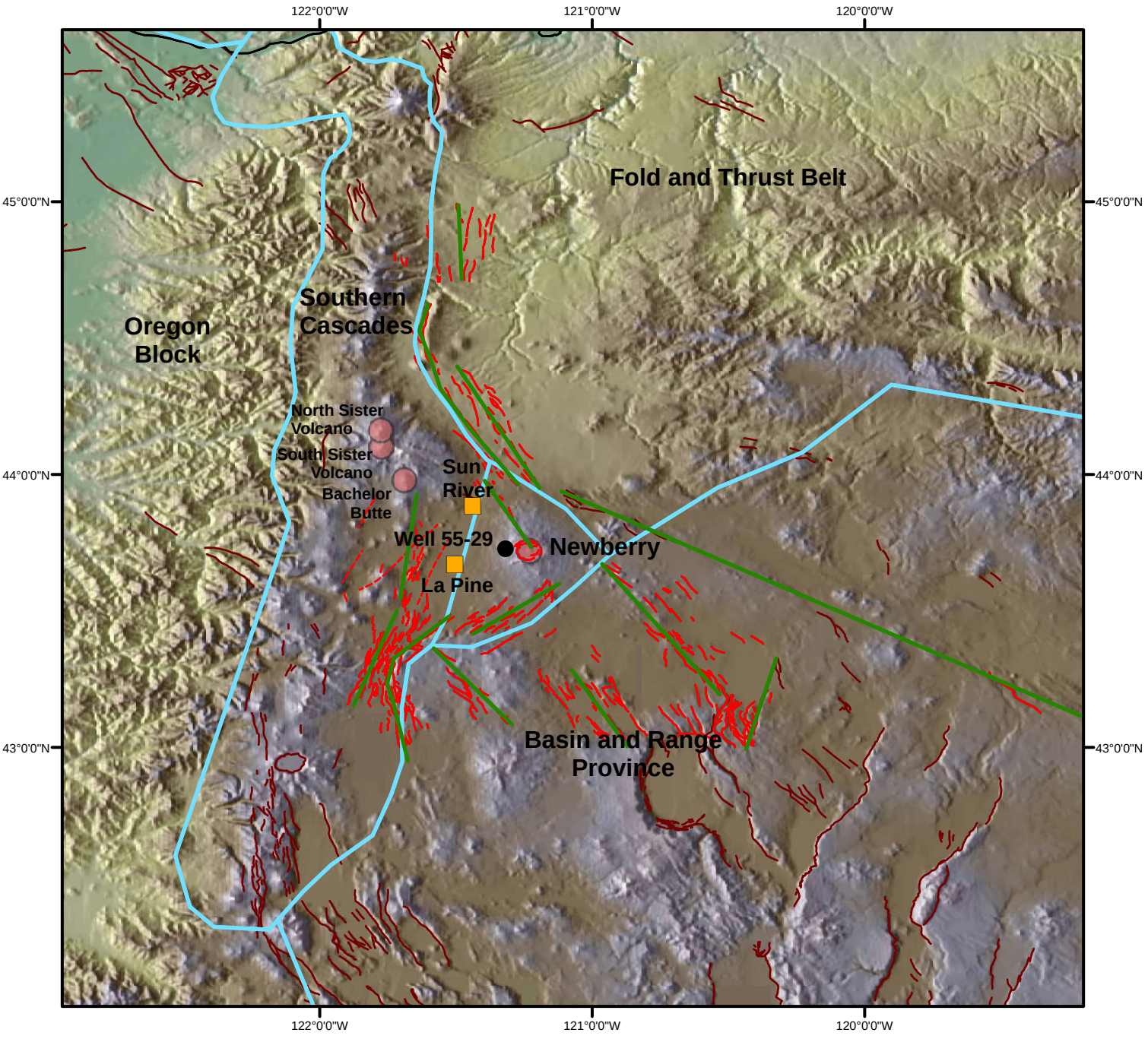

URS	Project No. 26817879 Newberry Volcano Oregon	SEISMIC SOURCE ZONES INCLUDED IN THE ANALYSIS	Figure 10

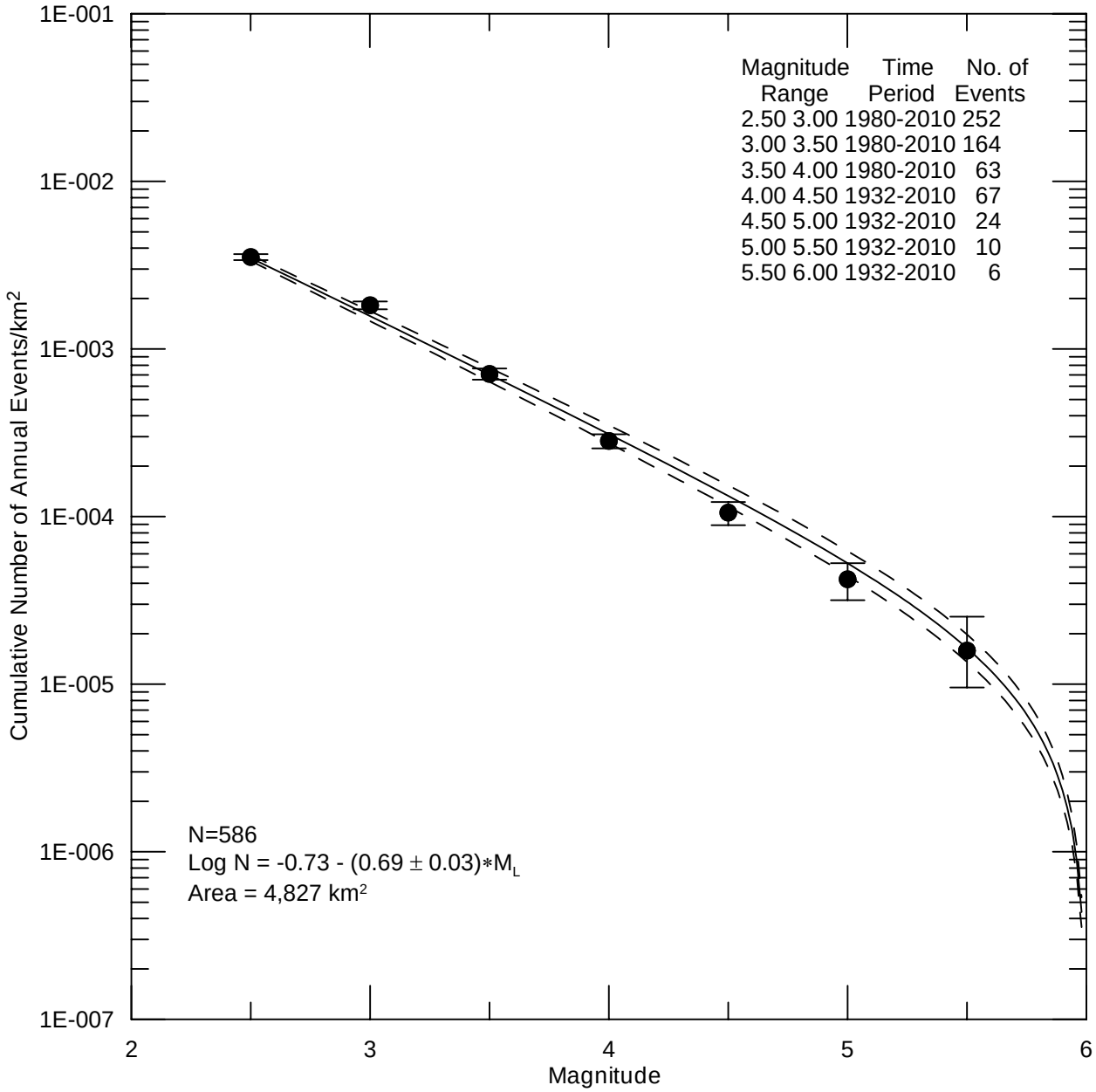

URS	Project No. 26817879 Newberry Volcano Oregon	EARTHQUAKE RECURRENCE OF LONG VALLEY CALDERA	Figure 11

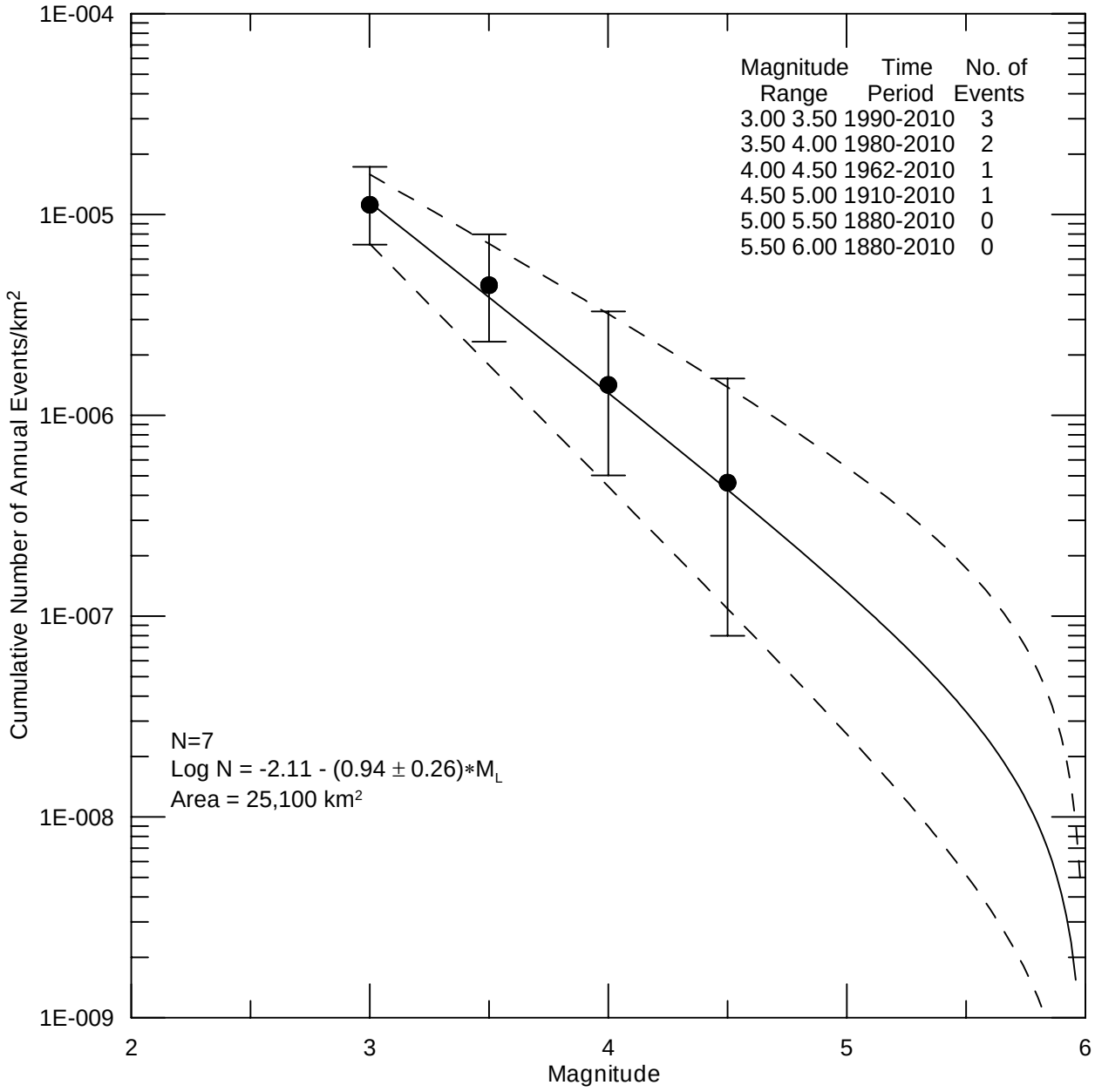

URS	Project No. 26817879 Newberry Volcano Oregon	EARTHQUAKE RECURRENCE OF SOUTHERN CASCADES	Figure 12

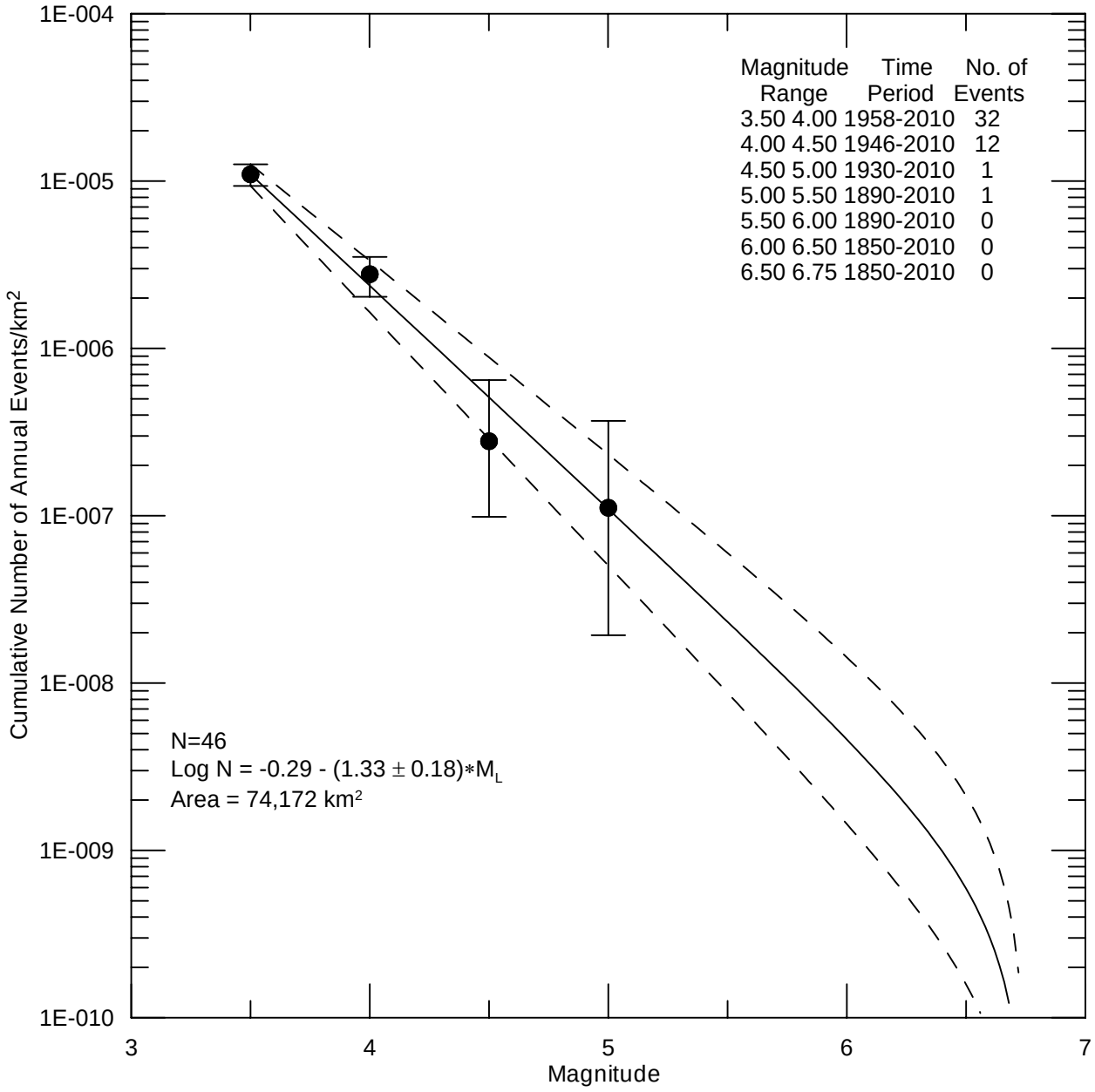

URS	Project No. 26817879 Newberry Volcano Oregon	EARTHQUAKE RECURRENCE OF FOLD AND THRUST BELT	Figure 13

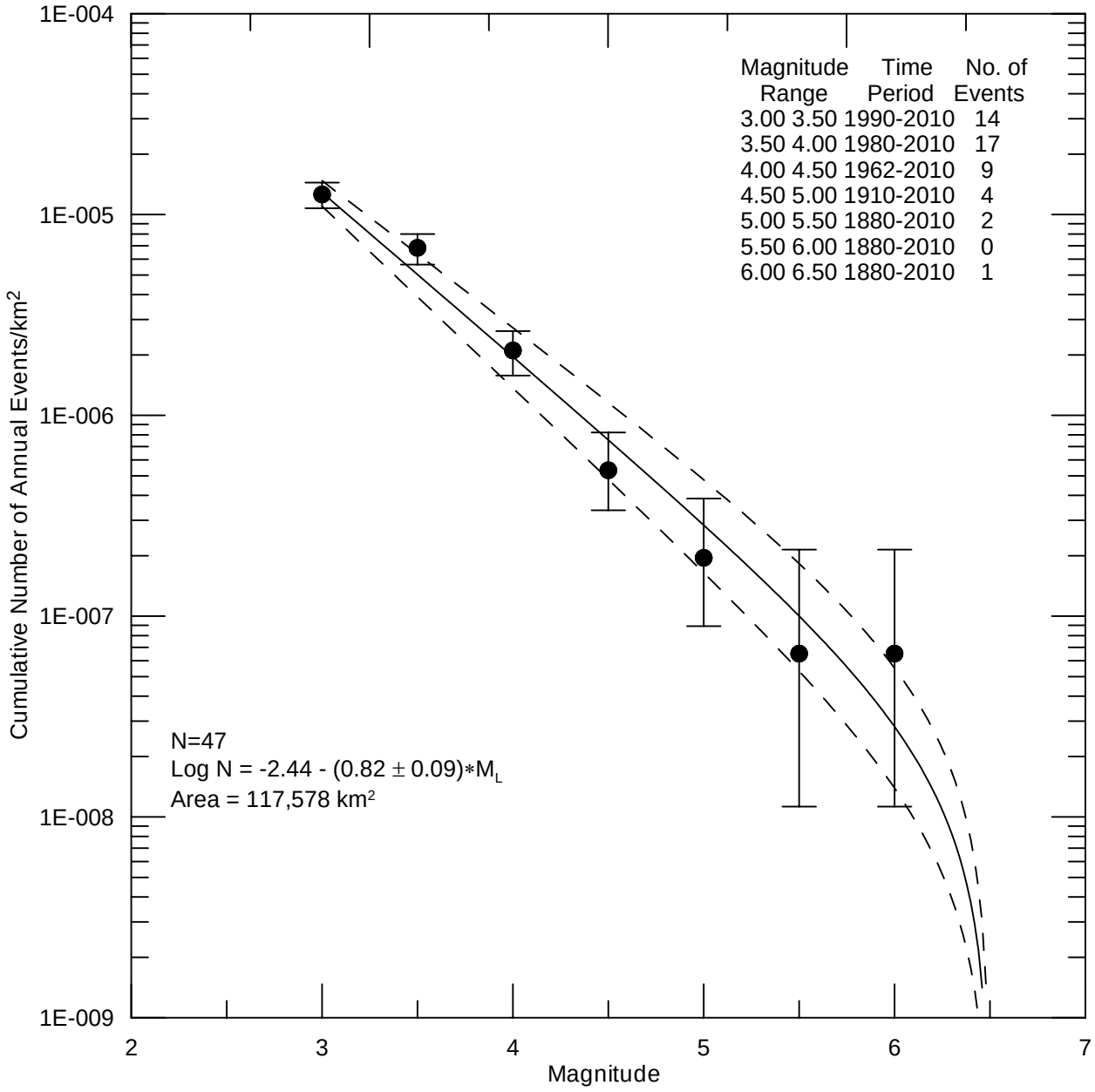

URS	Project No. 26817879 Newberry Volcano Oregon	EARTHQUAKE RECURRENCE OF BASIN AND RANGE PROVINCE	Figure 14

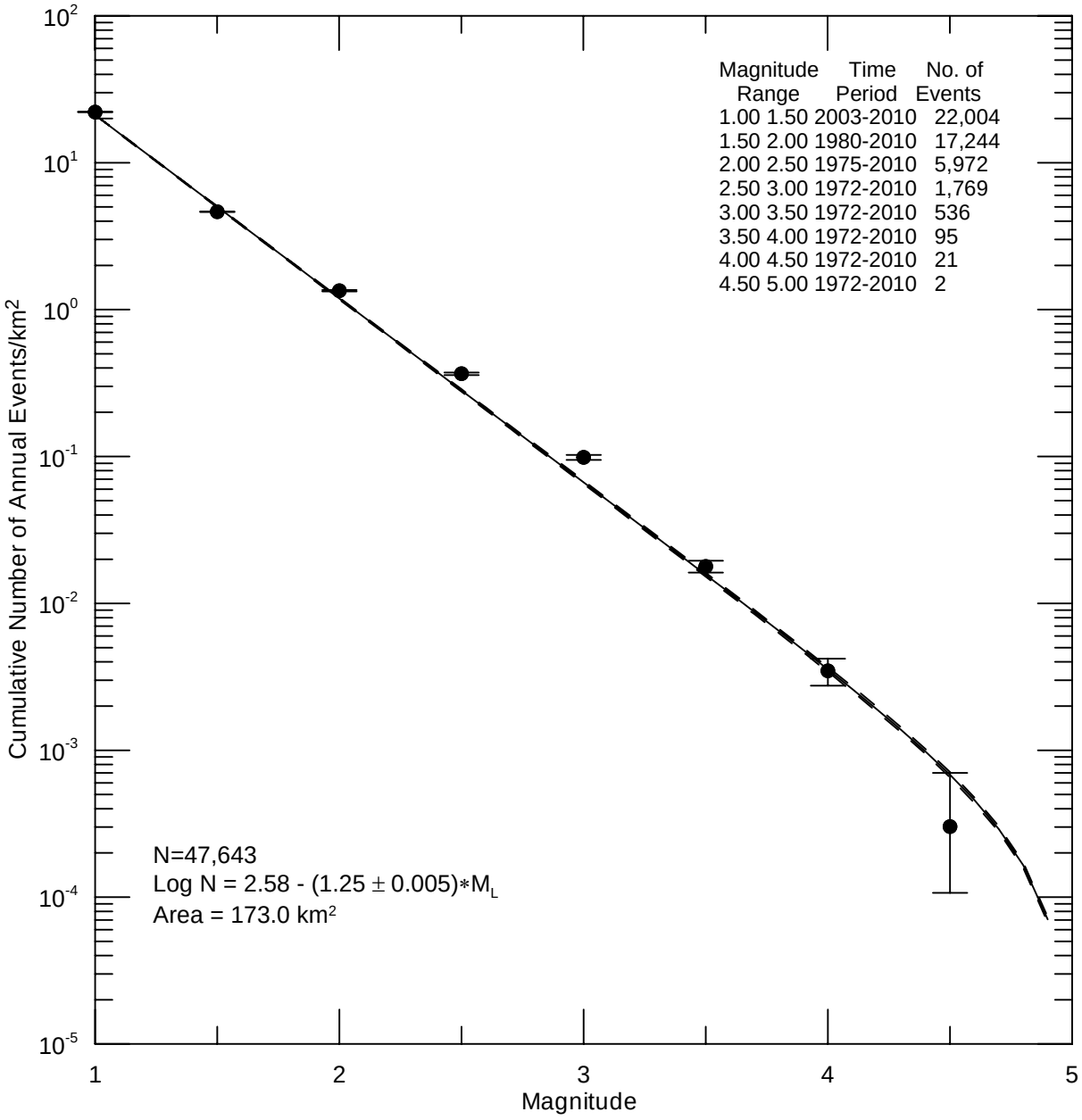

URS	Project No. 26817879 Newberry Volcano Oregon	EARTHQUAKE RECURRENCE OF THE GEYSERS	Figure 15

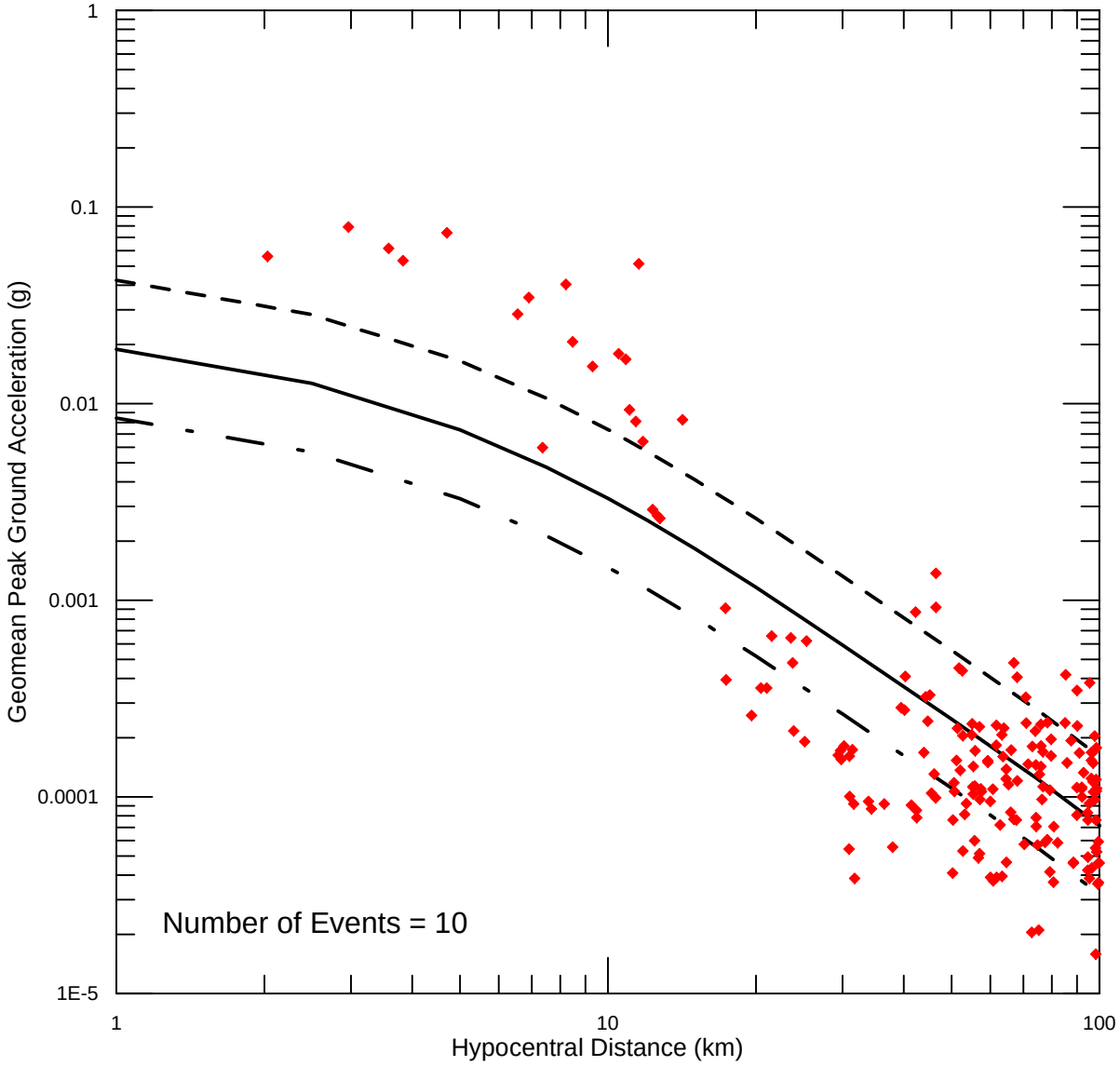

URS	Project No. 26817289 Newberry Volcano Oregon	RECORDED GEYSERS PGA VALUES COMPARED WITH CHIOU *ET AL.* GROUND MOTION MODEL FOR **M**3.5	Figure 16

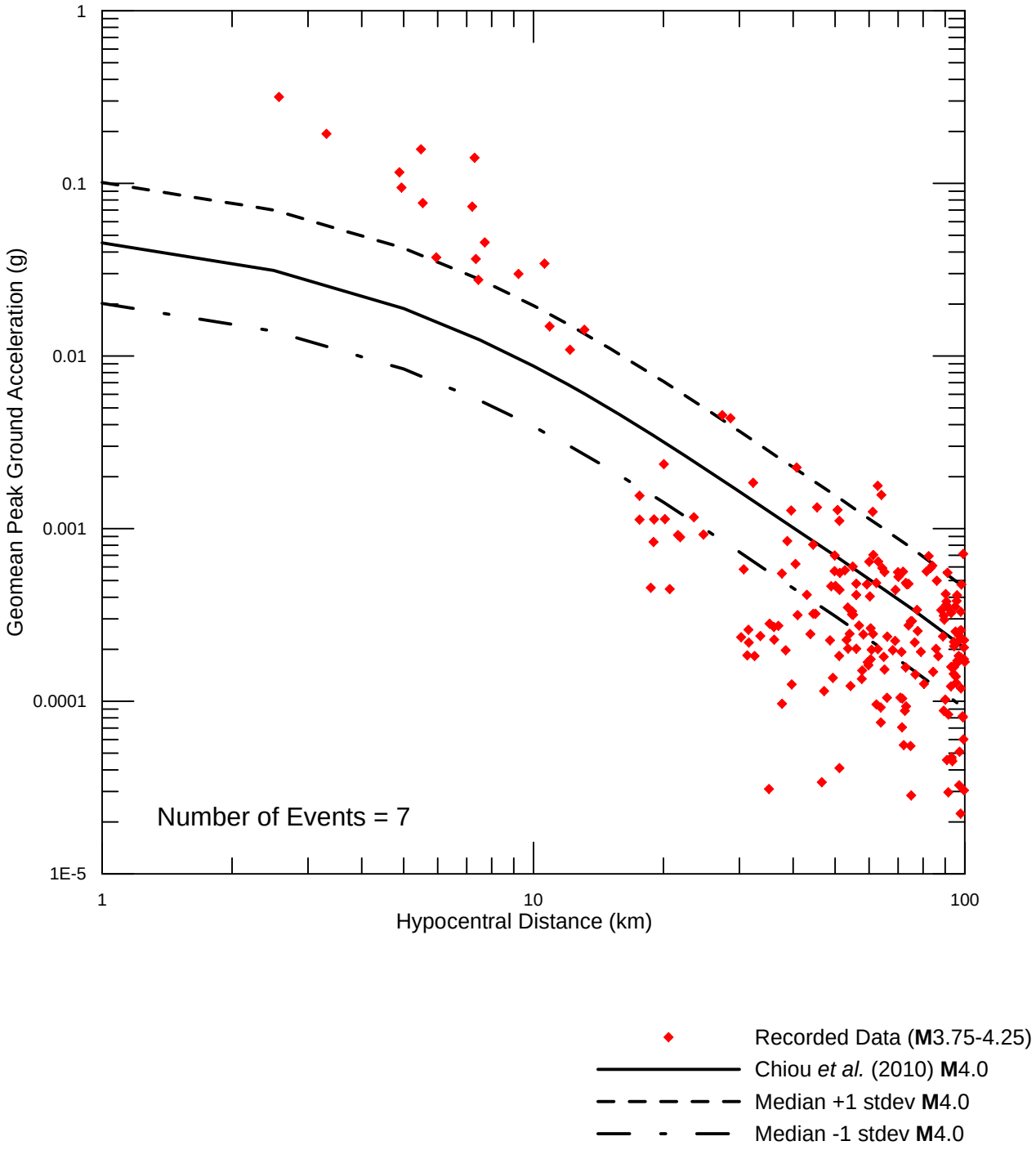

URS	Project No. 26817289 Newberry Volcano Oregon	RECORDED GEYSERS PGA VALUES COMPARED WITH CHIOU *ET AL.* GROUND MOTION MODEL FOR **M**4.0	Figure 17

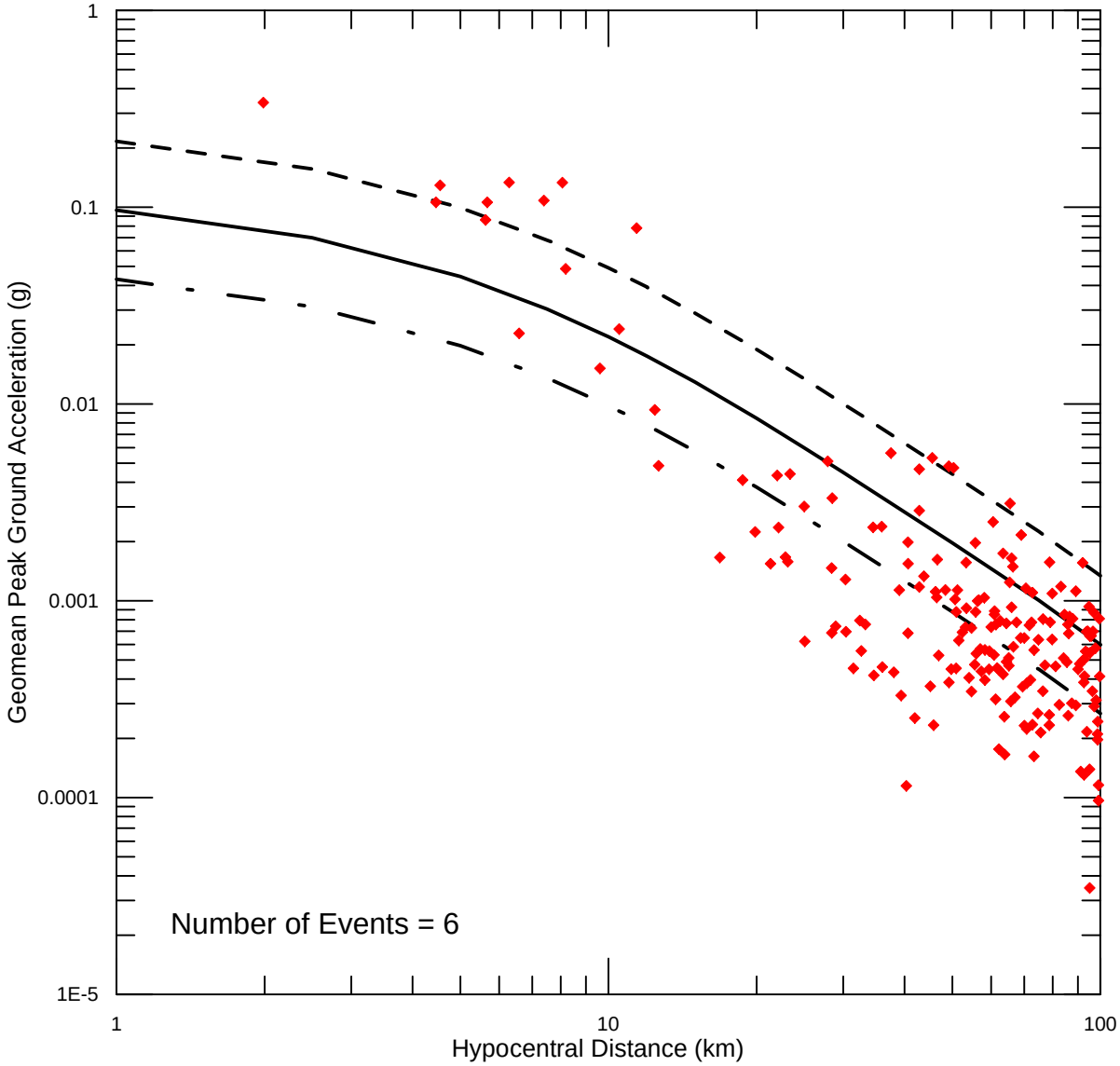

URS	Project No. 26817289 Newberry Volcano Oregon	RECORDED GEYSERS PGA VALUES COMPARED WITH CHIOU *ET AL.* GROUND MOTION MODEL FOR **M**4.5	Figure 18

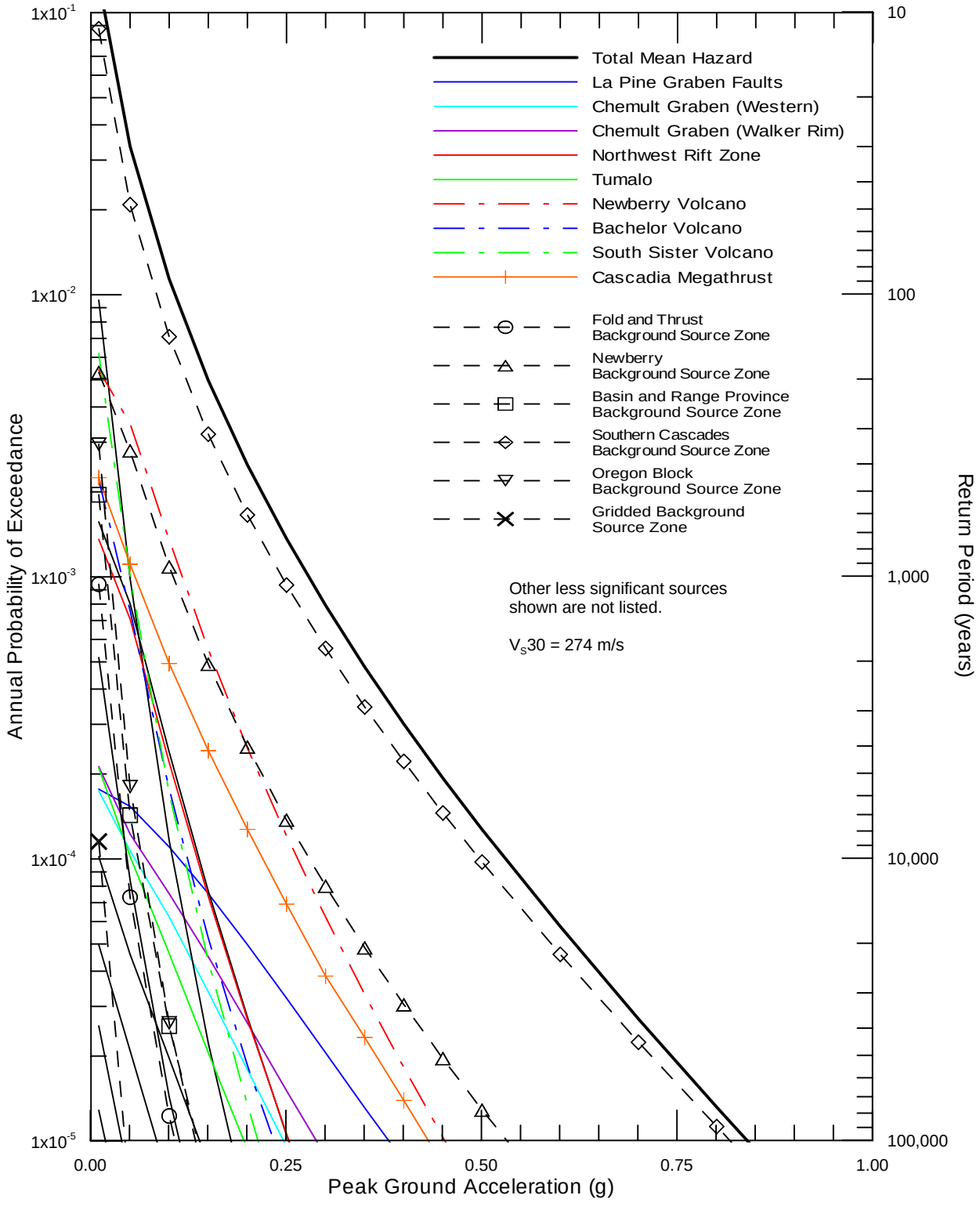

URS	Project No. 26817879 Newberry Volcano Oregon	SEISMIC SOURCE CONTRIBUTIONS TO MEAN PEAK HORIZONTAL ACCELERATION HAZARD AT LA PINE	Figure 19

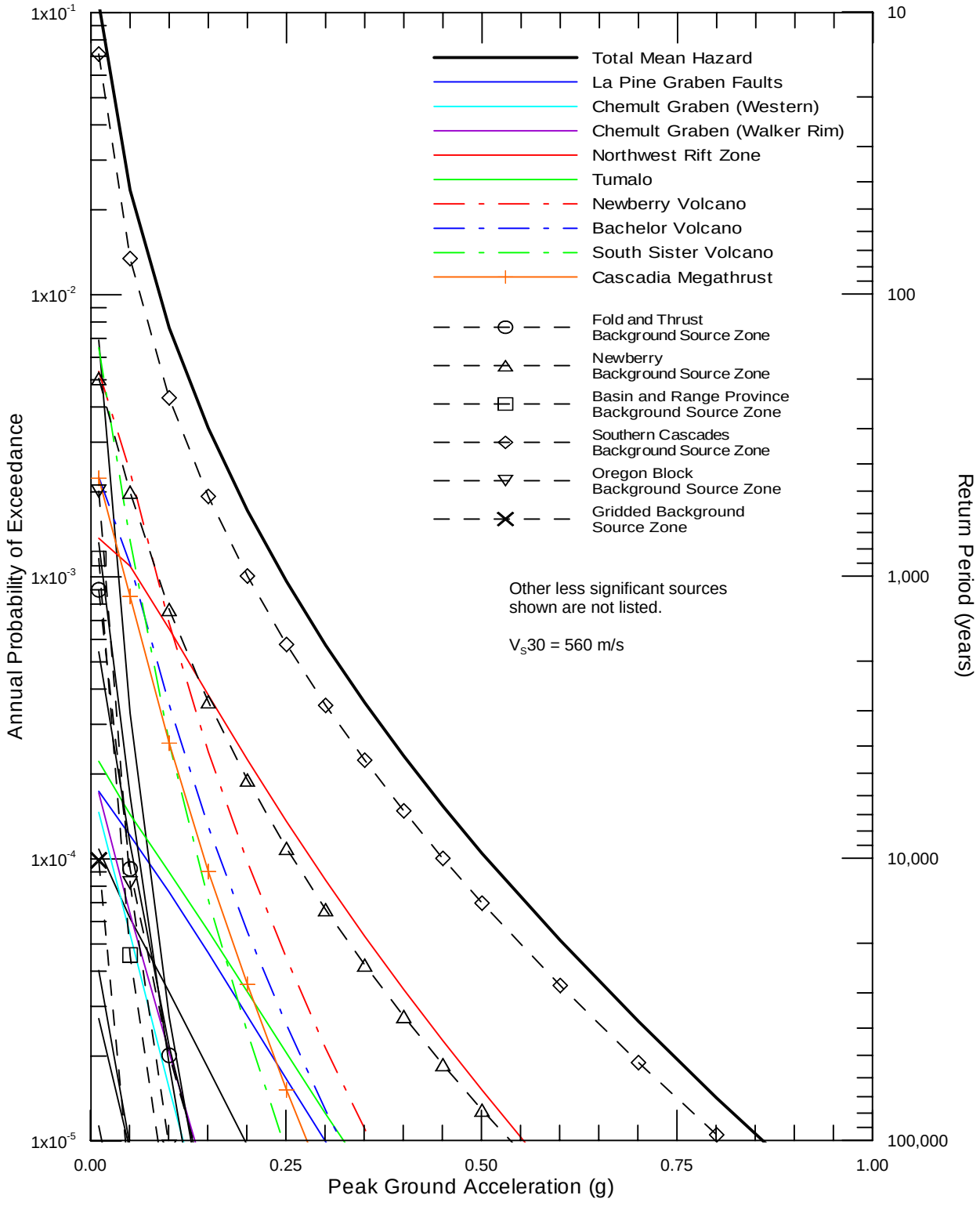

URS	Project No. 26817879 Newberry Volcano Oregon	SEISMIC SOURCE CONTRIBUTIONS TO MEAN PEAK HORIZONTAL ACCELERATION HAZARD AT SUNRIVER	Figure 20

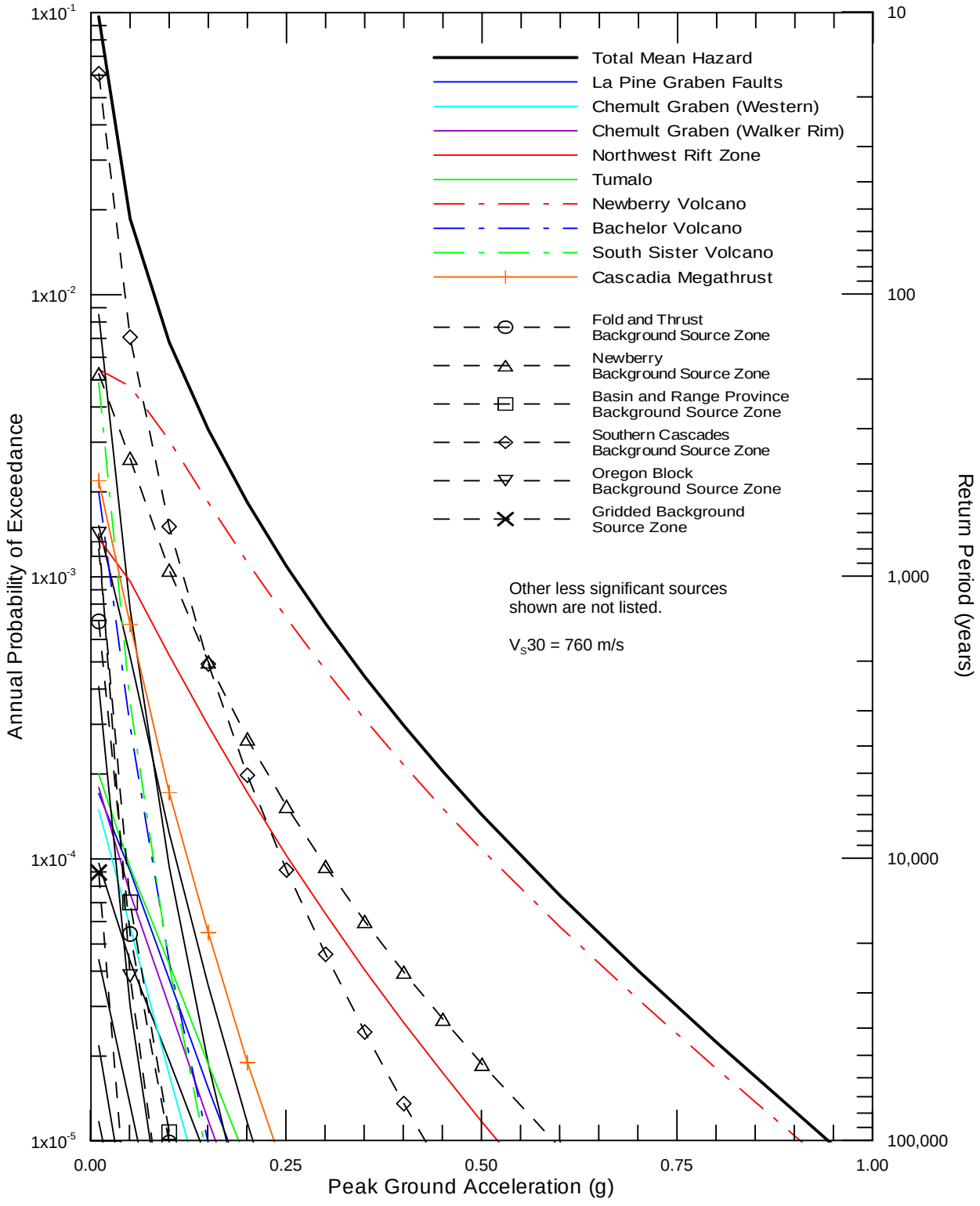

URS	Project No. 26817879 Newberry Volcano Oregon	SEISMIC SOURCE CONTRIBUTIONS TO MEAN PEAK HORIZONTAL ACCELERATION HAZARD AT WELL 55-29	Figure 21

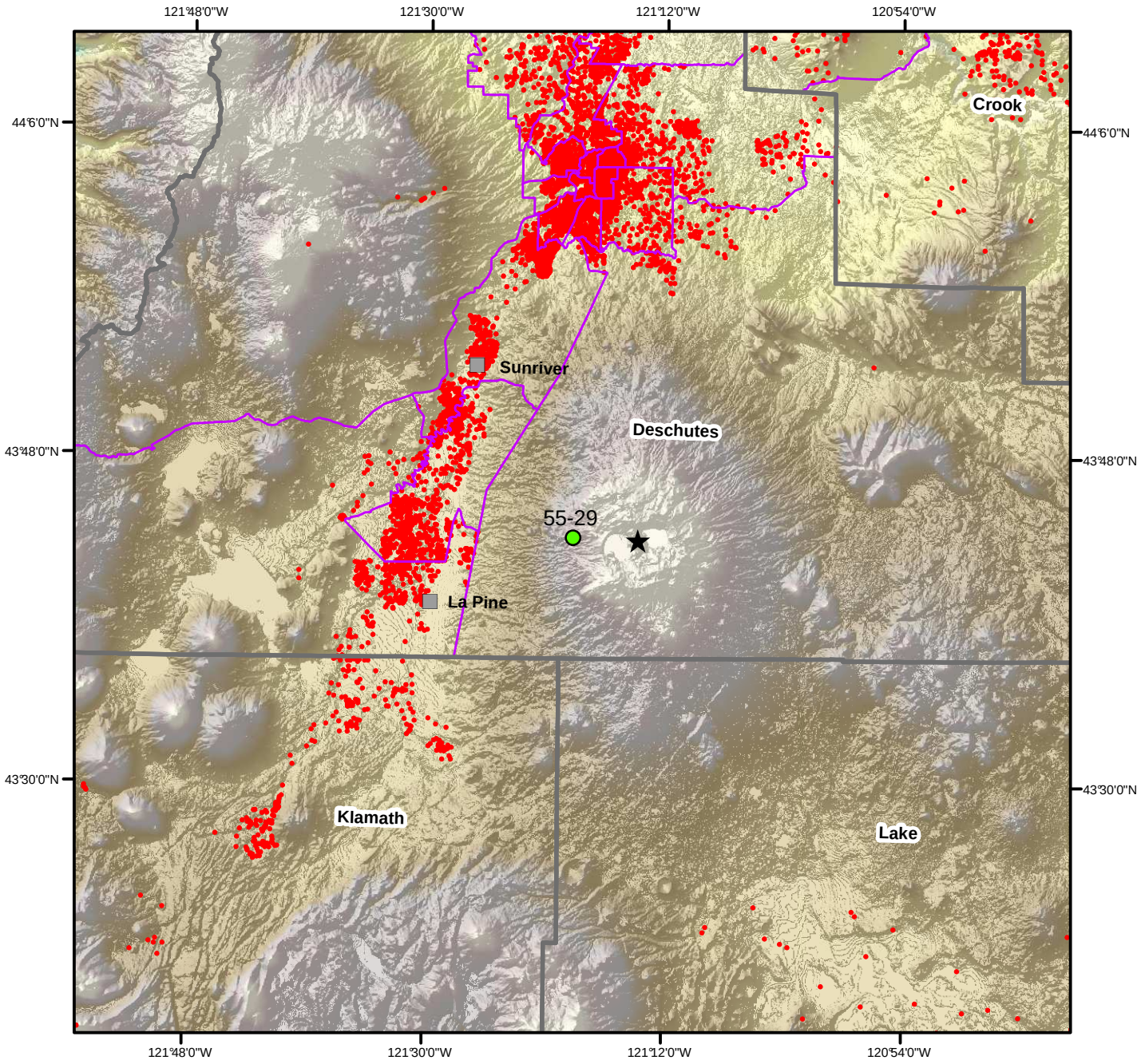

URS	Project No. 03017016 Newberry Volcano Oregon	POPULATION DISTRIBUTION AND DENSITY IN THE SITE REGION	Figure 22

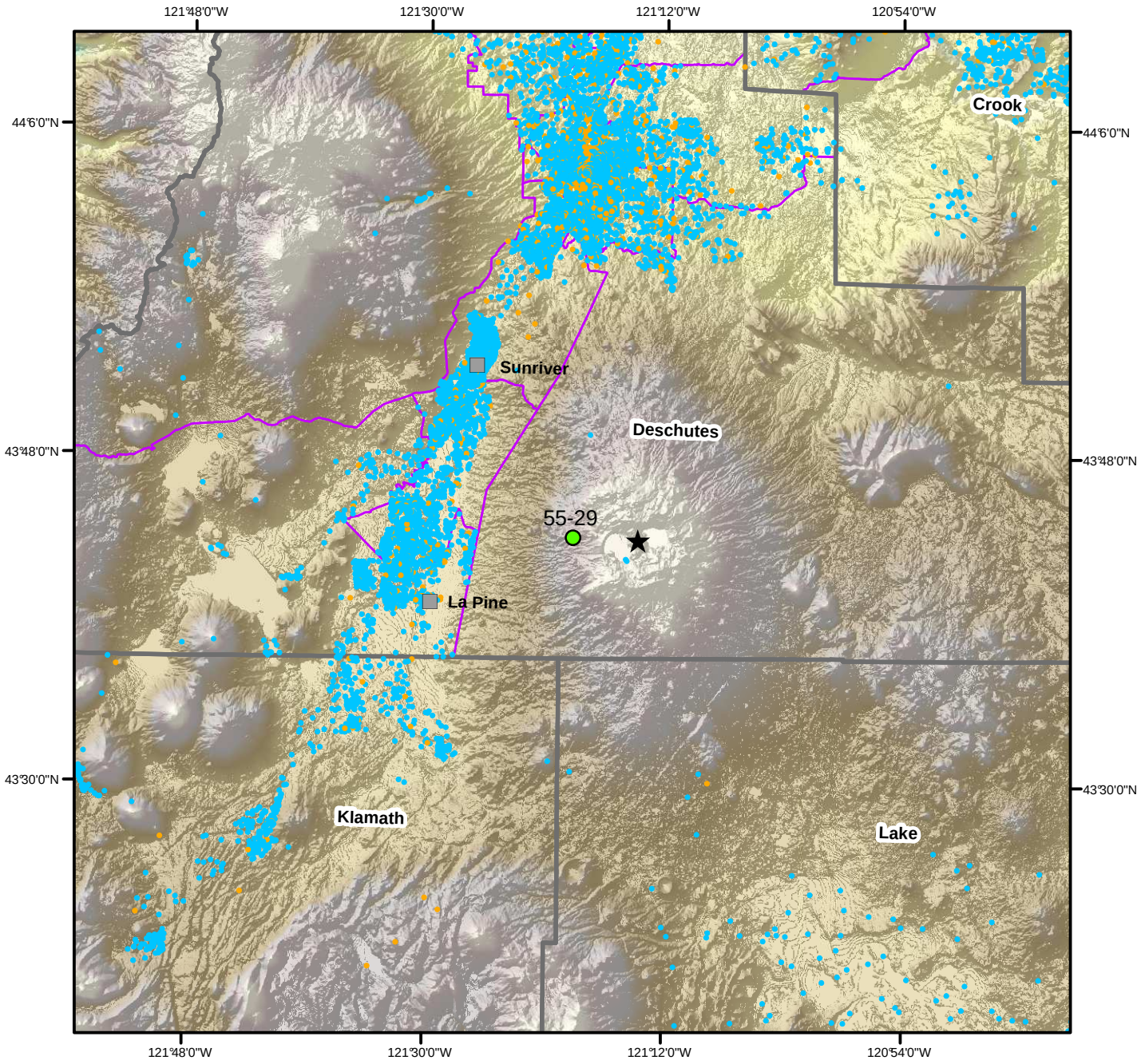

URS	Project No. 03017016 Newberry Volcano Oregon	BUILDING DISTRIBUTION AND DENSITY IN SITE REGION	Figure 23

Appendix
Site-Specific Probabilistic Hazard Results

We have computed the probabilistic hazard at the towns of La Pine and Sunriver, and Well NGC 55-29 without and with the contribution of potential EGS-induced seismicity. Figures A-1 to A-18 summarize the results of the PSHA without EGS seismicity. Figures A-1 to A-3 show the mean, median (50th percentile), 5th, 15th, 85th, and 95th percentile hazard curves for PGA for the three sites. The 1.0 sec SA hazard is shown on Figures A-4 to A-6. These fractiles indicate the range of uncertainties about the mean hazard. At a return period of 2,475 years, there is a factor of 4 between the 5th and 95th percentile values for La Pine (Figure A-1).

The contributions of the various seismic sources to the mean PGA hazard at the three sites are shown on Figures A-7 to A-9. For La Pine and Sunriver, the controlling source at PGA is background seismicity within the Basin and Range Province. The Newberry Volcano source controls the PGA hazard at NGC 55-29 (Figure A-9). For long-period ground motions at a period of 1.0 sec, the CSZ controls the hazard at return periods greater than 1,000 years (Figures A-10 to A-12). At shorter return periods, the Basin and Range background earthquakes control the hazard.

Figures A-13 to A-18 illustrate the contributions by events that were obtained by deaggregating the PGA and 1.0 sec SA hazard by magnitude and distance bins. The PGA hazard at 2,475 years is from local events of **M** 5.0 to 6.5 at distances less than 20 km, corresponding to background seismicity. At long periods, e.g., 1.0 sec SA, the CSZ megathrust contributes mostly to the 1.0 sec SA hazard with contributions also from background earthquakes (Figures A-16 to A-18).

In Figures A-19 to A-24, the PGA and 1.0 sec SA hazard with EGS seismicity is deaggregated by seismic sources. As shown, the contribution of EGS seismicity at the three selected sites is insignificant.

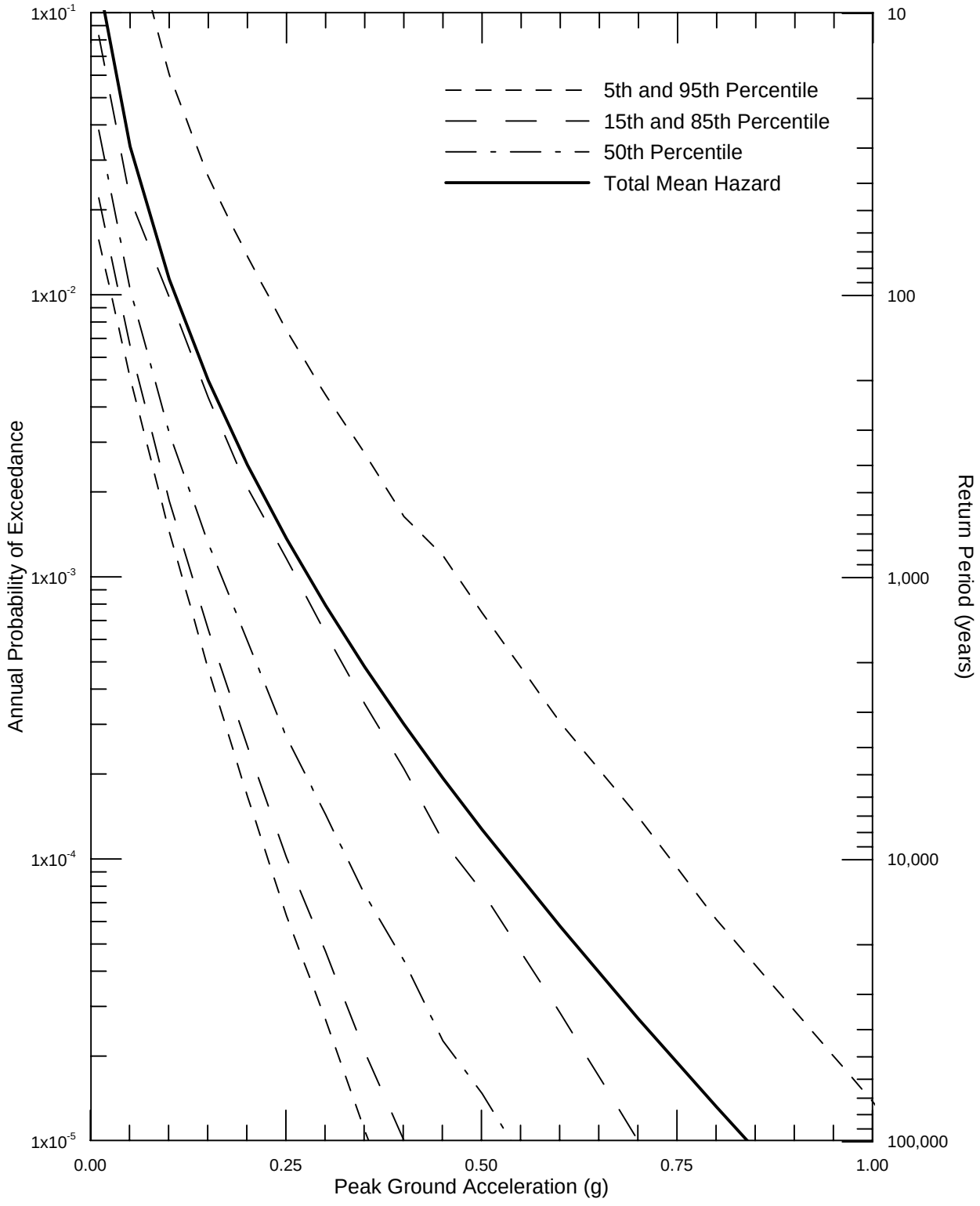

URS	Project No. 26817879 Newberry Volcano Oregon	SEISMIC HAZARD CURVES FOR PEAK HORIZONTAL ACCELERATION AT LA PINE	Figure A-1

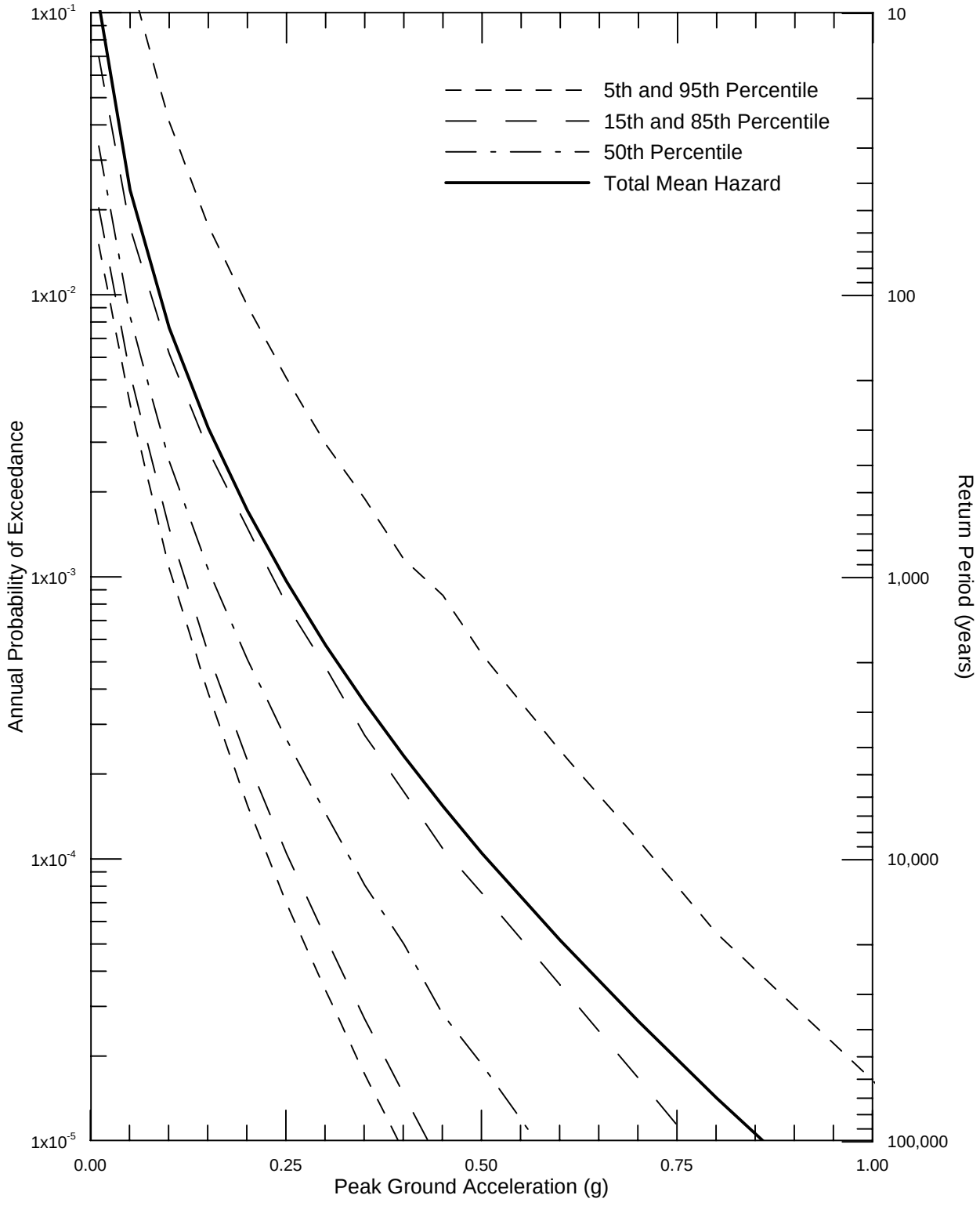

URS	Project No. 26817879 Newberry Volcano Oregon	SEISMIC HAZARD CURVES FOR PEAK HORIZONTAL ACCELERATION AT SUNRIVER	Figure A-2

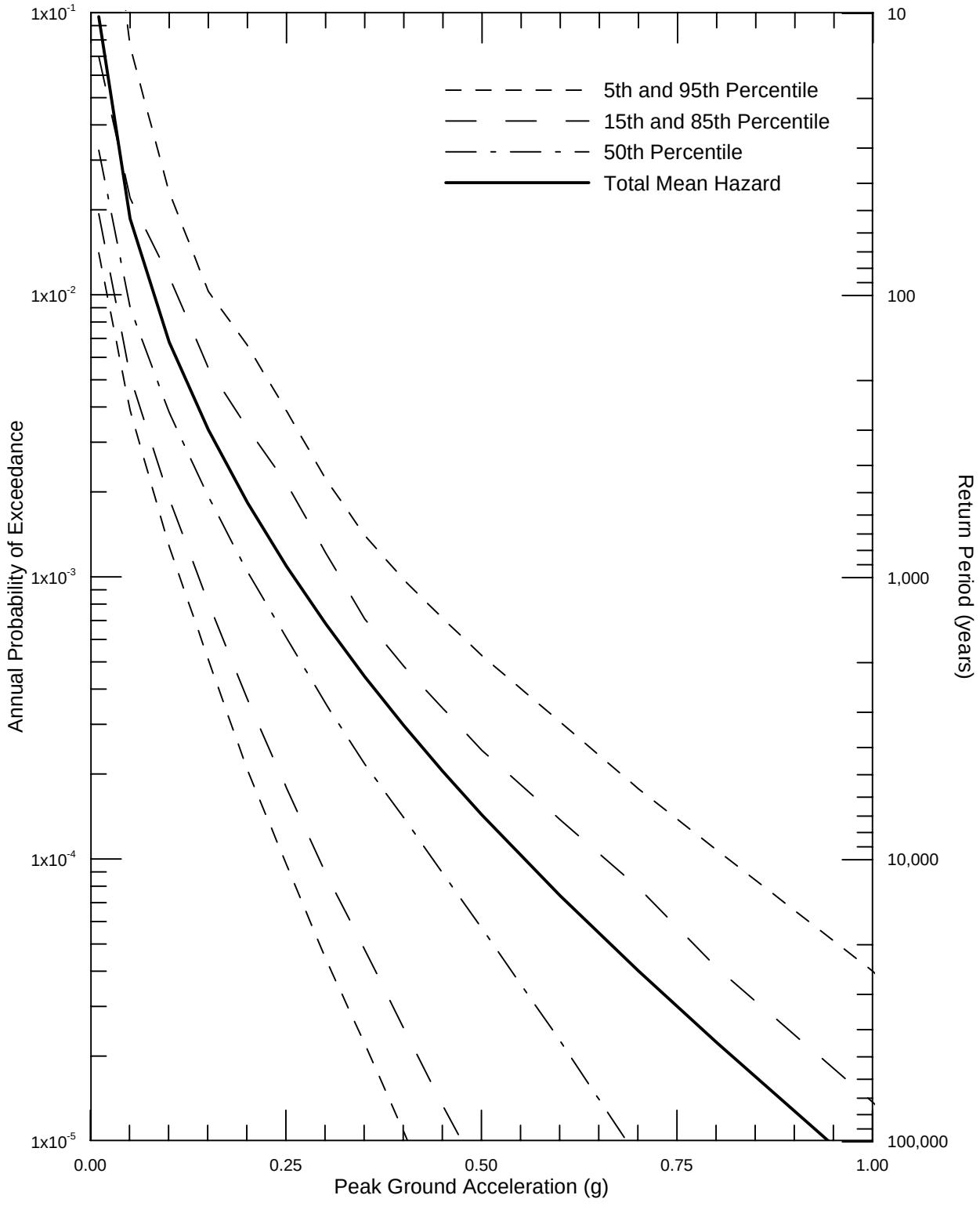

URS	Project No. 26817879 Newberry Volcano Oregon	SEISMIC HAZARD CURVES FOR PEAK HORIZONTAL ACCELERATION AT WELL 55-29	Figure A-3

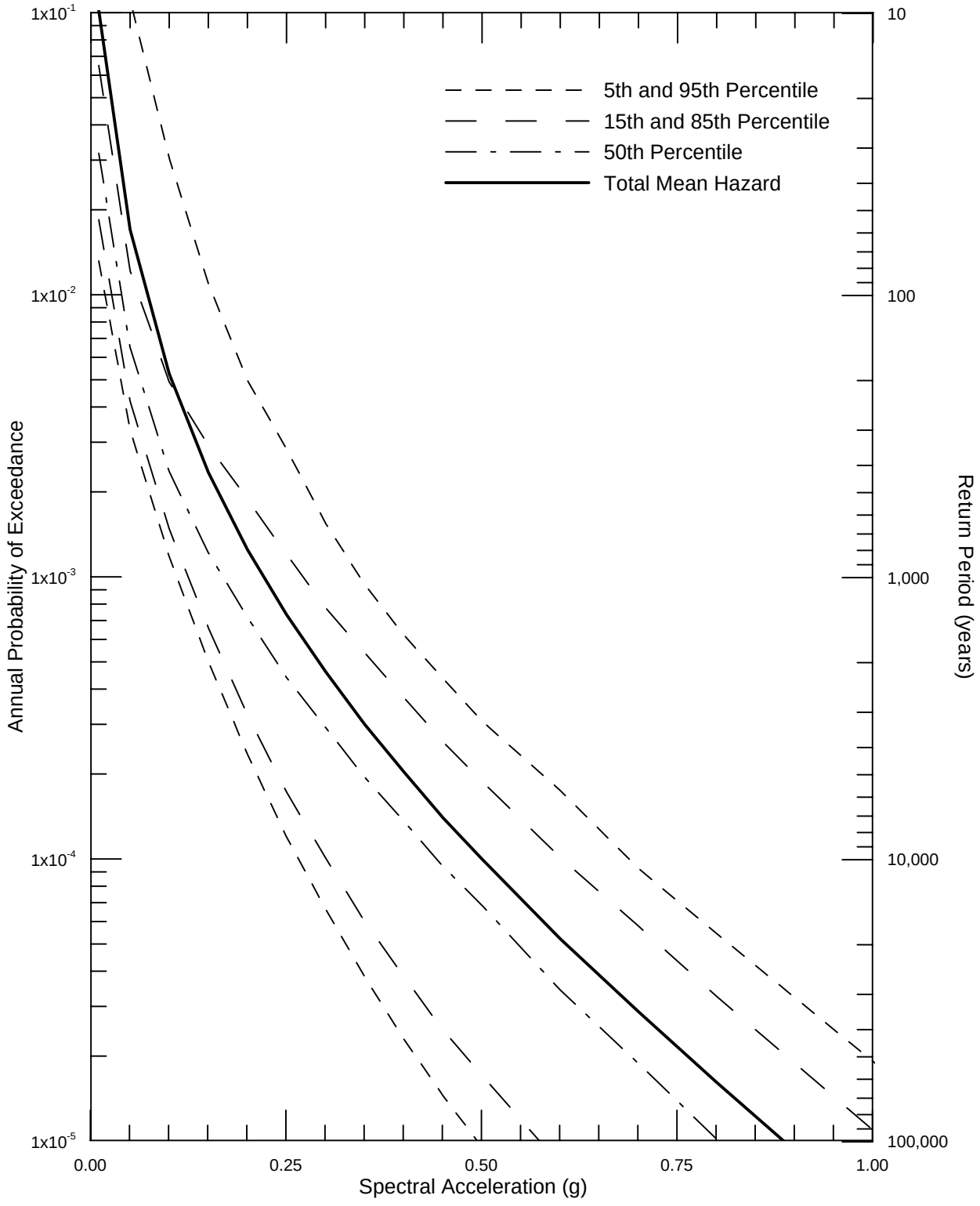

URS	Project No. 26817879 Newberry Volcano Oregon	SEISMIC HAZARD CURVES FOR 1.0 SEC HORIZONTAL SPECTRAL ACCELERATION AT LA PINE	Figure A-4

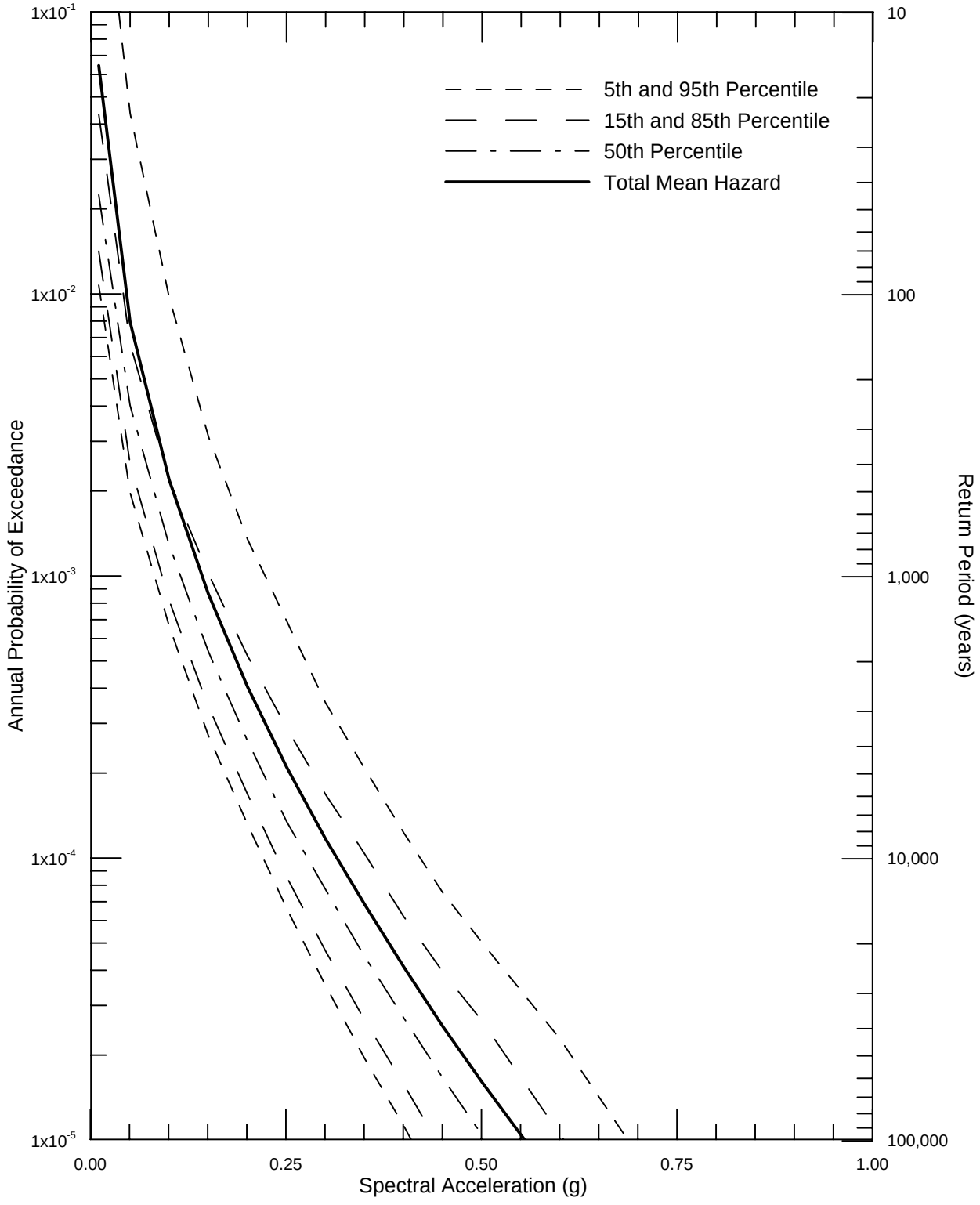

URS	Project No. 26817879 Newberry Volcano Oregon	SEISMIC HAZARD CURVES FOR 1.0 SEC HORIZONTAL SPECTRAL ACCELERATION AT SUNRIVER	Figure A-5

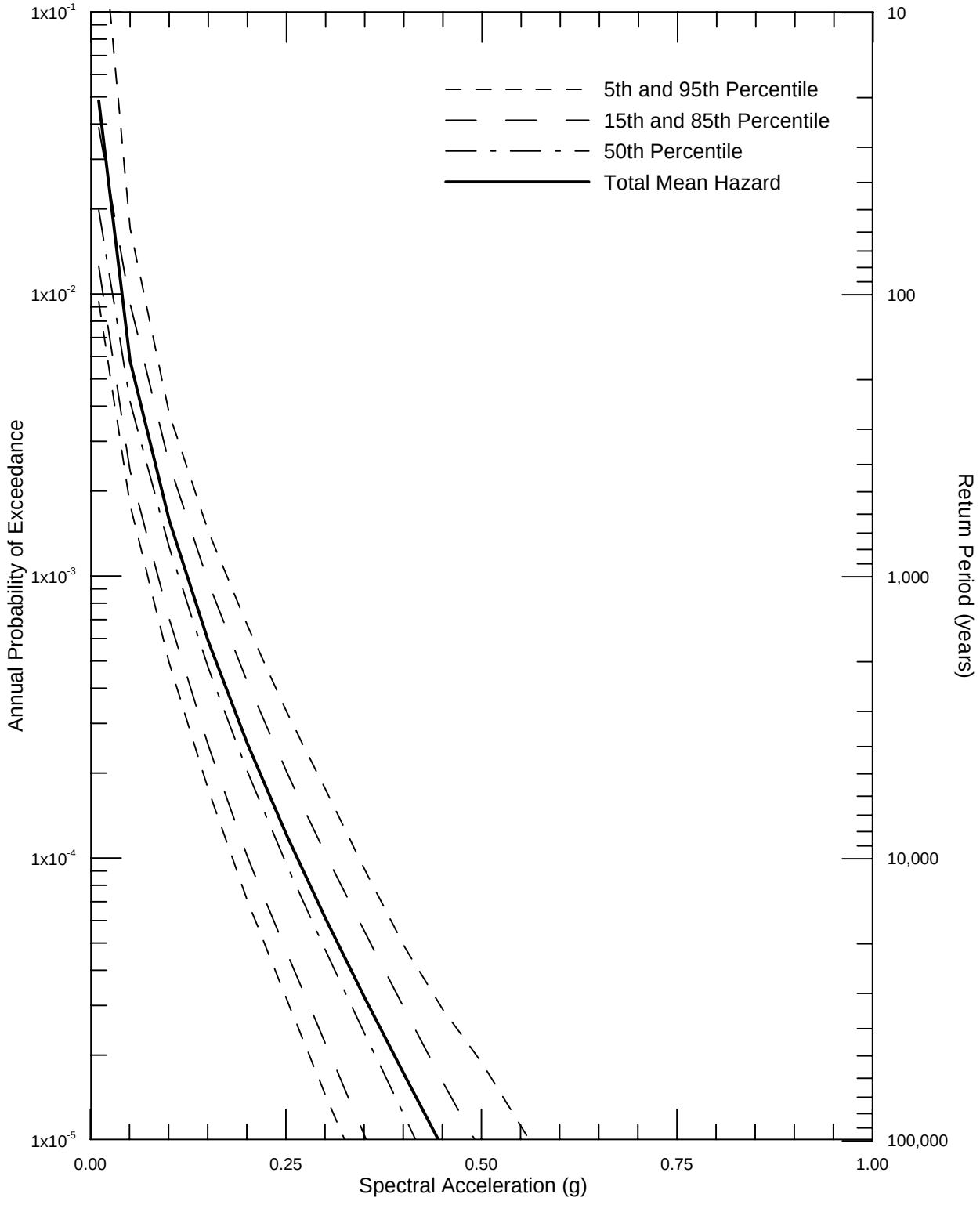

URS	Project No. 26817879 Newberry Volcano Oregon	SEISMIC HAZARD CURVES FOR 1.0 SEC HORIZONTAL SPECTRAL ACCELERATION AT WELL 55-29	Figure A-6

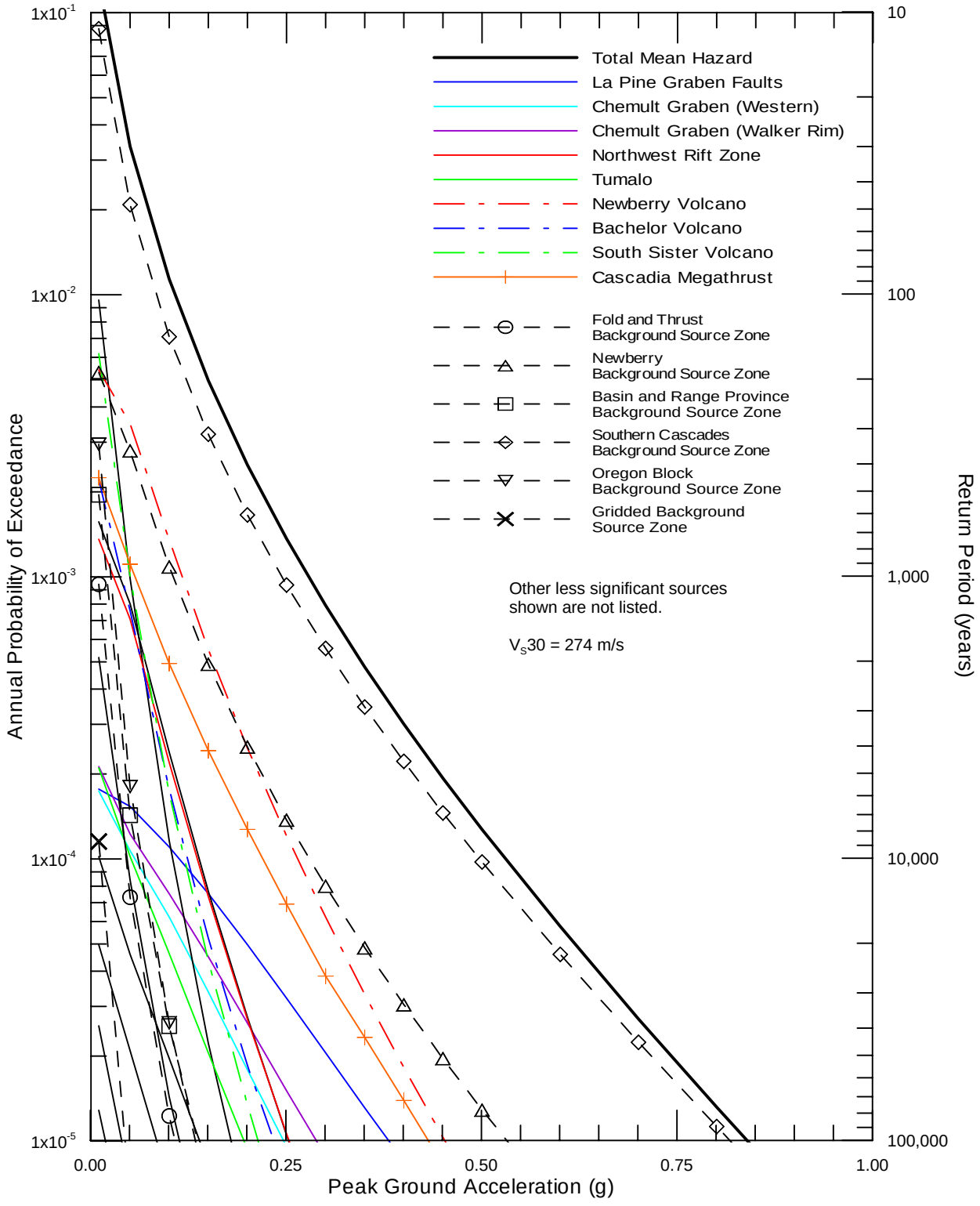

URS	Project No. 26817879 Newberry Volcano Oregon	SEISMIC SOURCE CONTRIBUTIONS TO MEAN PEAK HORIZONTAL ACCELERATION HAZARD AT LA PINE	Figure A-7

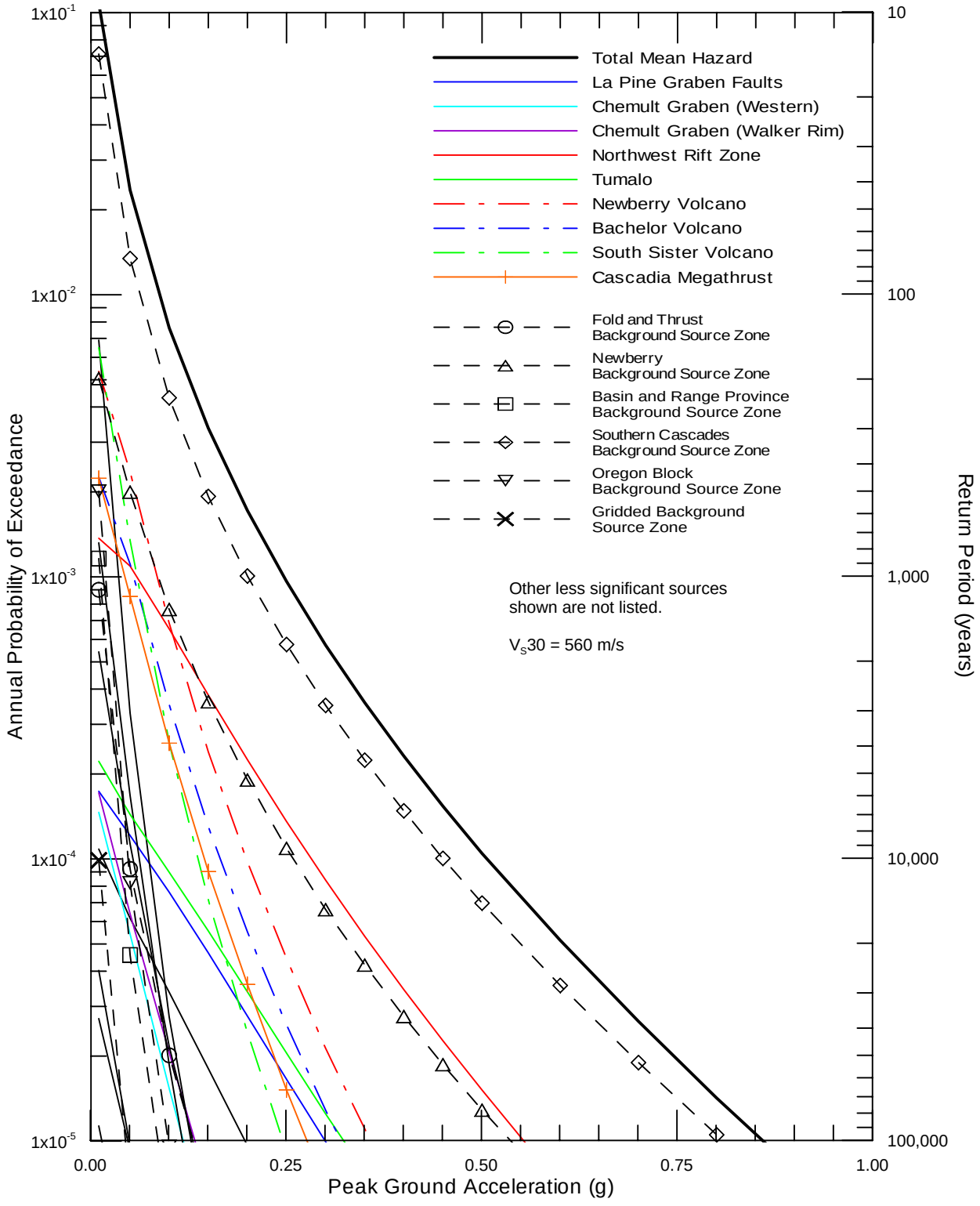

URS	Project No. 26817879 Newberry Volcano Oregon	SEISMIC SOURCE CONTRIBUTIONS TO MEAN PEAK HORIZONTAL ACCELERATION HAZARD AT SUNRIVER	Figure A-8

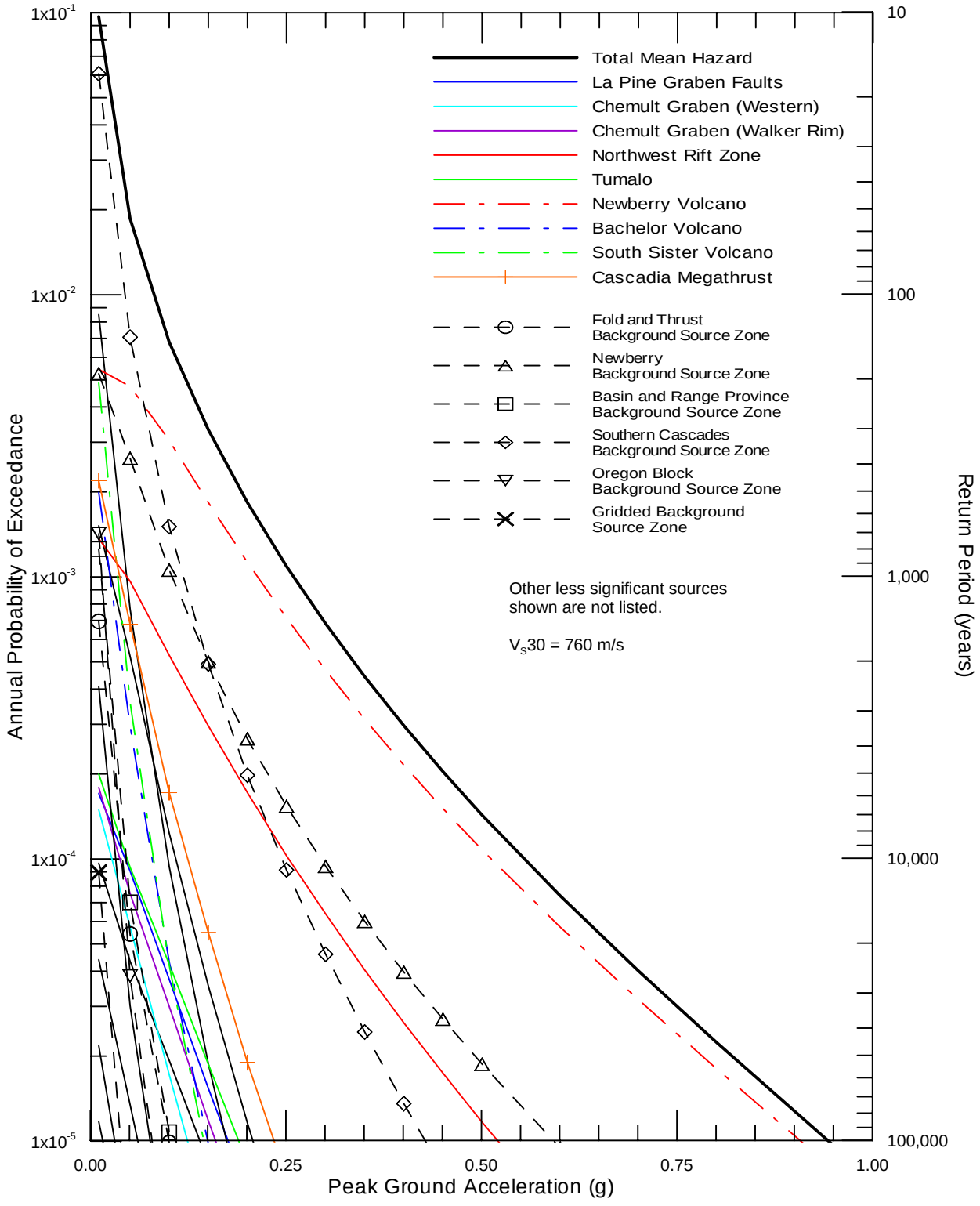

URS	Project No. 26817879 Newberry Volcano Oregon	SEISMIC SOURCE CONTRIBUTIONS TO MEAN PEAK HORIZONTAL ACCELERATION HAZARD AT WELL 55-29	Figure A-9

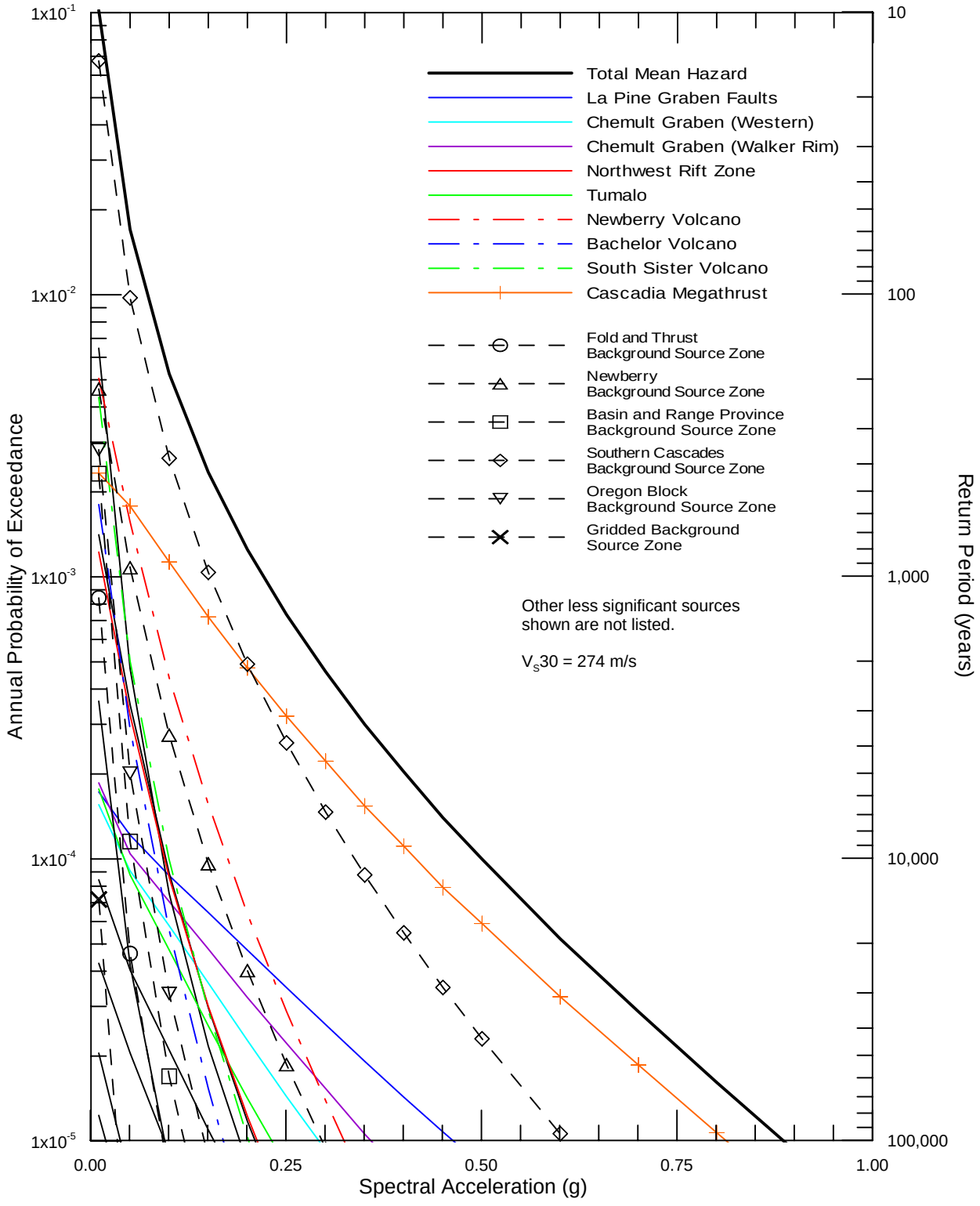

URS	Project No. 26817879 Newberry Volcano Oregon	SEISMIC SOURCE CONTRIBUTIONS TO MEAN 1.0 SEC HORIZONTAL SPECTRAL ACCELERATION HAZARD AT LA PINE	Figure A-10

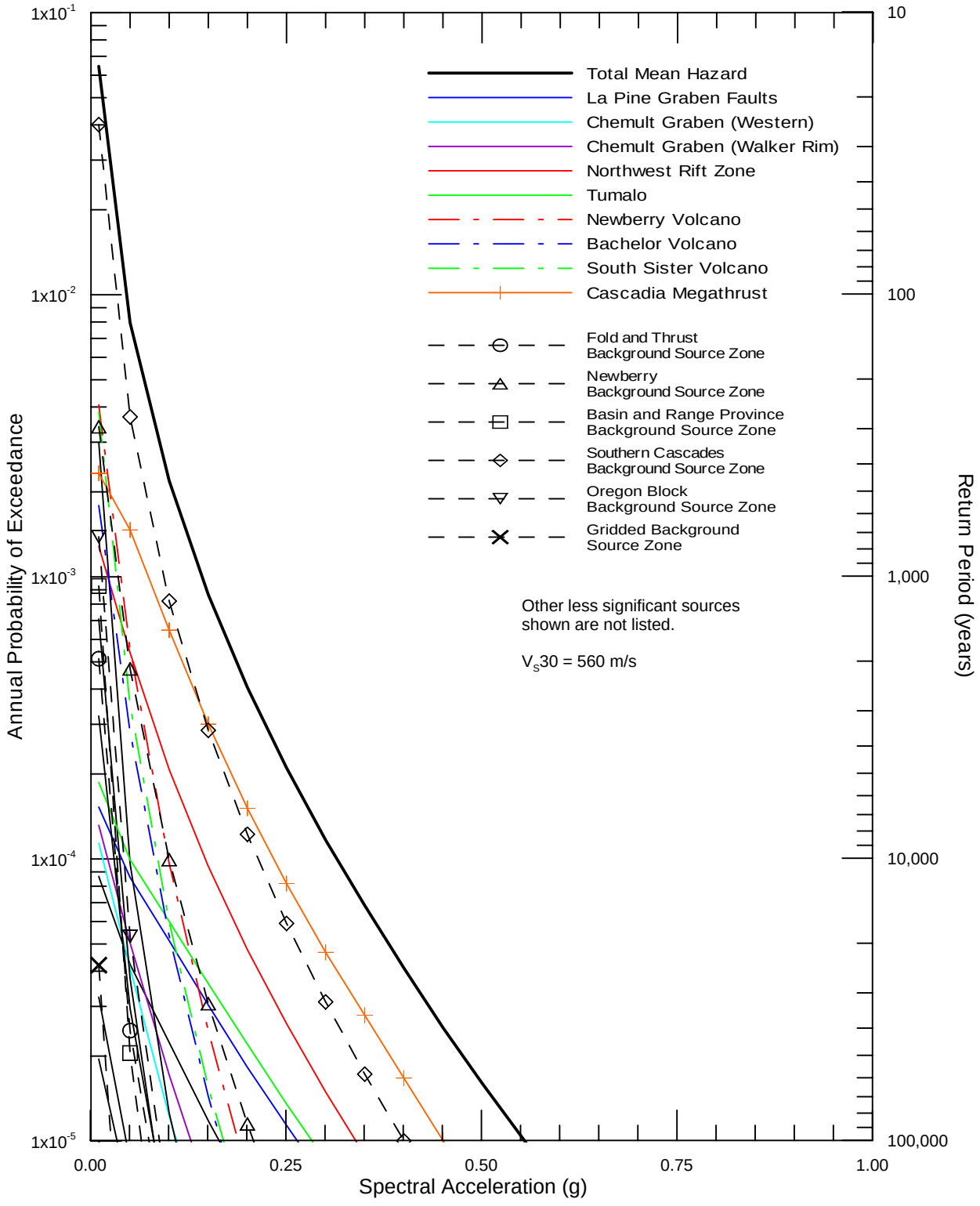

URS	Project No. 26817879 Newberry Volcano Oregon	SEISMIC SOURCE CONTRIBUTIONS TO MEAN 1.0 SEC HORIZONTAL SPECTRAL ACCELERATION HAZARD AT SUNRIVER	Figure A-11

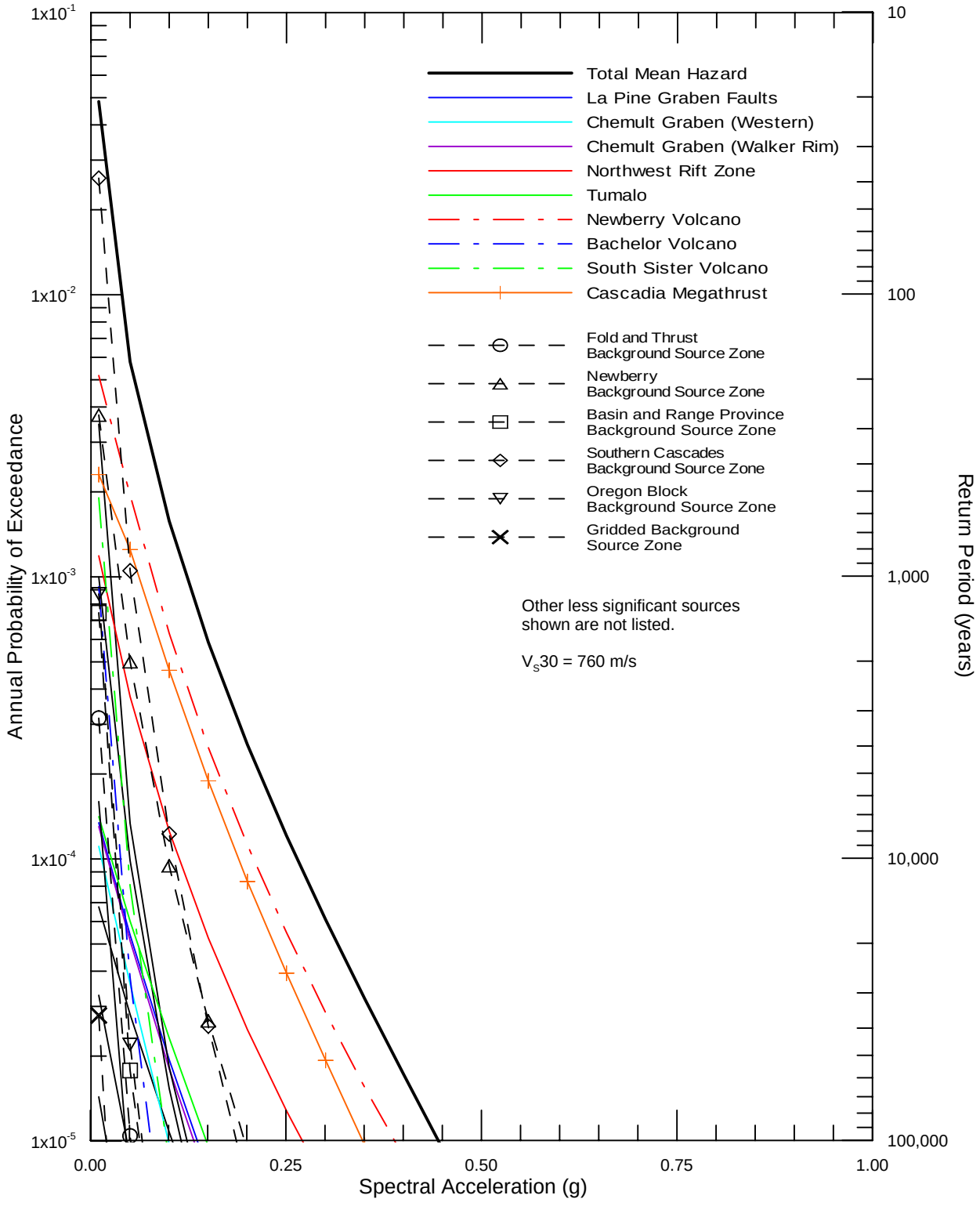

URS	Project No. 26817879 Newberry Volcano Oregon	SEISMIC SOURCE CONTRIBUTIONS TO MEAN 1.0 SEC HORIZONTAL SPECTRAL ACCELERATION HAZARD AT WELL 55-29	Figure A-12

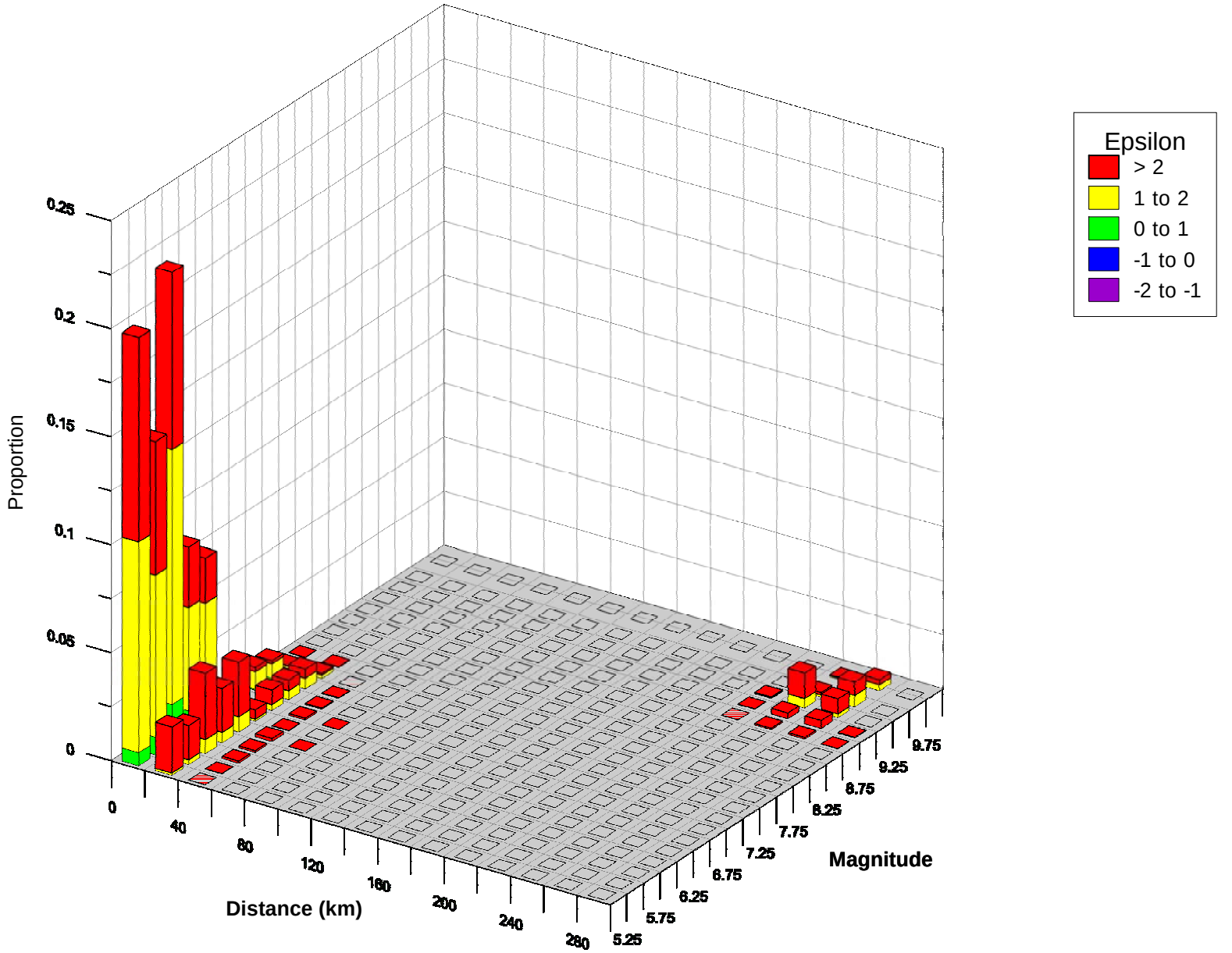

URS	Project No. 26817879 Newberry Volcano Oregon	MAGNITUDE AND DISTANCE CONTRIBUTIONS TO THE MEAN PEAK HORIZONTAL ACCELERATION HAZARD AT 2,475-YEAR RETURN PERIOD AT LA PINE	Figure A-13

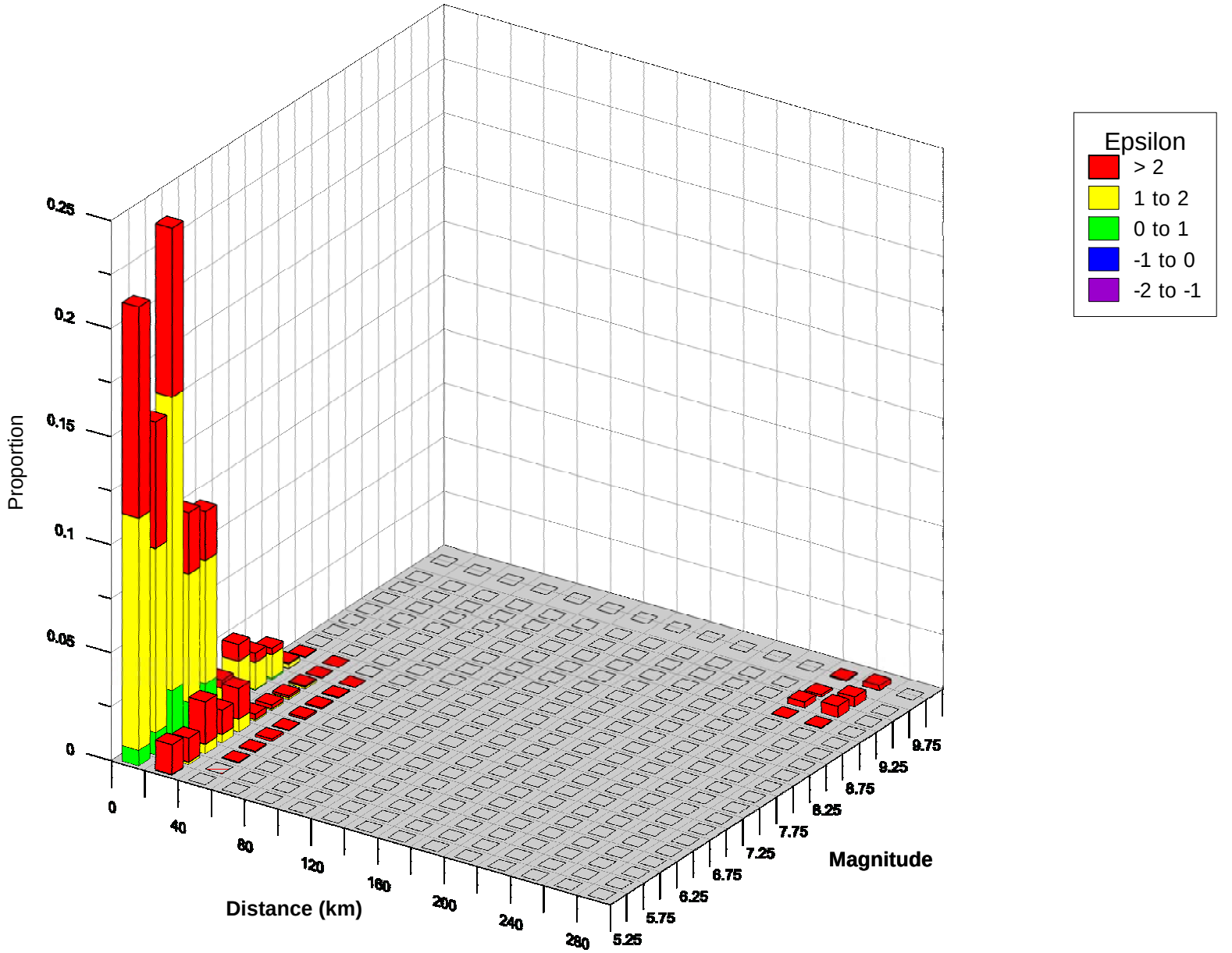

URS	Project No. 26817879 Newberry Volcano Oregon	MAGNITUDE AND DISTANCE CONTRIBUTIONS TO THE MEAN PEAK HORIZONTAL ACCELERATION HAZARD AT 2,475-YEAR RETURN PERIOD AT SUNRIVER	Figure A-14

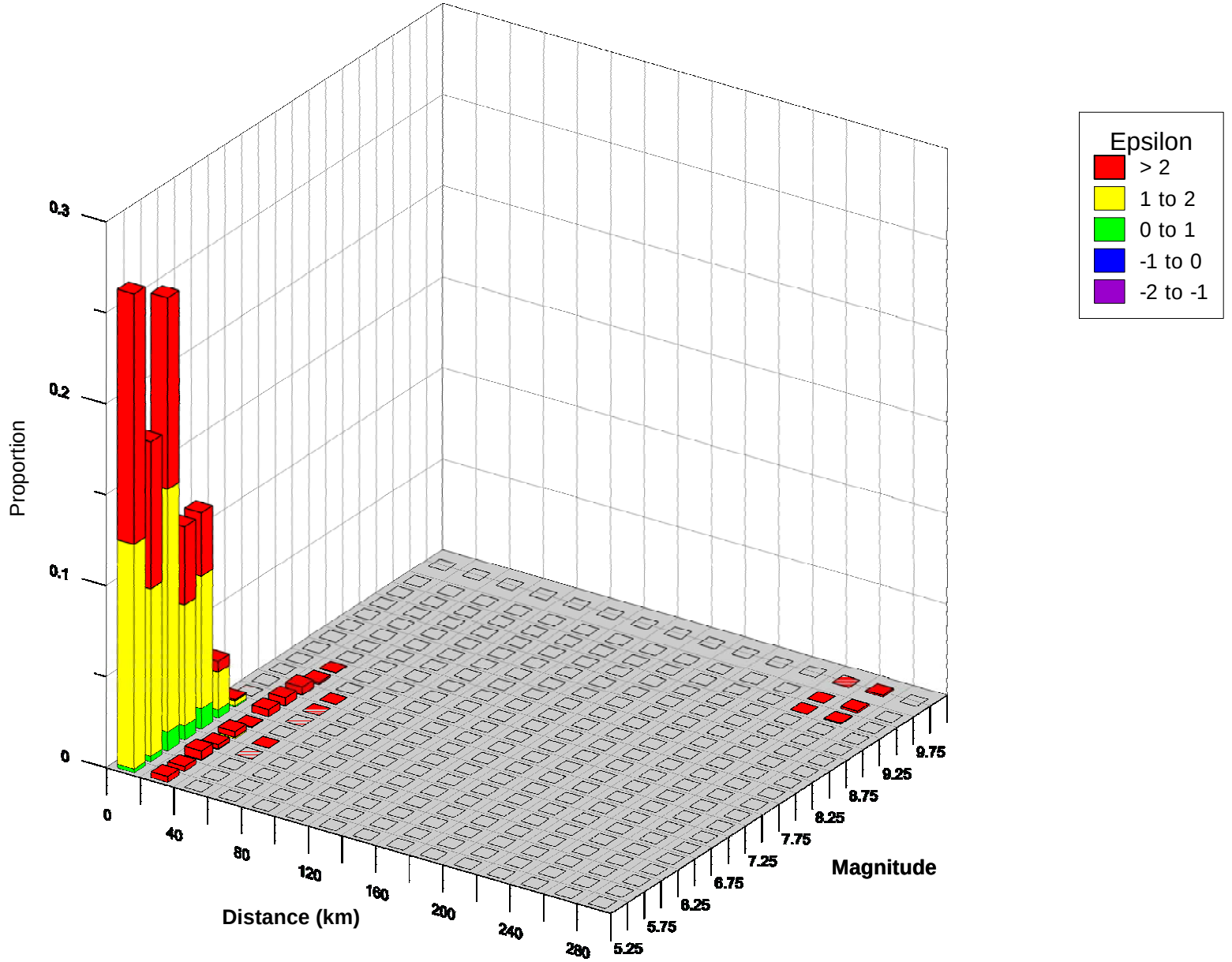

URS	Project No. 26817879 Newberry Volcano Oregon	MAGNITUDE AND DISTANCE CONTRIBUTIONS TO THE MEAN PEAK HORIZONTAL ACCELERATION HAZARD AT 2,475-YEAR RETURN PERIOD AT WELL 55-29	Figure A-15

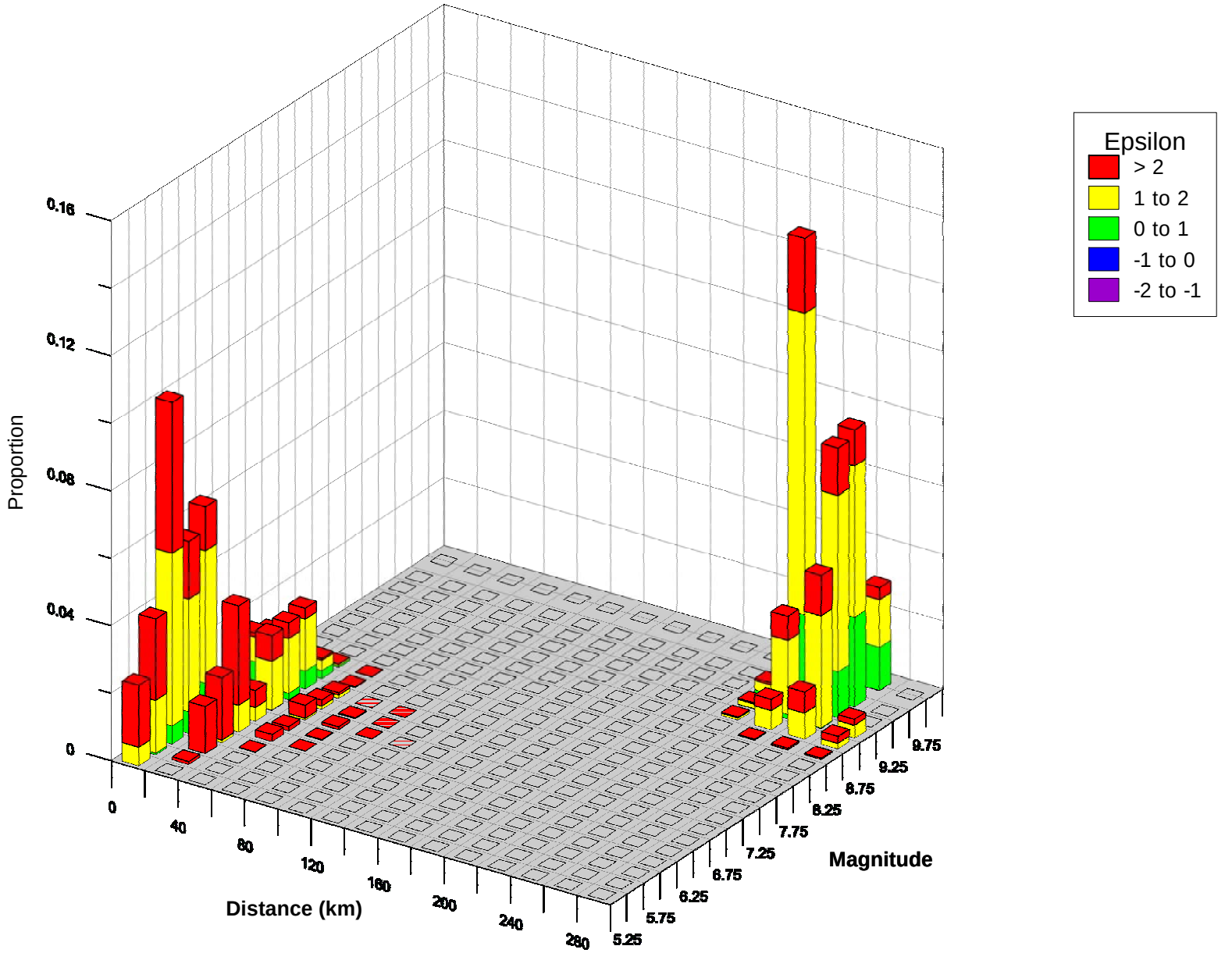

URS	Project No. 26817879 Newberry Volcano Oregon	MAGNITUDE AND DISTANCE CONTRIBUTIONS TO THE 1.0 SEC HORIZONTAL SPECTRAL ACCELERATION HAZARD AT 2,475-YEAR RETURN PERIOD AT LA PINE	Figure A-16

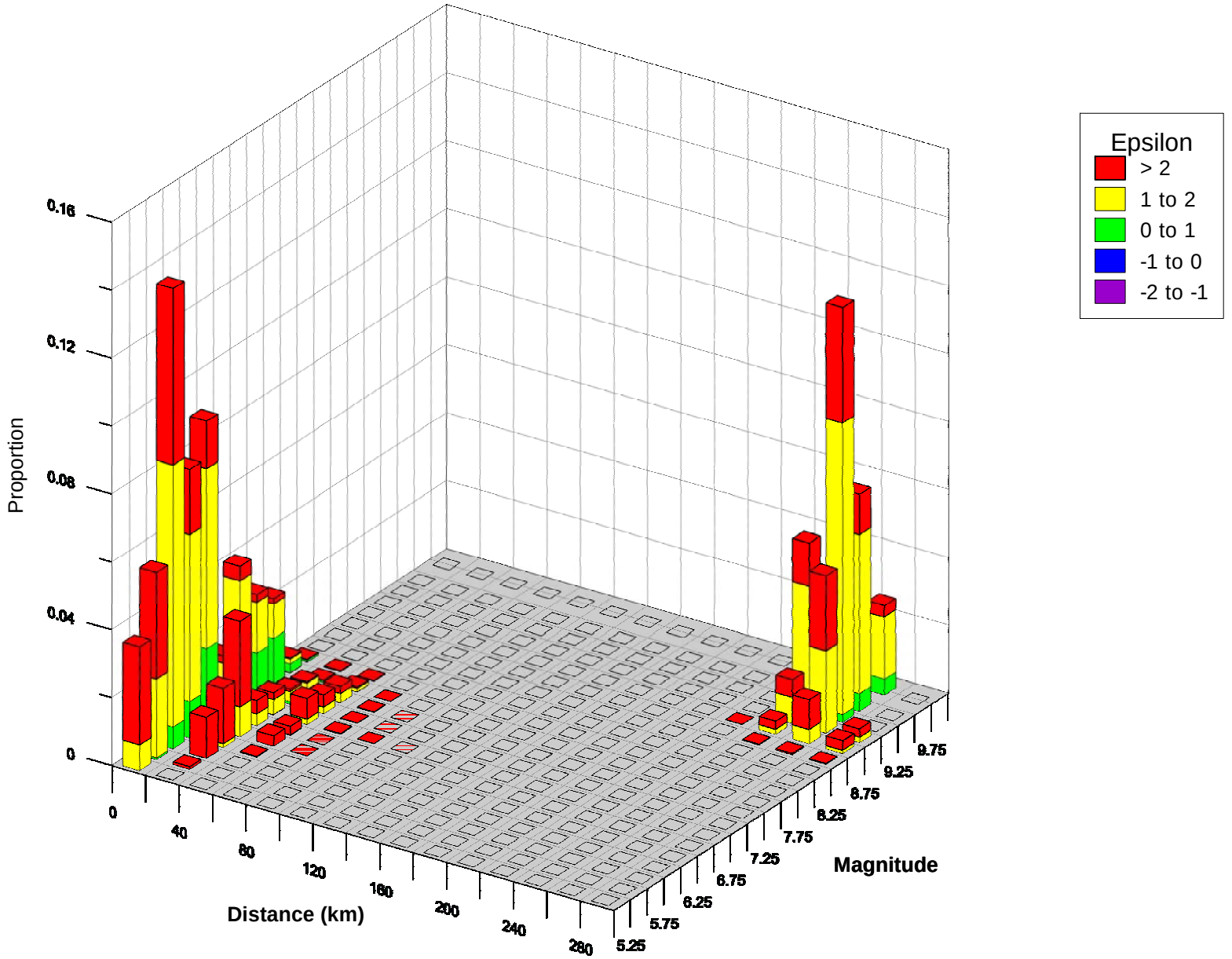

URS	Project No. 26817879 Newberry Volcano Oregon	MAGNITUDE AND DISTANCE CONTRIBUTIONS TO THE 1.0 SEC HORIZONTAL SPECTRAL ACCELERATION HAZARD AT 2,475-YEAR RETURN PERIOD AT SUNRIVER	Figure A-17

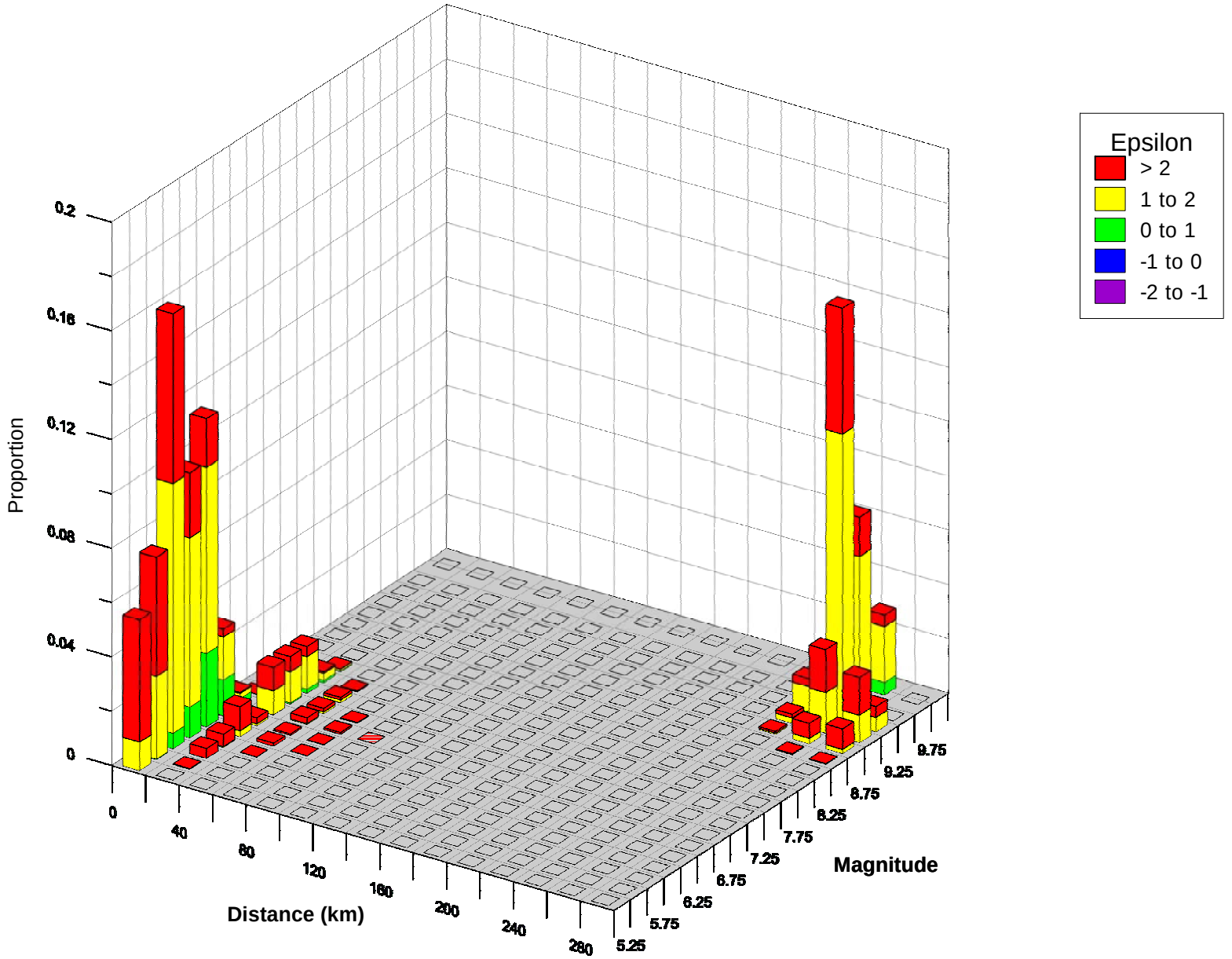

URS	Project No. 26817879 Newberry Volcano Oregon	MAGNITUDE AND DISTANCE CONTRIBUTIONS TO THE 1.0 SEC HORIZONTAL SPECTRAL ACCELERATION HAZARD AT 2,475-YEAR RETURN PERIOD AT WELL 55-29	Figure A-18

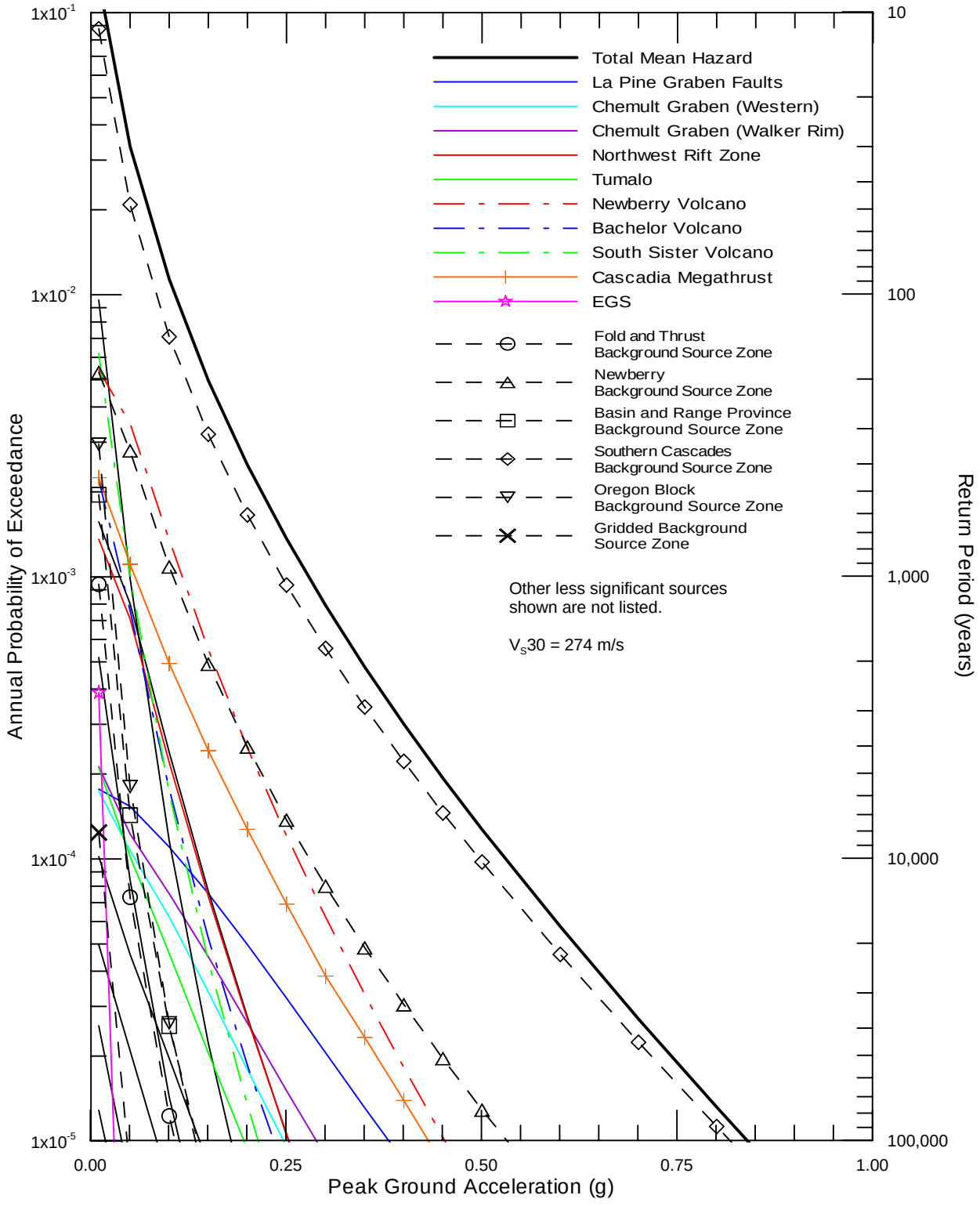

URS	Project No. 26817879 Newberry Volcano Oregon	SEISMIC SOURCE CONTRIBUTIONS TO MEAN PEAK HORIZONTAL ACCELERATION HAZARD AT LA PINE WITH EGS	Figure A-19

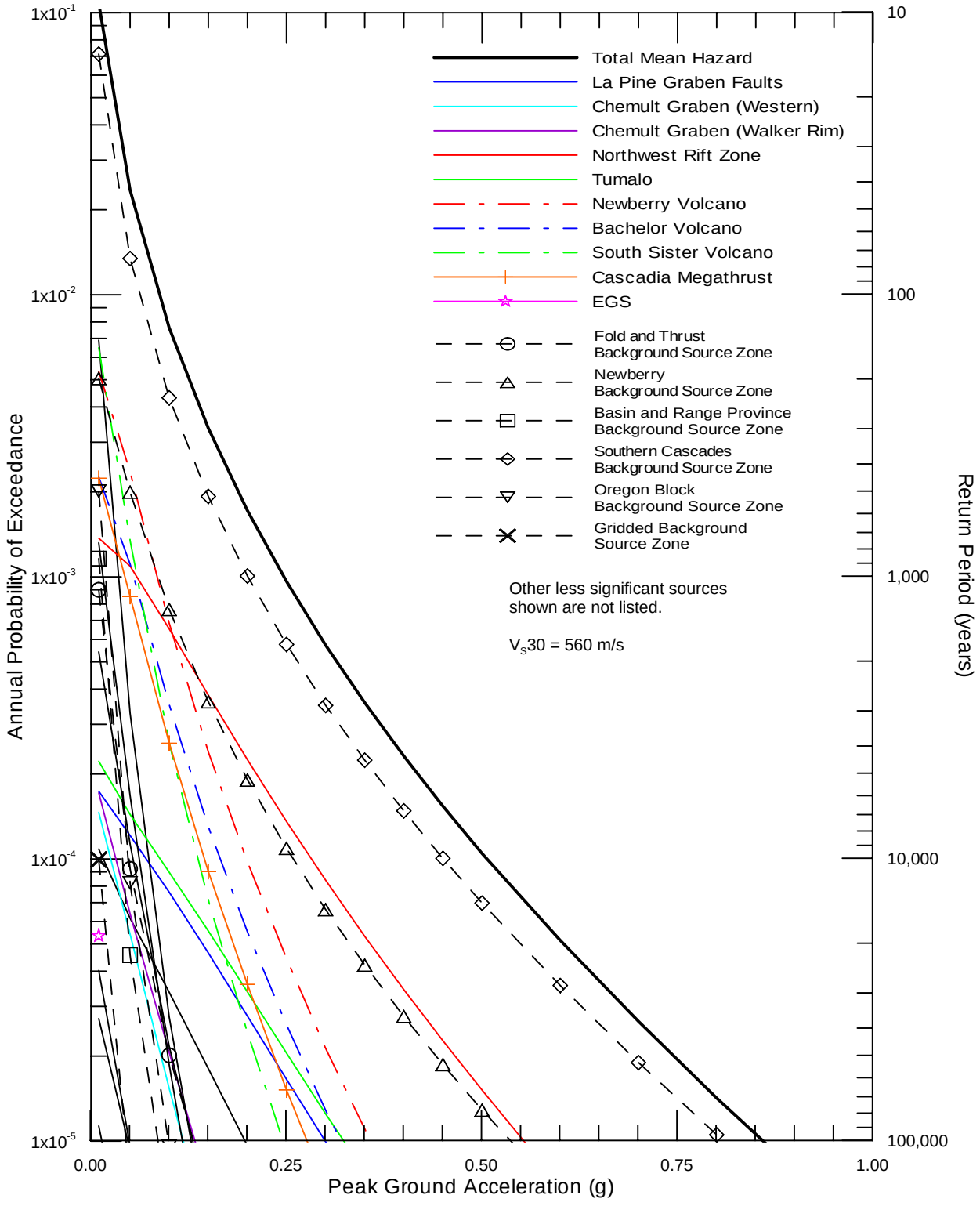

URS	Project No. 26817879 Newberry Volcano Oregon	SEISMIC SOURCE CONTRIBUTIONS TO MEAN PEAK HORIZONTAL ACCELERATION HAZARD AT SUNRIVER WITH EGS	Figure A-20

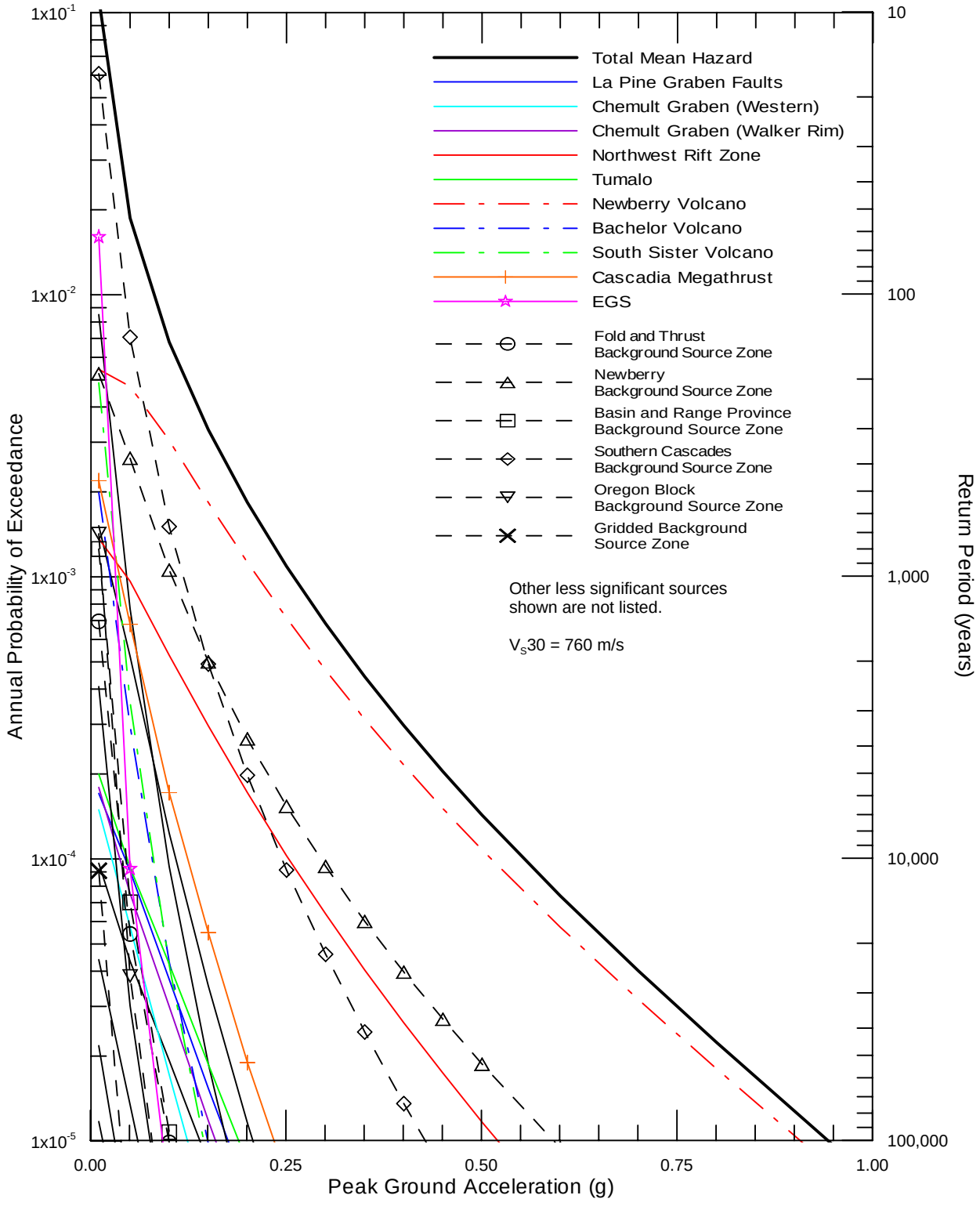

URS	Project No. 26817879 Newberry Volcano Oregon	SEISMIC SOURCE CONTRIBUTIONS TO MEAN PEAK HORIZONTAL ACCELERATION HAZARD AT WELL 55-29 WITH EGS	Figure A-21

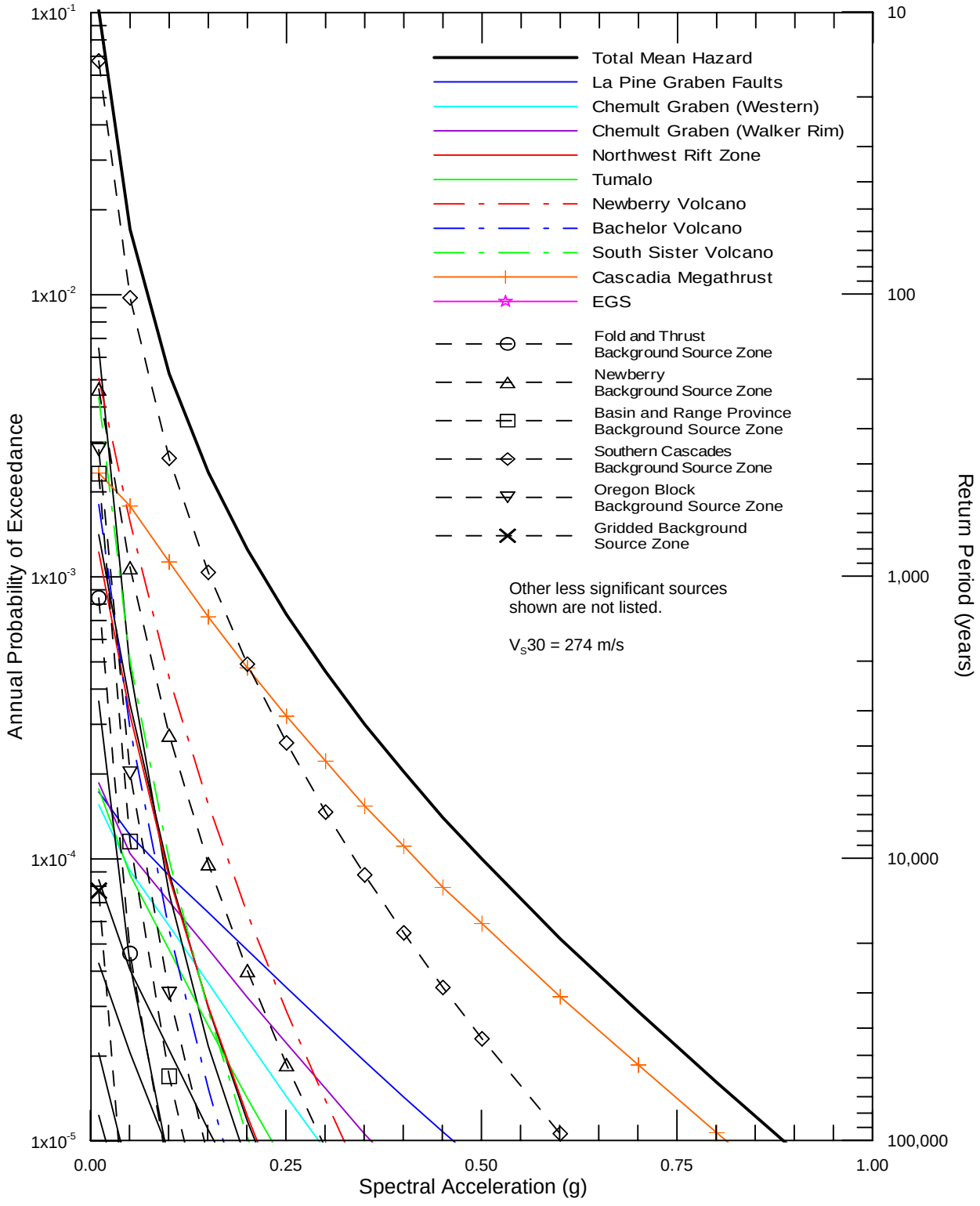

URS	Project No. 26817879 Newberry Volcano Oregon	SEISMIC SOURCE CONTRIBUTIONS TO MEAN 1.0 SEC HORIZONTAL SPECTRAL ACCELERATION HAZARD AT LA PINE WITH EGS	Figure A-22

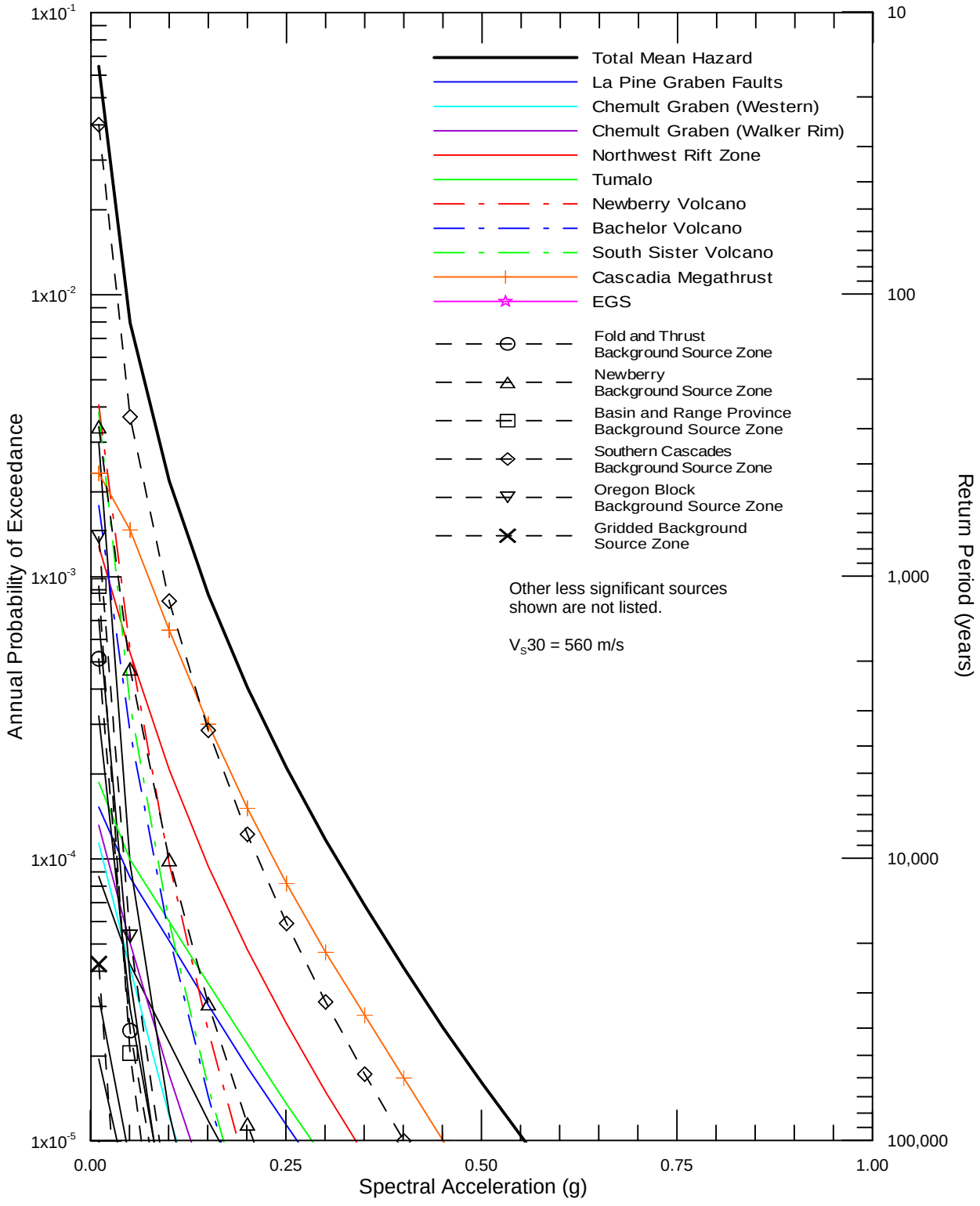

URS	Project No. 26817879 Newberry Volcano Oregon	SEISMIC SOURCE CONTRIBUTIONS TO MEAN 1.0 SEC HORIZONTAL SPECTRAL ACCELERATION HAZARD AT SUNRIVER WITH EGS	Figure A-23

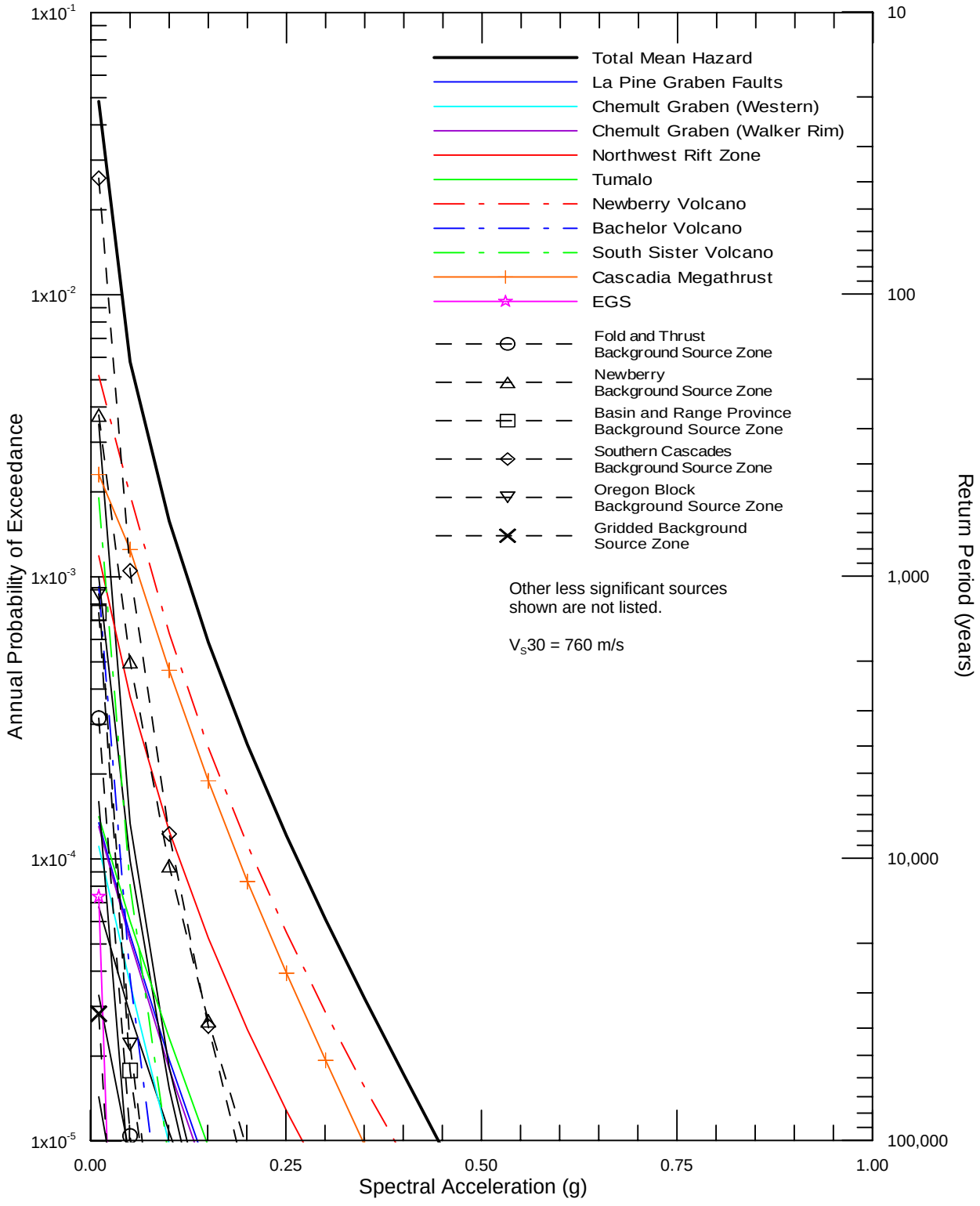

URS	Project No. 26817879 Newberry Volcano Oregon	SEISMIC SOURCE CONTRIBUTIONS TO MEAN 1.0 SEC HORIZONTAL SPECTRAL ACCELERATION HAZARD AT WELL 55-29 WITH EGS	Figure A-24